Terms and Conditions of Use of Digitised Theses from Trinity College Library Dublin

Copyright statement

All material supplied by Trinity College Library is protected by copyright (under the Copyright and Related Rights Act, 2000 as amended) and other relevant Intellectual Property Rights. By accessing and using a Digitised Thesis from Trinity College Library you acknowledge that all Intellectual Property Rights in any Works supplied are the sole and exclusive property of the copyright and/or other IPR holder. Specific copyright holders may not be explicitly identified. Use of materials from other sources within a thesis should not be construed as a claim over them.

A non-exclusive, non-transferable licence is hereby granted to those using or reproducing, in whole or in part, the material for valid purposes, providing the copyright owners are acknowledged using the normal conventions. Where specific permission to use material is required, this is identified and such permission must be sought from the copyright holder or agency cited.

Liability statement

By using a Digitised Thesis, I accept that Trinity College Dublin bears no legal responsibility for the accuracy, legality or comprehensiveness of materials contained within the thesis, and that Trinity College Dublin accepts no liability for indirect, consequential, or incidental, damages or losses arising from use of the thesis for whatever reason. Information located in a thesis may be subject to specific use constraints, details of which may not be explicitly described. It is the responsibility of potential and actual users to be aware of such constraints and to abide by them. By making use of material from a digitised thesis, you accept these copyright and disclaimer provisions. Where it is brought to the attention of Trinity College Library that there may be a breach of copyright or other restraint, it is the policy to withdraw or take down access to a thesis while the issue is being resolved.

Access Agreement

By using a Digitised Thesis from Trinity College Library you are bound by the following Terms & Conditions. Please read them carefully.

I have read and I understand the following statement: All material supplied via a Digitised Thesis from Trinity College Library is protected by copyright and other intellectual property rights, and duplication or sale of all or part of any of a thesis is not permitted, except that material may be duplicated by you for your research use or for educational purposes in electronic or print form providing the copyright owners are acknowledged using the normal conventions. You must obtain permission for any other use. Electronic or print copies may not be offered, whether for sale or otherwise to anyone. This copy has been supplied on the understanding that it is copyright material and that no quotation from the thesis may be published without proper acknowledgement.

Aspects of landscape evolution, lineaments and fault zone mineralisation in southeast Ireland

by

David Jordan

Submitted for the degree of Doctor of Philosophy

Department of Geology

University of Dublin, Trinity College

March 2008

Declaration

This thesis has not been submitted as an exercise for a degree at this or any other university. Except where duly acknowledged, this thesis is entirely my own work. I agree that the Library of Trinity College Dublin may lend or copy this thesis upon request.

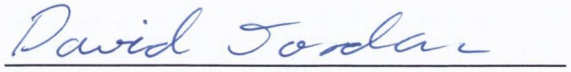

David Jordan

Summary of Thesis

The findings of this work are presented in 8 chapters. Chapter 2 deals with a deep weathering profile in limestone at the Timahoe, County Kildare. Detailed analysis of materials collected from an investigatory borehole show that the weathering profile is a pocket deposit. It is proposed that weathering of a pyrite rich rock generated sulphuric acid that dissolved carbonate leaving behind an insoluble silica rich residuum. The Timahoe pocket deposit was initially mistaken for a buried palaeoriver due to its linearity, therefore other claimed palaeorivers in the region may also be pocket deposits. Furthermore, the practice of reconstructing the missing section above a pocket deposit to the Namurian level, for the purpose of landscape evolution studies, may be justified if the local Namurian rocks contain appreciable pyrite.

Chapter 3 investigates lineaments in the study area. Past studies relied on subjective identification of lineaments, leading to bias and error. Here, a work flow incorporating Feature Network Extraction (FNE) is developed. FNE is a computer based method that automatically detects lineaments, negating bias and error. FNE detected numerous lineaments that mostly follow rivers, including two previously unrecognised major lineaments.

Chapter 4 tests the hypothesis that lineaments that find expression in the landscape channelled hydrothermal fluids that caused hydrothermal alteration and weakening of wall rocks. This chapter describes the Shankill Fracture Zone (SFZ), a mineralised normal fault in north west County Wicklow. The Cloghleagh Iron Mine lies along the SFZ and it allowed excellent access to the fault. Examination of the SFZ and materials collected confirm that the SFZ channelled hydrothermal fluids, which generated a fault hosted epithermal manganese oxide deposit. These observations confirm that lineaments in the study area channelled hydrothermal fluids.

Chapter 5 describes intriguing microscopic filamentous structures found in a late fault that cuts supergene weathering and a hydrothermal breccia at the Cloghleagh Iron Mine. The filaments are formed of chains of microscopic cells, which resemble

fossilised bacteria. However, it is shown that the inorganic growth process Viscous Fingering may have formed the filaments in a natural analogue of the Silica Garden. This conclusion undermines the pantheon of Archean microfossils for which evidence of biogenicity often hinges on morphology alone. Additionally, these observations support the recent laboratory simulation of a fault zone that encountered extraordinarily low friction due to the generation of lubricating silica gel on the sliding fault surface.

Chapter 6 describes hydrothermally altered granite at a site overlooking Lough Tay, County Wicklow. It is shown via detailed mineralogical analysis carried out using X-ray diffraction analysis, that the clay mineral assemblage of montmorillonite-beidellite, kaolinite and illite is argillic alteration. Argillic alteration is typical of low temperature near surface hydrothermal activity, frequently $\sim<$200 metres below ground. Additionally, a tepid spring and galena mineralisation are found at the site. It is suggested that the tepid spring represents waning hydrothermal activity. Finally, the hydrothermally altered granite further supports the hypothesis that faults in the study area hosted hydrothermal fluids that promoted alteration of wall rocks.

Finally, chapter 7 investigates the topographic and fluvial development of the study area. In an effort to avoid subjectivity, Trend Surface Analysis (TSA) is used to determine the slope, trend and flatness of topography. It is shown that the Calary Plateau of east County Wicklow is gently tilted to the south and it appears to connect with the Rathdrum Surface. The second section of the chapter describes the oldest drainage pattern in the study area, which is a NW to SE drainage that appears to follow fractures. Finally, its is proposed that landscape tilting was caused by isostatic readjustment in response to erosional unloading of limestone.

Acknowledgements

I wish to express my deep gratitude to my late supervisor Prof. Adrian Phillips, who offered me the opportunity to study at Trinity College and whose enthusiasm inspired me at the outset of my project. I am similarly indebted to Dr. John Graham, whose crucial encouragement helped me to complete my project. I also pay thanks to Dr. Gareth Ll. Jones, who taught me the craft of scientific writing by co-writing a paper with me, Prof. George Sevastopulo for helpful discussions and Dr. Mike Philcox for providing me with depth to bedrock data. I also wish to thank Dr. David Chew, Prof. Geoff Clayton, Dr. Pete Coxon, Dr. Alex Densmore, Dr. Chris Nicholas, Dr. Ian Sanders, Prof. Christopher Stillman, Dr. Valentin Troll and Dr. Patrick Wyse Jackson for their help and support over the years. I am also grateful to Dr. Mike Cunningham for many stimulating and enlightening conversations regarding the Irish landscape.

My project also benefited from cooperation with Tobin Consulting Engineers, who allowed me to collect samples from a drill site at Timahoe, County Kildare. I'd also would like to thank Dr. David Ball and David Blaney who also attended the drill site, and Adrian Briody whose skill at operating the drill rig ensured that the borehole reached bedrock despite difficult conditions. Many thanks also go to Dr. David Doff and Dr. Robbie Goodhue who introduced me to the methods of clay mineral analysis. I also wish to thank Ric Pasquali for providing me with borehole data. A special thanks goes to Dr. Mags Duncan for her words of encouragement, especially towards the end of my project. I'm am also indebted to the geology department's technicians Neil Kearney, Declan Burke, Frank Hendron and Maura Morgan.

I also wish to I thank Dr. Sarah Taylor, Dr. Brian McSharry, Dr. Francois-Xavier (Fx) Devuyst and Dr. Stuart Bennett for their help and friendship during my studies. I'm also grateful to my postgraduate friends Fiona, Graeme and Marc-Antoine for their patience and help, and of course Paul, Jane, Jo, Alastair, Eleanor, Eoghan, Sarah, Aoife, Niall, Eloise and Maja. I also remember with great fondness my late friend Mary Corcoran, who I will always miss. I am sorry if I have forgotten anyone, all those who helped and supported me are remembered with gratitude. Lastly, but most of all, many thanks to my parents for their support and encouragement over the years.

Table of Contents

Figures

Tables

Chapter 1 - Introduction

The initial aim of the research presented in this thesis was to determine whether palaeorivers crossed the study area of south eastern Ireland, directed away from the Irish Sea towards the west. This goal was motivated by the proposal of the Irish Sea Dome, whereby the Irish Sea area was uplifted and was land during the early-Palaeogene, forming a drainage that flowed westward across Ireland (Cope, 1994). However, no evidence for a west directed palaeodrainage was found but from work entailed in looking for it, other lines of enquiry arose and were followed up. In addition to drainage analysis, investigations of palaeoweathering, lineaments, hydrothermal phenomena and topography were undertaken, as follows:

1.1 Overview of chapters

Chapter 2 investigates a large silica clay deposit in limestone at Timahoe, County Kildare, which was discovered by remote sensing. An investigatory borehole was drilled into the centre and presumed deepest part of the geophysical anomaly, and it returned mostly silica rich clays to a depth of *c.* 128 metres. The results of detailed mineralogical and geochemical analysis of the materials collected from the borehole show that is a pocket deposit. The origin and nature of the deposit is discussed in relation to the work of Walsh *et al.* (1972) who studied pocket deposits elsewhere and Pasquali (2002) who proposed the existence of several buried palaeochannels in the Irish Midlands

The aim of chapter 3 is to develop and use an objective method to detect lineaments in the study area. Lineaments are normally identified using subjective judgement, which can lead to user bias and error. Thus there is need for an objective method of lineament identification. Here, a simple work-flow incorporating Feature Network Extraction is developed. This is a computer based method that automatically detects topographic lineaments, minimising user bias and error. Two previously unknown major lineaments are reported and it will be shows that rivers follow most of the lineaments.

Chapter 4 tests the hypothesis that faults and fractures in the study area, that find expression in the landscape, channelled hydrothermal fluids that caused wall-rock alteration that is liable to erosion. This chapter describes a hydrothermally altered and mineralised fault, the Shankill Fracture Zone (SFZ) of east County Wicklow. The Cloghleagh Iron Mine is located along a mineralised section of the SFZ, and the mine allowed excellent access to the fault. A genetic model describing the formation of the mineralisation is developed and the deposit is compared with other similar deposits abroad.

Chapter 5 describes the serendipitous discovery of microscopic filamentous structures in a fault rock at the Cloghleagh Iron Mine. The filaments resemble fossilised microbial life, indeed some filaments appear to be formed of chains of bacilli shaped cells. Both organic and inorganic origins are carefully evaluated and it is shown that the inorganic process Diffusion Limited Aggregation can create structures that resemble the biomorph in question. The conclusions are discussed in relation to supposed fossil microbial life of the Archean and the recent observation of silica gel formation in a simulated fault zone (Marone, 2004).

Chapter 6 returns to the subject of hydrothermal alteration and it describes a chemically altered granite at a site overlooking Lough Tay, County Wicklow. The altered granite looks like a typical granite saprolite, the product of surficial chemical weathering. However, detailed mineralogical analysis of the chemically altered granite carried out using X-ray Diffractometry revealed a hydrothermal origin. Furthermore, analysis provided an approximate depth of formation of the chemically altered granite.

Chapter 7 relates to landscape analysis and is separated into two main sections. The first section examines the Calary Plateau and Rathdrum Surface of east County Wicklow. Once again in an effort to avoid subjective judgement, Trend Surface Analysis is used to determine the flatness, trend and slope of the Calary Plateau and Rathdrum Surface. It is shown that the surfaces are tilted to the south and they may have been part of larger contiguous surface in the past. The second half of the chapter endeavours to identify the oldest drainage pattern in the region and comment on the

nature of its associated surface. It is shown that the oldest drainage pattern in southern Wicklow and northern Wexford, appears to have flowed along NW to SE faults/fractures across a surface gently tilted to the south east. A hypothesis involving isostatic readjustment in response to erosional unloading is offered to explain the observed surface tilting.

Finally, chapter 8 contains the conclusions resulting from work of this thesis and suggestions for further research.

Chapter 2 – The Timahoe Weathering Profile

2.1 Summary of Chapter

The subject of this chapter is the Timahoe limestone weathering profile, a pocket deposit (Walsh *et al.*, 1999) near Timahoe, County Kildare. The weathering profile was discovered using remote sensing and was at first interpreted by O'Connel (2003) as a pre-glacial palaeochannel filled with stiff clays; *c.* 300 metres wide, at least 2 km long and more than 50 metres deep.

Drilling of the Timahoe weathering profile was conducted at its mid-line and presumed deepest part (borehole designation: BH-7). Drilling encountered 64.6 metres of Quaternary overburden followed by 63.7 metres of silica-clays with rotted chert that represents a weathering profile in limestone. Bedrock was reached at 128.3 metres depth, some 33.3 metres below sea-level. A compete drill log, mineralogical and geochemical analysis of the materials collected allowed a detailed examination of the Timahoe weathering profile. The work of Chigira & Oyama (1999) regarding pyritic weathering profiles in sedimentary rocks and Rose & Cravotta's (1998) work on Acid Mine Drainage (AMD) in particular were helpful in understanding the processes that were involved in the formation of the Timahoe weathering profile.

It is suggested that pyrite oxidation played an important role in the formation of the Timahoe weathering profile and that pyrite oxidation may have also played an important role in some other pocket deposits. The implications of this proposal are discussed in relation to earlier studies that relied on pocket deposits to understand the Cenozoic landscape evolution of Ireland and Britain (Walsh & Brown, 1971, Walsh *et al.*, 1972; Walsh *et al.*, 1996; Walsh *et al.*, 1999) and Pasquali (2002) who claimed that gravity lows and areas of deep depth-to-bed-rock values found in the Carboniferous Midlands of Ireland are hidden palaeorivers.

2.2 Introduction: Pocket Deposits

Pocket deposits are features of limestone karst. They are typically pipe shaped bodies in limestone, up to a kilometre wide and up to 200 metres deep that contain silica rich clays and weathered chert, representing the insoluble residuum of limestone dissolution (Walsh *et al.*, 1972; Beese *et al.*, 1983). Some pocket deposits additionally contain surface derived materials such as palaeosols, lignite, fossil leaves, fluvial sands and gravels (Walsh *et al.*, 1972).

Walsh *et al.* (1972), who employed 2-dimensional sandbox modelling, proposed that pocket deposits form when limestone dissolution at depth causes surface materials to subside into a growing depression. However, Reynolds (1974) indicated that the Dunshaughlin pocket deposit is a surficial weathering profile. Furthermore, it lies close to an extensive occurrence of pyrite rich Namurian shales, and Reynolds (1974) suggested that the Dunshaughlin pocket deposit could have formed when pyritic oxidation generated sulphuric acid that dissolved the limestone. This proposal followed Reynold's (1974) observation that limestone collected beside the Dunshaughlin pocket deposit left a residue of silica-clays following acetic acid treatment (which removed calcium carbonate) that looked very like the Dunshaughlin pocket deposit clays.

2.2.1 History of research

Maw (1865) was the first to provide a geological description of a pocket deposit near Little Ormes Head, Llandudno, North Wales. He described two pocket deposits that were mined for pipe clays; impure silica rich clays were used to make poor quality pottery and clay pipes. Later, Maw (1867) described several more pocket deposits in the same region of North Wales and included several field sketches that show sedimentary bedding, and he described for the first time bleached and porous "decomposed chert" from the Pant Du pocket. Maw (1867) proposed the pocket deposits were pre-glacial Tertiary in age and that they formed via tropical weathering of limestone. According to Walsh *et al.* (1972), the term "Pocket Deposit" was first used in 1897 in relation to the Derbyshire and Staffordshire pocket deposits.

A number of the pocket deposits described by Maw (1867) were situated amongst the copper sulphide and iron oxide mines of the Halkyn ore field. Walsh & Brown (1971) greatly extended Maw's (1867) work on the pocket deposits of North Wales. They described several pocket deposits that trend along faults and sulphide mineral veins, namely the Berthddu pocket deposit that trends along the Pant-y-ffrith mineralised fault, the Plascerrig Main Pit pocket deposits and the Loggerheads Inn pocket deposit that coincide in part with the Cat Hole mineral veins and other "cross-course" veins. The pocket deposits and mineral veins form an interesting association considering that sulphide oxidation might cause limestone dissolution

2.2.2 Importance in landscape evolution studies

Pocket deposits are potentially valuable in reconstructing a history of landscape evolution. If a pocket deposit contains datable in-fill materials that subsided from a higher palaeosurface and the missing stratigraphic section can be reconstructed to that original surface, then the altitude and age of the palaeosurface may be estimated (Walsh *et al.*, 1972). Following from this, the degree and rate of erosion may be ascribed to the present day landscape (Walsh *et al.*, 1996; Walsh *et al.*, 1999).

Walsh *et al.* (1999) used several pocket deposits and other Cenozoic deposits to propose that various separate landscapes of low relief (including the Menian Surface of north Wales, the Bosherston-Castlemartin Surface of south west Wales, the Reskajeage Surface of south west England, the Tullow lowlands of County Carlow, Ireland and the South Ireland Plain of east County Cork and south County Waterford) are the fragmentary remnants of a once extensive palaeosurface surface of upper-Oligocene to mid-Miocene age (*c.* 28 to 15 Ma). One of the "corner stone" pocket deposits analysed by Walsh *et al.* (1999), was the Hollymount pocket deposit of County Laois, where the missing stratigraphic section was reconstructed to the Namurian level following Mitchell's (1997) brief description of the in-fill materials that were interpreted as "insoluble millstone grit"; a total subsidence of *c.* 210 metres was suggested from an upper-Miocene palaeosurface, indicating an average landscape lowering rate of 0.02 mm per year.

2.3 The Timahoe Weathering Profile

The Timahoe weathering profile is situated mid way between Drehid crossroads and Timahoe village County Kildare at NGR 274750 232500, some 40 km due west of Dublin (figure 2.1). The location of the drill site (drill hole designation BH-7) was at the mid-line and presumed deepest part of the anomaly, as determined by remote sensing (figure 2.2). The local relief is subdued, with an altitude of 90 ± 5 metres. The vegetation is sparse, with just a few hedgerows and areas of gorse. Accordingly, the site was easy to survey and drill.

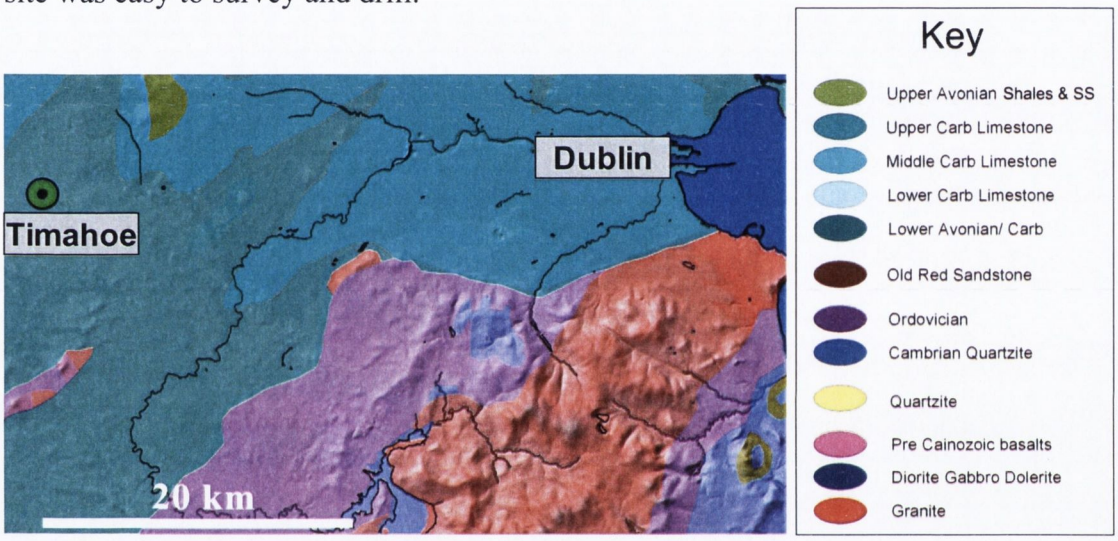

Fig. 2.1: Location and regional geological map of the Timahoe weathering profile.

2.3.1 Discovery

The Timahoe weathering profile was discovered beneath the proposed Drehid landfill site that is intended to accommodate domestic waste from County Kildare. It is a significant development that could have an impact on the local environment. Accordingly, an Environmental Impact Statement (EIS) is required. Potentially toxic fluids are generated by landfill waste during and after operations. These fluids must not contaminate water supplies. An important factor influencing the location of a landfill is the local geology and hydrogeology; there should be no aquifer or limestone karst beneath a landfill site. In addition, all landfill sites are lined with clays and geotextile, a plastic membrane that prevents fluid contaminating the water table.

In order to check for karstification at the proposed Drehid landfill site, detailed VLF-R, resistivity and seismic surveys were carried out. The resistivity survey identified a linear area of high conductivity that was initially interpreted as a Tertiary palaeoriver filled with clays, the Timahoe weathering profile.

2.4 Local Geology

Prior to recent site surveying, the bedrock geology at Drehid was poorly understood. The bedrock geology of the Drehid area, detailed on Sheet 16 produced by the Geological Survey of Ireland (GSI) (McConnell & Philcox, 1994) relies on widely spaced mineral exploration boreholes and rare rock outcrops (David Blaney pers. comm., 2003). The Drehid area is blanketed by peat, glacial and lacustrine deposits with depth to bedrock (DtoB) values averaging 5 to 15 metres (O'Connel, 2003).

GSI's Sheet 16 (McConnell & Philcox, 1994) indicates that the Timahoe weathering profile is in Waulsortian Limestone (Marchant & Sevastopulo, 1980) and that Waulsortian Limestone changes laterally to Calp Limestone, and that the contact separating the two lithologies is *c.* 700 metres west of BH-7 and it trends NNE – SSW, with Calp Limestone west of the boundary. A restricted occurrence of the Boston Hill Formation is indicated *c.* 1 km to the south of the Timahoe weathering profile and it dips gently to the north (O'Connel, 2003).

Calp Limestone was not found in BH-7, nor was it found in any earlier boreholes drilled within *c.* 2 km west of the Timahoe pocket deposit (O'Connel, 2003). Instead, Boston Hill Formation was encountered at 127.32 metres depth in BH-7. It is possible that Calp Limestone near the Timahoe weathering profile is was misidentified because it is also deeply weathered. If so, weathered Calp Limestone could account for the deep depth to bedrock values (up to 50 metres) seen in boreholes just north of Drehid cross roads, *c.* 1.75 km west of the Timahoe pocket deposit.

2.4.1 Waulsortian Limestone Formation

Waulsortian Limestone Formation is composed largely of pale grey biomicrite with Stromatactis structures (McConnell & Philcox, 1994). The formation may contain mud mounds. Mud mounds consist of individual and coalesced mounds of fossiliferous micritic limestone, with primary dips up to 40° (McConnell & Philcox, 1994). Mud mounds may represent a symbiotic seabed living ecosystem involving methanotrophic carbonate depositing bacteria and opportunistic faunas that included bryozoa, brachiopods, goniatites and corals (McConnell & Philcox, 1994). Due to its lack of clay minerals, Waulsortian Limestone is susceptible to karstification.

2.4.2 Calp Limestone

Calp Limestone is a dark argillaceous limestone typically interbedded with shales that was laid down by deep sea turbidity currents (McConnell & Philcox, 1994). It can physically overlie and laterally translate to Waulsortian Limestone. Below the Calp and possibly separated by a unconformity, is the Boston Hill Formation (McConnell & Philcox, 1994). The basal section of the Calp is locally known as the Tober Colleen Formation on the east of Sheet 16 (McConnell & Philcox, 1994). Calp Limestone may be pyrite and chert rich. Chert can form black hard stratigraphically bound and laterally extensive bands (Marchant & Sevastopulo, 1980). Pyrite may be similarly stratigraphically confined and can form rich layers of disseminated brassy cubes. Calp Limestone is clay rich and is resistant to normal karstification (O'Connel, 2003).

Regarding the area of the Timahoe weathering profile, according to the GSI's bedrock map, sheet 16 (McConnell & Philcox, 1994), Calp Limestone here is transitional to Waulsortian Limestone *c.* 700 metres west of BH-7, with the contact running NNW to SSE. However, no Calp Limestone was found in the several boreholes drilled in the area prior to the present study, however as earlier suggested, it is possible that it is deeply weathered.

2.4.3 Boston Hill Formation

Boston Hill Formation consists of coarse calcarenites and thin shales (McConnell & Philcox, 1994). GSI's sheet 16 indicates that Boston Hill Formation occurs *c.* 3 km south of BH-7 and it dips shallowly to the north, so is should occur at depth below BH-7. Above the Boston Hill Formation is Calp Limestone and Waulsortian Limestone (McConnell & Philcox, 1994). The top of the Boston Hill Formation is demarcated by a sharp boundary that may be unconformable (McConnell & Philcox, 1994).

2.5 Geophysical Survey

The geophysical survey results presented here are part of a survey carried out by APEX Geoservices Limited. Surveying methods employed include: VLF-R, 2D-resistivity, seismic profiling, digging of trial pits and depth probing of peat. In all, *c.* 650 hectares of bog were surveyed.

2.5.1 Very Low Frequency-Resistivity (VLF-R)

The VLF-R survey measured the subsurface interaction with very low frequency radio waves from the military transmitter at Rugby, England (16 kHz at 60 kW near Lat 52° 22" Long 01° 11"). The surveying was carried out using a Geonics EM16/16R with ground electrode (O'Connel, 2003). The Geonics EM16/16R measures apparent resistivity of the underlying overburden and bedrock by measuring the interaction of very low frequency (VLF) radio waves with the underlying stratigraphy. A strong VLF signal at 16 kHz was provided by a military time signal station at Rugby, Warwickshire, England. Two parameters are recorded, apparent resistivity (ρ) and phase angle (φ). VLF-R measurements were taken at 50 meter intervals over three 1.5 km lines and two 0.75 km lines (O'Connel, 2003). The position of each survey location was recorded using a Garmin12XL global positioning receiver with a horizontal accuracy of 15 metres (O'Connel, 2003). In all, 120 VLF-R readings were taken and the computed apparent resistivity (ρ) and phase angle (φ) readings were displayed on a plan map over the surveyed area (O'Connel, 2003).

VLF-R surveying can determine the overburden thickness and overburden type. In some cases, VLF-R surveying can also help identify areas of karstification, faulting, fracturing or dolomitisation. These areas have a much lower resistivity than the surrounding bedrock due to groundwater that is electrically conductive

2.5.2 2D resistivity

2D resistivity profiling was carried out with a Tiger resistivity meter using a Wenner type electrode array (O'Connel, 2003). Resistivity profiling measures a large number of resistivity values vertically throughout a profile. The Tiger resistivity meter speeds up the surveying process by using 32 or 64 placed electrodes, from which a subset of 4 active electrodes are computer selected (O'Connel, 2003).

The Wenner array consists of 4 in line electrodes. The two outer electrodes provide current that passes through the ground then the potential difference is measured by the two inner electrodes. The voltage detected by the inner electrodes is proportional to the resistivity of the ground through which the current passes. By incrementally increasing electrode spacing, the resistivity at ever greater depths is resolved. The recorded resistivity values were processed using RES2-DVINV with five iterations for each surveyed line (O'Connel, 2003). Resistivity surveying can define overburden thickness and type, bedrock resistivity and possible areas of low resistivity indicating groundwater flow and karstification. The method clearly visualised the Timahoe weathering profile in cross section. Resistivity surveying has a maximum depth of resolution of *c.* 50 metres, but despite this, the bottom of the pocket deposit could not be resolved (O'Connel, 2003).

2.5.3 Seismic refraction profiling

Seismic refraction profiling was carried out using a Geode 12 channel seismograph with a geophone spacing of 5 and 10 metres (O'Connel, 2003). Acoustic energy was generated using a sledge hammer and buffalo gun with five shots per profile (O'Connel, 2003). The location of the seismic refraction profile measurements were

based on earlier VLF-R and 2D-resistivity survey locations (O'Connel, 2003). However, attenuation caused by peat resulted in poor results and at best the method only confirmed earlier surveys (O'Connel, 2003).

2.5.4 Trial pits

Trial pits and depth probing of peat outlined in the survey reports, did not elucidate the nature of the Timahoe deposit due to shallow penetration depths of just a few metres and shall not be discussed further (O'Connel, 2003).

2.5.5 The implications of survey results

Immediately apparent in VLF-R and resistivity surveys (Fig. 2.2) was a linear area of low resistivity, interpreted by O'Connel (2003) as a deep clay filled Tertiary palaeoriver up to 2 km long and 500 metres wide. Its depth, judged by resistivity surveying was greater then 50 metres. However, the actual depth of the anomaly was not determined due to instrumental limitations (Adrian Phillips, pers. comm., 2003).

Using conservative estimates of 200 x 2,000 x 50 metres for the dimentions of the deposit, a volume of 20,000,000 m^3 of clay is indicated. Reynolds (1974) studied a large pocket deposit near Dunshaughlin County Meath and determined a density of 2.2 g/cm^3 for the pocket deposit there. Using these values, the Timahoe weathering profile comprises around 44,000,000 tons of silica-clay. The northern and the southern extent of the deposit continues beyond the surveyed area and therefore the size of the deposit is larger than indicated by remote sensing. The form of the deposit appears similar to a slot canyon i.e. it is almost as deep as it is wide (Adrian Phillips, pers. comm., 2003). The sides of the Timahoe weathering profile imaged by resistivity survey (Fig. 2.2) appear scalloped, with a similar morphology to the buried limestone karst at Sepang, Kuala Lumpur, Malaysia that was imaged by seismic refraction profiling prior to the construction of an international airport there (Twidale, 2002).

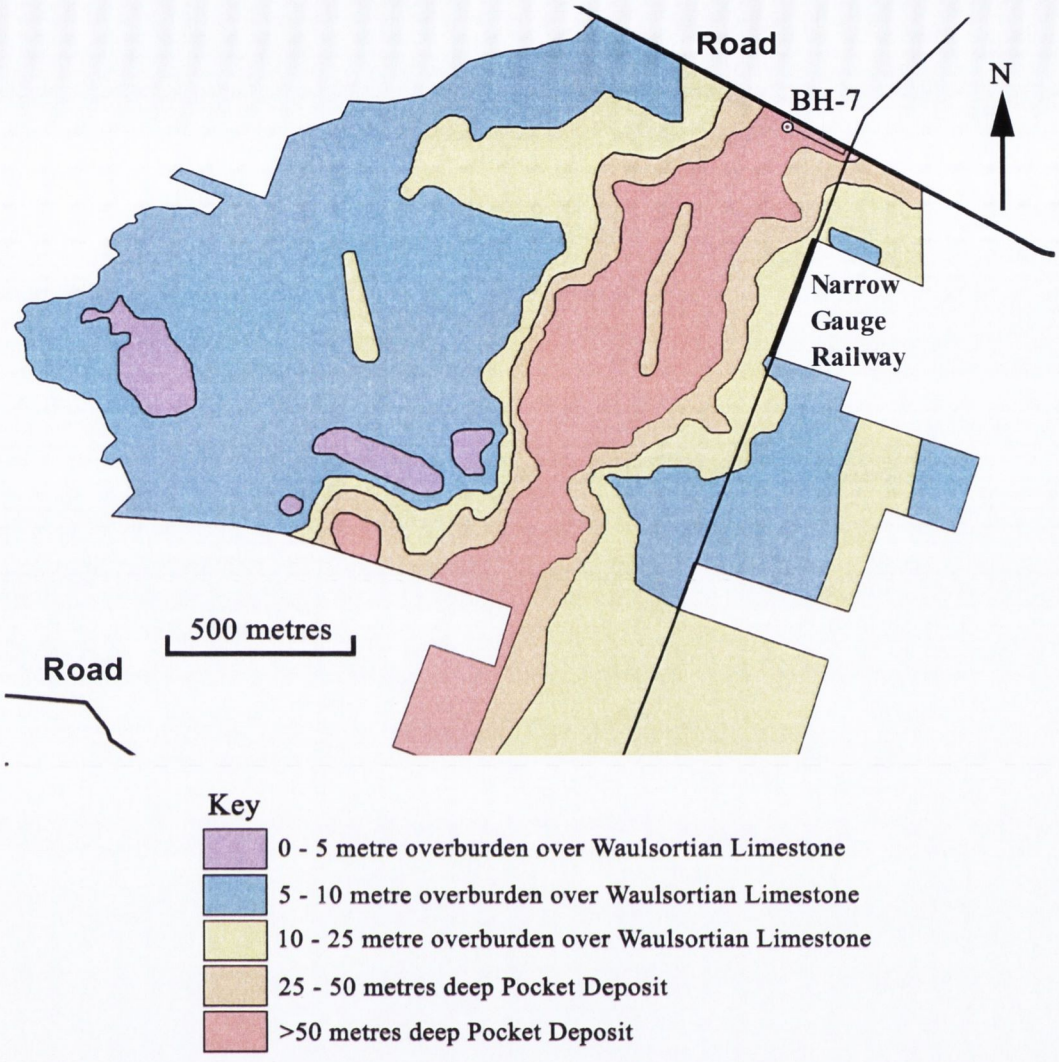

Fig. 2.2: An interpretation of resistivity survey that reveals the shape Timahoe weathering profile.

2.6 Drilling the Timahoe Weathering Profile

It was decided to drill at the centre line and assumed deepest part of the anomaly, near a public road for heavy equipment access. Drilling commenced on the 27th May and bedrock was reached on the 5th June 2003. The borehole, BH-7, was located at NGR 274784 232999, 90.1 OD. The position was measured using GPS with a horizontal accuracy of 8 metres (David Blaney, pers. comm., 2003). Present during drilling were hydrogeologist Dr. David Ball and David Blaney of TES Ltd. Drilling of the anomaly was undertaken by Birody Aquadrill Ltd., with a 505 horsepower Drilltech D40K, a former British Coal Board machine (figure 2.3) (Adrian Birody, pers. comm., 2003).

2.6.1 Drilling method

The drilling method was "down the hole hammer" (DHH) with forward air circulation (Adrian Birody, pers. comm., 2003). The DHH method uses a high-pressure air driven percussion hammer at the end of the drill-string to break ground. The air exits the hammer at high velocity and returns cuttings to the surface between the drill-string and drill hole. Water mixed with detergent was added on occasion to help raise cuttings in foam. There are limitations to the DHH method. It does not win a continuous core but only gives cuttings, and this can cause sampling bias and contamination as material can fall down the hole from above. On two occasions drilling encountered incohesive ground, and thus it was necessary to prevent a collapse by reinforcing the drill hole to a depth of 48 metres with 10-inch steel pipe and from 48 to 66.14 metres with 8-inch steel pipe. Pipe was driven down the hole with the drill rig's percussion hammer. The drill hole casing prevented contamination falling down the hole from above the depth pipe was hammered to.

Fig. 2.3: The Timahoe drill site during drilling through the dark silica-clays.

2.6.2 Sample collection

Samples were gathered at 3 feet intervals by catching the returns in sieves and basins. The returned cuttings at each interval were displayed on the ground and were inspected, bagged and labelled with the depth reached. What was thought to be interesting material was bagged separately, including possible organic remains or unusual clasts. The rows of unbagged material helped to visualise the gradual change in the character of the returns as drilling progressed.

Catching returns with sieves and basins is not ideal as sampling bias can occur. Also, because the cuttings are brought to the surface by air, larger clasts of clay and chert are not raised but can remain at the bottom of the hole until broken down to a smaller size. However, unbroken clods of clay were brought to the surface on occasion and these faithfully reflected the section drilled. Additionally, at the end of drilling the hole was flushed out with water when a high rate aquifer was struck. The flow of water brought to the surface numerous large unbroken clasts, including abundant "rotted" cherts to 10 cm and numerous ocherous fragments, including a ferricrete corona sample that will be described later.

2.7 Summary of Drilling Results

The hole was drilled to a depth of 128 metres and the results are as follows (see figure 2.4). The presumed post-glacial section began at 1.83 metres and continued to *c.* 63.70 metres depth. At first fluvial-glacial gravels, sands and clays were encountered. When dry, these were grey to yellow/brown, clayey to sandy gravels with green sandstone, limestone and a single clast of pink granite. Below were yellow/brown gravels that were wet due to a minor aquifer. At 21 metres depth, there was an abrupt transition from dry fluvial-glacial gravels to lacustrine muds. When wet the lacustrine muds were blue-black but dried to a grey-brown colour. Rare, small angular to sub-angular clasts of limestone were encountered as drilling progressed through this section.

Small white particles were noted in intact mud fragments and these crumbled to a fine white powder. They were possibly diatomaceous matter common in lake sediments. Lacustrine muds are common below peat deposits in Ireland (David Blaney, pers. comm., 2003). It is likely that the soft Timahoe weathering profile was scoured by glacial erosion and a deep lake formed in the eroded depression, not less than *c.* 25 metres deep.

After 44.2 metres depth there was a gradual return to sandy and clayey gravels. However, clast content included an increasing number of white siliceous clasts that were not seen before. There was an impression, particularly towards the base of this section, that the siliceous clasts content increased. The top of the pocket deposit is set at 63.7 metres depth, but this is an approximation. It is likely that the siliceous clasts were derived from the pocket deposit via glacial scouring. Thus the transition to pristine pocket deposit is gradual. Transition to the pocket deposit was indicated by the loss of limestone, siltstone and sandstone clasts whereas the siliceous clasts increased and the clay darkened and reddened.

Siliceous clasts were present throughout the pocket deposit but were most common in the dark silica-clays section. They were later identified as chert subjected to varying degrees of silica dissolution. Many were snow white, easily scratched and microporous. Chert clasts varied up to cobble size. Some cherts appeared to preserve original bedded contacts. None were macroscopically fossiliferous (compare with Beese *et al.*, 1983). Ferricrete fragments were also common in the dark silica-clays section. They were red to dark red brown in colour and varied in size, from flecks to several centimetres. Most were lenticular whilst a minority where rounded and these sometimes enveloped clay. Those that envelope clay are termed ferricrete corona.

There was a sudden and dramatic change to pale silica-clays at 100.27 metres depth. The chert clasts were smaller in the pale silica-clays. They averaged granule to 1 cm and appeared less weathered or unweathered with a bluish-grey colour. Many cherts were tablet shaped with surface roughening indicating subtle bedded contacts. Ferricrete was much less common, forming small flecks and rare larger fragments to 0.5 cm.

While drilling through the pocket deposit silica-clays, the drill hole did not collapse as feared (David Ball, pers. comm., 2003). A collapse occurs if more material falls down the drill hole from the sides then can be cleared by the returning air, foam or water. It appears that collapse was prevented by competent chert layers that acted as scaffolding, supporting the soft silica-clays between (David Ball, pers. comm., 2003).

Near the end of drilling, several clasts of Boston Hill Formation, initially weathered brown with a roughened texture, were returned with the pale silica-clays. But within another 30 cm of drilling, fresh bedrock was returned. A good aquifer of *c.* 10,000 gallons per hour (visual estimate by David Ball) was struck at the end of drilling. The water level settled just 3 metres below the top of the drill hole. Thus, the Timahoe weathering profile extends to just over 32 metres below sea level.

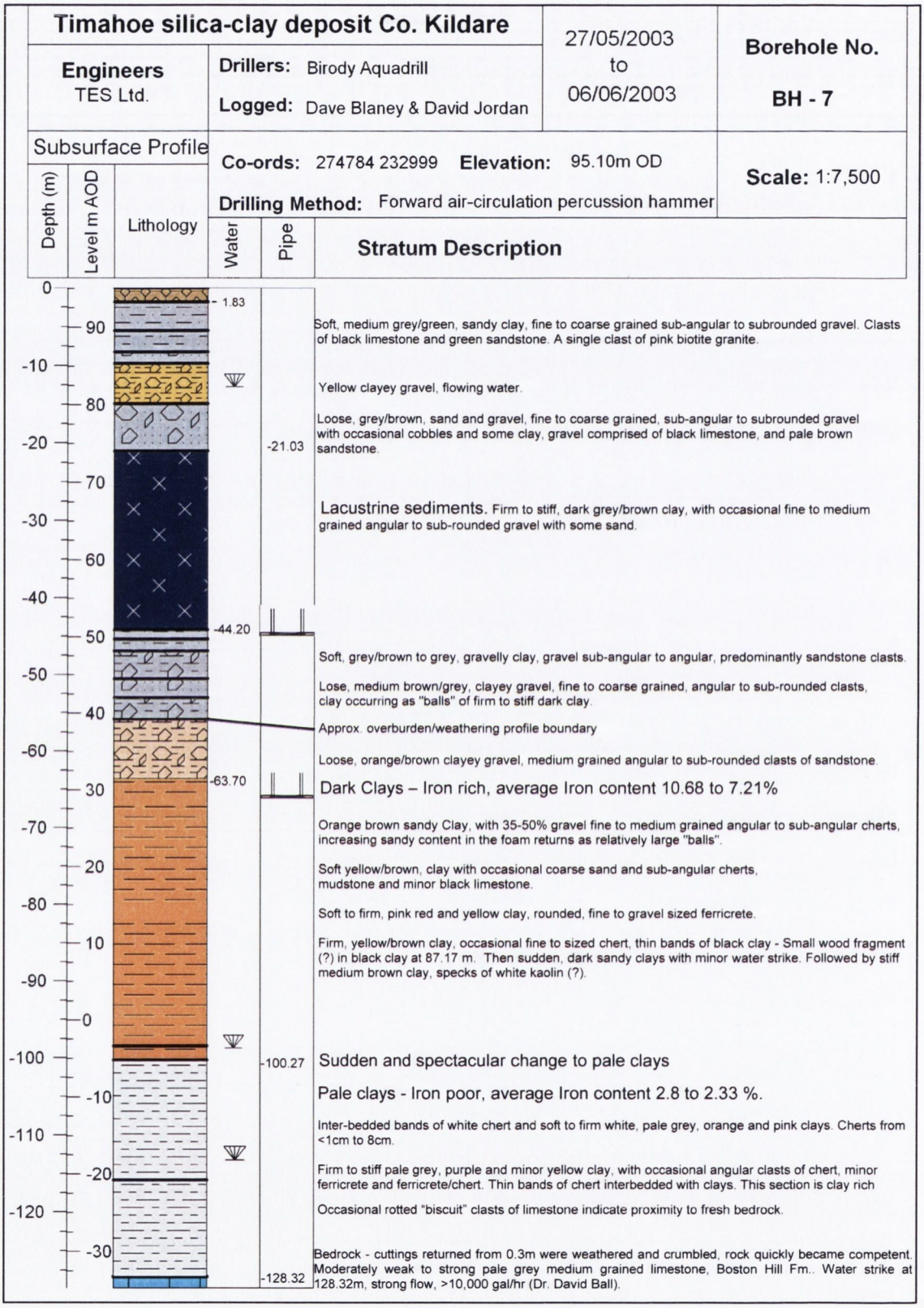

Fig. 2.4: Summary drill log for the Timahoe weathering profile encountered in BH-7. Note the sharp break from pale to dark clays and that the bottom of the Timahoe weathering profile is 33 metres below sea-level.

2.8 Analysis of the Timahoe Silica-Clays

The dark silica-clays were returned between 63.70 to 100.27 metres. The Munsell® colour of the dark silica-clays between 63.70 metres to *c.* 80 metres varied from Olive Brown (2.5Y 4/4) to Light Olive Brown (2.5Y 5/6). After *c.* 80 metres the dark silica-clays became redder, tending to towards Yellowish Brown (10YR 5/6 - 5/8) to Brownish Yellow (10YR 6/6) with wisps of red clay becoming more common towards the end of the dark silica-clays section. The red clay whips were Yellowish Red (5YR 5/6).

The light silica-clays began suddenly at 100.27 metres, suggsting a bedded or unconformable contact. Munsell® colour for pale silica-clays are Light Grey (5Y 7/2) to Light Brownish Grey (2.5Y 6/4). Occasional, small particles of conspicuous purple clay was intermixed with the predominanty pale silica-clays. The purple clay was Reddish Grey (10R 5/1).

2.8.1 XRD analysis

Two silica-clay samples were analysed using X-ray diffraction analysis (XRD). Both were 2-micron water sedimented air-dried samples, one from the dark clays section (TIM 270-82) from 82 metres and one from the pale clays section (TIM 378-115) from 115 metres.

In addition, the ferricrete corona sample was analysed (figure 2.5). The ferricrete corona sample fell down the borehole from above, so its original depth is unknown but it is likely that is was derived from the iron rich dark silica-clay section that contained numerous small red ferricrete fragments. The ferricrete corona sample was analysed by XRD bulk powder and 2 micron liquid sedimentation method.

Fig. 2.5: Ferricrete corona sample, (A) intact clast with red iron oxides enveloping a yellowish clay centre and (B) with the iron oxides removed from the clay centre.

2.8.1.1 Sample preparation

5 grams of silica-clays were placed in a 100 ml graduated cylinder with 80 ml of de-ionised water, then 20 ml 10% Calgon® dispersing agent (sodium hexametaphosphate) was added by pipette. The graduated cylinder was sealed and shaken vigorously for 15 minutes to fully disperse the silica-clays. The silica-clays were allowed to settle in the graduated cylinder for 4 hours and then an eyedropper was used to draw slurry from 3.8 cm depth. This ensured that <2 micron clay sized particles were selected for XRD analysis (Moore & Reynolds, 1989; Poppe *et al.*, 2001). The slurry was placed on a silicon slide and air-dried overnight. Silicon slides generate less X-ray fluorescence then glass slides that could otherwise obscure weak and broad diffraction peaks.

The samples were analysed with a Philips PW-1720 XRD machine at 10,000 volts and 6 milliamps with a Cu-Kα anode providing a 1.5418Å collimated X-ray source. The scan angle was between 2 and 35 degrees with a step size of 0.02 degrees and a scan speed of 1 degrees per minute. The recorded scans were recorded as a digital file and analysed with Traces v.5.0.5 by Diffraction Technology.

2.8.1.2 XRD results

The dark silica-clays, TIM 270-82 from 82 metres contains kaolinite, illite/smectite, quartz and goethite, whereas the pale silica-clays, TIM 378-115 from 115 metres contains kaolinite, illite/smectite and quartz (figure 2.6). Only the dark silica-clays contain goethite, whch is the colouring agent. Both the pale and dark clays contain micron sized quartz (figure 2.6). The outer rim of the ferricrete corona sample was composed of goethite (figure 2.7). Whilst the inner yellow clay centre was composed of micron sized silica-clay with minor goethite, a trace amount of halloysite or poorly crystalline kaolinite is suggested by a weak diffraction peak at 7.15 Å. Another peak at 4.5 Å could not be identified. There are several rare secondary minerals found in oxidised sulphide deposits that possess a 4.5 Å peak but none of these seems plausable.

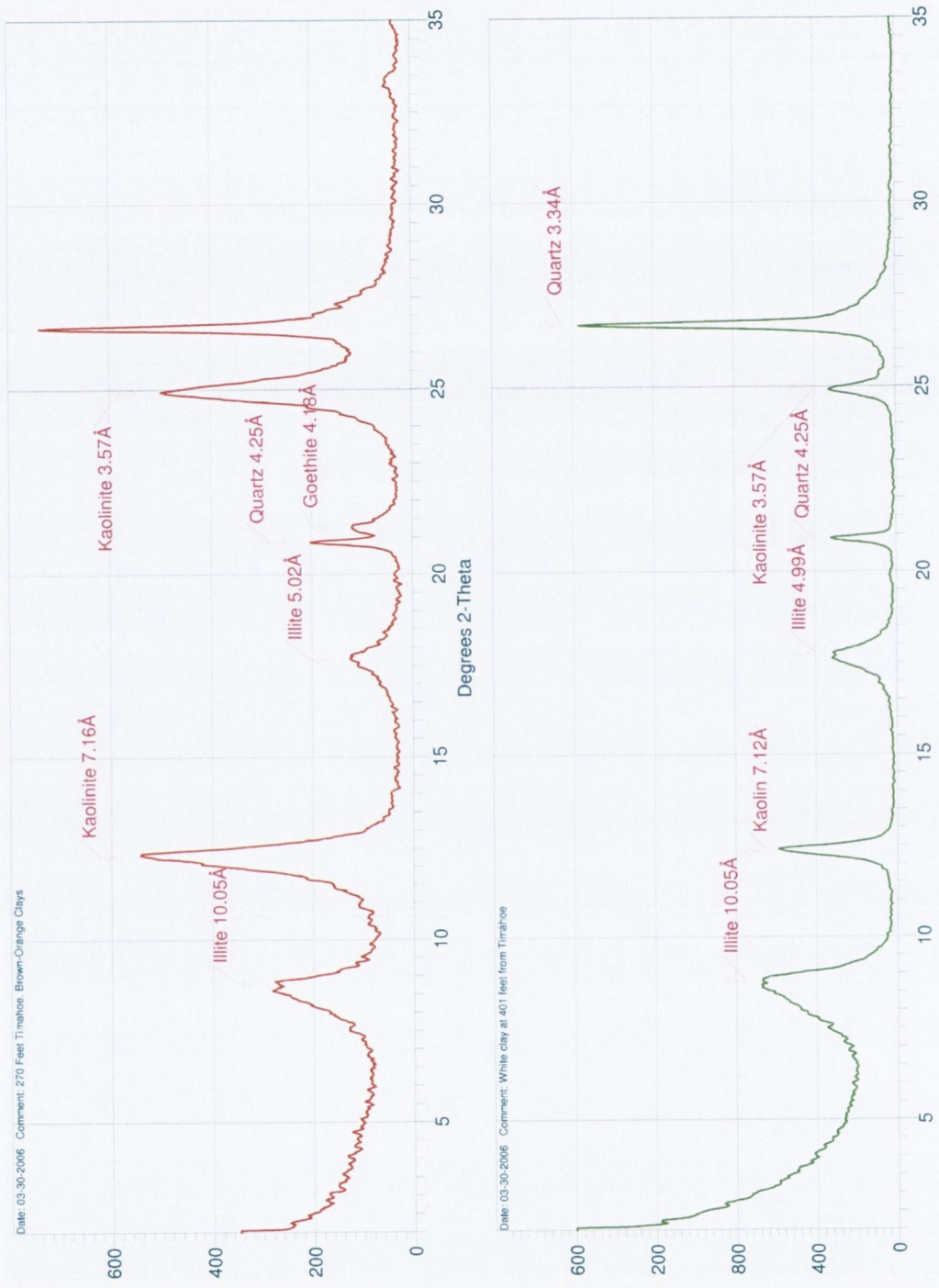

Fig. 2.6: XRD analysis results for TIM 270-82 (dark clays) and TIM 378-115 (pale clays).

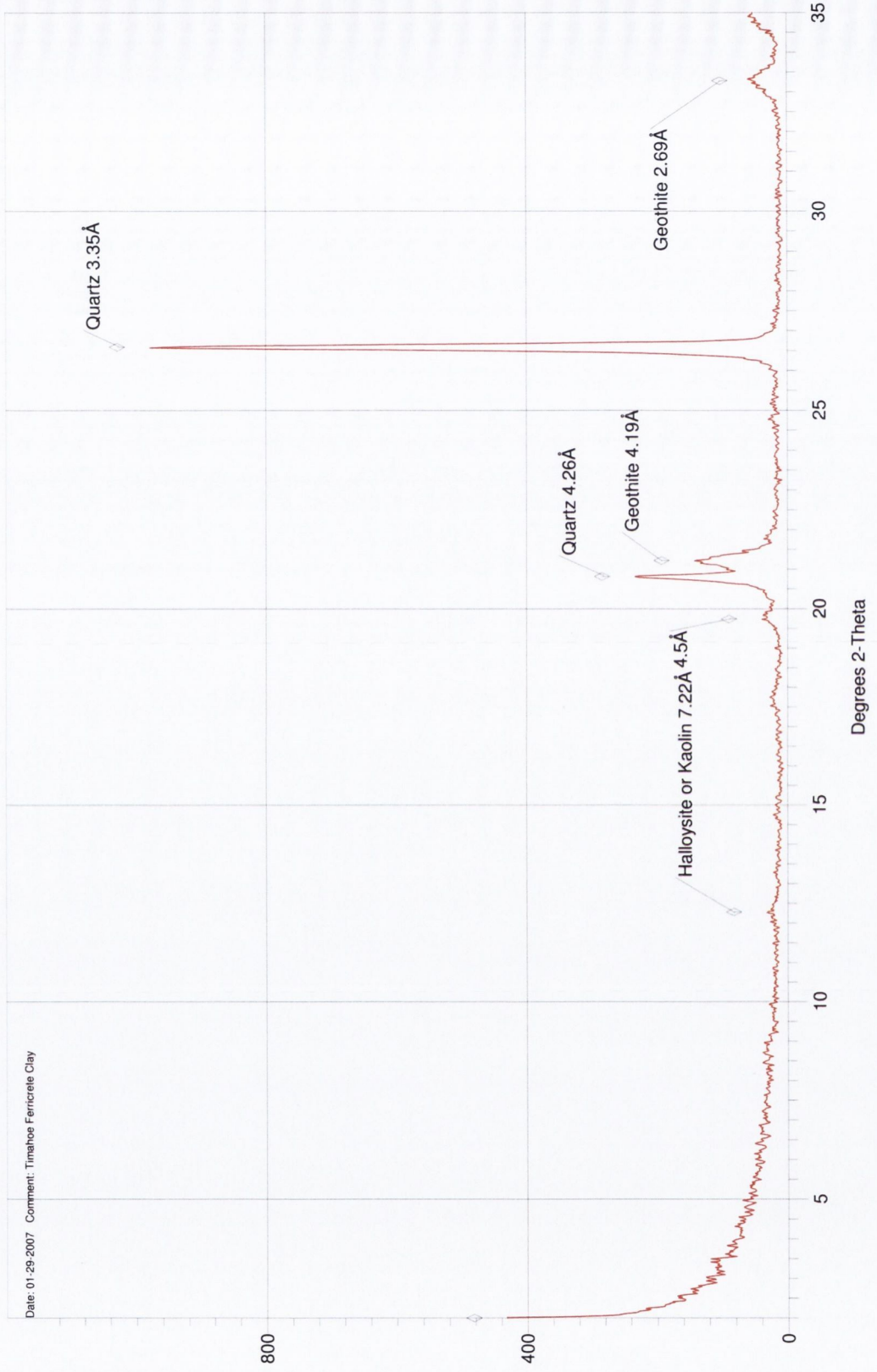

Fig. 2.7: XRD analysis results for the clays from the centre of the Timahoe ferricrete corona sample, revealing quartz, goethite and minor halloysite or kaolin. Clay mineralogy is similar to that of the dark silica clays.

2.8.1.3 Comparison with clays from pocket deposits

The silica-clay mineralogy of the Timahoe weathering profile is similar to several pocket deposits for which clay mineralogy is published. The Ballygaddy pocket deposit of County Offaly contains quartz rich clays with illite and kaolin (Beese *et al.*, 1983) and in North Wales, the Rhes-y-cae and Pant Du pocket deposits contain kaolin, illite and quartz (Walsh & Brown, 1971). Finally, the pocket deposits of the southern Pennines contain illite/mica and quartz, and a minority of samples also contain kaolin (Walsh *et al.*, 1972).

In addition, the clay sized quartz (<2 microns) detected in the Timahoe weathering profile is commonly seen in other pocket deposits e.g. the Ballygaddy pocket deposit, County Offaly (Beese *et al.*, 1983) and Dunshaughlin pocket deposits, County Meath (Reynolds, 1974). Reynolds (1974) imaged 1 to 2 micron euhedral quartz crystals in the silica-clays of the Dunshaughlin pocket deposit using scanning electron microscopy; inheritance from the dissolved lithology was suggested. Beese *et al.*, (1983) also detected abundant clay sized quartz and proposed that clay sized quartz in the Ballygaddy pocket deposit originated from the weathering of chert. Binocular microscope examination of the Timahoe silica-clays identified numerous transparent, elongated, euhedral grains of quartz averaging 0.25 mm along the c-axis. Similar macroscopic quartz was noted in the Ballygaddy pocket deposit (Beese *et al.*, 1983).

2.8.2 Geochemistry

Geochemical analysis of the Timahoe silica-clays was carried out in an attempt to determine the identity of the original, unweathered lithology. Immobile elements, elements not lost or gained during chemical weathering, are commonly used to "fingerprint" the source of Terra Rossa soils (Durn *et al.*, 1999). For this exercise, it was hypothesised that the Timahoe weathering profile was originally a shale or clay rich limestone such as Calp.

The Marine Sciences Group Samples (MSGS) shale geochemistry database and SDO-1, Ohio black shale USGS Geochemical Reference Standard, are compared (in Table 2.1) with the geochemistry of the Timahoe silica-clays (Quinby-Hunt *et al.*, 1989; Kane *et al.*, 1990). The MSGS database contains geochemical analyses of 341 shales distributed throughout the Phanerozoic; 19 of the samples are black shales from the Carboniferous of Wales (Quinby-Hunt *et al.*, 1989). Bulk and trace element geochemical analysis of the Timahoe silica-clays was carried out by OMAC Ltd. of Lough Rea, County Galway using ICP-MS for major elemental analysis and ICP multiacid for trace elemental analysis.

2.8.2.1 Sample preparation

It was decided to restrict analysis of the silica-clays to the fine fraction, <75 microns. This was achieved by wet sieving with a 75 microns sieve. Recall that as drilling progressed, it appeared that the bulk of the Timahoe weathering profile comprises clays, with occasional layers of chert. Accordingly, the geochemical analyses reflect the chemistry of the clays between the chert layers. The sieved silica-clays were collected in beakers and dried at 60°C overnight. The silica-clays were then weighed in 5 gram samples, bagged and labelled with depth in feet and metres e.g. TIM281-86. The drill rig's core barrels came in 20 foot sections, thus samples were bagged in feet, the second number is the depth in metres.

Whole-rock analyses were carried out on samples TIM281-86 and 359-109, whilst trace element analyses were carried out on samples TIM250-76, 261-80, 281-86, 301-62, 304-93, 333-101, 359-109 and 404-123 with 421-123. Samples TIM404-123 and 421-123 were combined as too little clay was obtained from individual samples. TIM250-76, 261, 281, 301, 304 and 333 were dark silica-clays, whereas TIM359-109 and TIM404-123 and Tim 421-123 were pale silica-clays. Elements determined were:

Whole Rock analysis:

SiO_2, Al_2O_3, Fe_2O_3, MgO, CaO, Na_2O, K_2O, TiO_2, P_2O_5, MnO, Cr_2O_3, Ba, Ni, Sr, Zr, Y, Nb, Sc, LOI (loss on ignition), TOC (total organic carbon), TOT/S (sulphur content)

Trace elemental analysis:

Ag, Al, As, Ba, Be, Bi, Ca, Cd, Ce, Co, Cr, Cu, Fe, Ga, Ge, Hg, K, La, Li, Mg, Mn, Mo, Na, Nb, Ni, P, Pb, Rb, S, Sb, Sc, Se, Sn, Sr, Ta, Te, Th, Ti, Tl, U, V, W, Y, Zn, Zr

2.8.2.2 Results and interpretation

The elements Ce, Ga, La, Sc, Th, Nb and Zr, less so Sr, Ti and V (Table 2.1 & 2.2) show consistent values through the Timahoe profile, suggesting that they are immobile elements. There was variation in the titanium/zirconium ratios, indicating that titanium was leached at the top of the profile where the weathering was perhaps more intense. The element Nb appeared immobile but was too close to instrumental detection limit and was not used. The immobile elements identified in the Timahoe silica-clays correspond with the immobile elements used by Durn *et al.* (1999) to determine the source lithology of Terra Rossa soils in Istria, Croatia. Also, most of the immobile elements in the Timahoe silica-clays also express a narrow range of variation in the MSGS database.

SAMPLE NO.	SiO_2	Al_2O_3	Fe_2O_3	MgO	CaO	Na_2O	K_2O	
	%	%	%	%	%	%	%	
TIM 281	67.31	12.26	**10.03**	0.44	0.25	0.08	1.06	
TIM 359	79.42	10.19	**2.8**	0.46	0.27	0.11	1.31	
MSGS Mean	N/A	14.97	5.1	1.7	2.9	0.72	3.4	
SDO-1	49.28	12.27	9.34	1.54	1.05	0.38	3.35	
	TiO_2	P_2O_5	MnO	Cr_2O_3	Ba	Ni	Sr	
	%	%	%	%	ppm	ppm	ppm	
TIM 281	0.35	0.5	**0.18**	0.012	319	304	282	
TIM 359	0.45	0.29	**0.01**	0.018	266	< 20	130	
MSGS Mean	0.7	N/A	0.05	0.02	1006	N/A	291	
SDO-1	0.71	0.11	0.042	0.009	397	99.5	75.1	
	Zr	Y	Nb	Sc	LOI	TOT/C	TOT/S	
	ppm	ppm	ppm	ppm	%	%	%	SUM
TIM 281	64	159	< 10	14	7.3	0.12	0.01	%
TIM 359	64	31	< 10	15	4.4	0.18	0.02	99.92
MSGS Mean	227	N/A	N/A	15				99.79
SDO-1	165	40.6	11.4	13.2	21.7	9.95	5.35	

Table 2.1: Bulk geochemistry for <75 micron fraction in TIM 281 dark silica-clays and TIM 359 pale silica-clays. Note the iron and manganese values in bold. MSGS mean values from Quinby-Hunt *et al.* (1989). SDO-1 is the Huron member of the Ohio Shale, a USGS Geochemical Reference Sample (Kane *et al.*, 1990).

LAB NO.	SAMPLE NO.	Ag ppm	Al %	As ppm	Ba ppm	Be ppm	Bi ppm	Ca %	Cd ppm	Ce ppm	Co ppm	Cr ppm	Cu ppm	Fe %	Ga ppm	Ge ppm	Hg ppm	K %	La ppm	Li ppm	Mg ppm	Mn ppm	Mo ppm	Na ppm
7	TIM 250	<.5	7.85	121	487	8	<5	0.3	3	60	35	79	795	10.68	6	<2	<1	0.77	54	29	0.29	2840	22	0.06
8	TIM 261	<.5	8.62	83	719	7	<5	0.37	2	81	54	96	880	9.29	8	<2	<1	0.87	76	40	0.31	2087	22	0.06
9	TIM 281	1	6.65	67	329	5	<5	0.19	3	66	25	90	527	7.63	8	<2	<1	0.87	58	22	0.29	1740	14	0.07
10	TIM 287	2	7.09	69	357	4	<5	0.19	2	68	23	92	509	7.21	8	<2	<1	0.9	60	23	0.3	1625	15	0.07
11	TIM 301	1.8	7.23	61	443	4	<5	0.22	3	66	14	90	452	8.44	8	<2	<1	0.85	60	22	0.29	1323	31	0.07
12	TIM 304	1.3	7.73	70	519	5	<5	0.22	3	66	18	87	530	9.84	8	<2	<1	0.81	60	23	0.29	1579	37	0.06
	Average	1.53	7.53	78.5	475.67	5.5	N/D	0.25	2.67	67.83	28.17	89	615.5	8.85	7.67	N/D	N/D	0.85	61.33	26.5	0.3	1865.67	23.5	0.07
	SD	0.46	0.69	22.03	139.91	1.64		0.07	0.52	7	14.52	5.73	176.29	1.33	0.82			0.05	7.55	7.12	0.01	538.27	9.01	0.01
SDO-1	Average	0.01-0.17	6.49	68.5	397	3.3	2 - <10	0.75	<2 - <10	79.3	46.8	66.4	60.2	6.53	16.8	1.3	0.19	2.78	38.5	28.6	0.93	325	134	0.28
	SD			8.6	38	0.57				7.8	6.3	7.6	9.6		1.8				4.4	5.5			21	
13	TIM 333	1.2	6.85	40	475	4	<5	0.24	2	71	14	114	428	2.33	12	2	<1	1.16	51	20	0.35	1226	30	0.1
14	TIM 404-421	0.8	7.01	57	241	4	<5	0.44	7	74	23	121	457	4.94	11	<2	<1	0.91	54	20	0.29	685	32	0.08
	Average	1	6.93	48.5	358	4	N/D	0.34	4.5	72.5	18.5	117.5	442.5	2.33	12	2	N/D	1.16	51	20	0.35	1226	30	0.1
	SD	0.43	2.66	26.44	187.83	1.77		0.24	2.41	31.63	13.13	46.95	240.19	3.81	6.06			1.01	25.49	9.87	0.34	660.96	45.83	0.11
SDO-1	Average	0.01-0.17	6.49	68.5	397	3.3	2 - <10	0.75	2 - <10	79.3	46.8	66.4	60.2	6.53	16.8	1.3	0.19	2.78	38.5	28.6	0.93	325	134	0.28
	SD			8.6	38	0.57				7.8	6.3	7.6	9.6		1.8				4.4	5.5			21	

LAB NO.	SAMPLE NO.	Nb ppm	Ni ppm	P %	Pb ppm	Rb ppm	S %	Sb ppm	Sc ppm	Se ppm	Sn ppm	Sr ppm	Ta ppm	Te ppm	Th ppm	Ti ppm	Tl ppm	U ppm	V ppm	W ppm	Y ppm	Zn ppm	Zr ppm
7	TIM 250	8	418	0.36	166	54	0.03	<5	15	<10	<5	243	<2	<5	6	1655	<5	54	411	<5	145	1086	61
8	TIM 261	<5	629	0.41	260	61	0.03	9	16	<10	<5	333	<2	<5	7	2115	8	45	337	<5	265	1188	66
9	TIM 281	7	308	0.24	152	52	0.01	6	14	<10	<5	279	<2	<5	7	2060	5	32	266	<5	157	1220	58
10	TIM 287	7	296	0.23	152	61	0.01	<5	13	<10	<5	259	<2	<5	6	2089	<5	31	256	<5	143	1003	59
11	TIM 301	7	219	0.27	200	54	0.01	<5	13	<10	<5	239	<2	<5	7	1998	<5	39	351	<5	88	945	66
12	TIM 304	<5	267	0.3	197	<50	0.01	6	14	<10	<5	231	<2	<5	7	1852	<5	48	424	<5	105	1025	65
	Average	7.25	356.17	0.3	187.83	56.4	0.02	7	14.17	N/D	N/D	264	N/D	N/D	6.67	1961.5	6.5	41.5	340.83	N/D	150.5	1077.83	62.5
	SD	0.5	148.97	0.07	41.19	4.28	0.01	1.73	1.17			37.86			0.52	177.08	2.12	9.14	70.36		61.99	108.12	3.62
SDO-1	Average	11.4	99.5	0.05	27.9	126	5.35	4.1-4.8	13.2	1.9-6.8	3.7	75.1	1.1		10.5	4257		48.8	160	3.3	40.6	64.1	165
	SD	1.2	9.9		5.2	3.9	0.44		1.5		1.2	11	0.13		0.55			6.5	21		6.5	6.9	24
13	TIM 333	11	141	0.15	137	67	0.09	8	14	22	<5	170	<2	<5	8	2571	<5	28	383	29	54	239	69
14	TIM 404-421	7	200	0.19	129	<50	0.04	<5	15	<10	<5	227	<2	<5	7	2442	<5	27	472	<5	94	558	70
	Average	11	141	0.15	137	67	0.09	8	14	22	N/D	170	N/D	N/D	8	2571	N/D	28	383	29	54	239	69
	SD	5.21	123.25	0.12	85.01	50.77	2.14	2.76	6.47	0		105.27			4.1	1469.06	3.1	18.98	171.66		50.84	495.2	55.62
SDO-1	Average	11.4	99.5	0.05	27.9	126	5.35	4.1-4.8	13.2	1.9-6.8	3.7	75.1	1.1		10.5	4257		48.8	160	3.3	40.6	64.1	165
	SD	1.2	9.9		5.2	3.9	0.44		1.5		1.2	11	0.13		0.55			6.5	21		6.5	6.9	24

Table 2.2: Trace element geochemistry for <75 micron fraction in TIM 250, 261, 281, 287, 301 and 304 dark silica-clays, and TIM 333 and TIM 404-421 pale silica-clays. The table includes SDO-1, element geochemistry for the Huron member of the Ohio Shale, a USGS Geochemical Reference Sample (Kane *et al.*, 1990).

Although vanadium is immobile in the Timahoe profile, it is variable in the MSGS database. This is because the solubility of vanadium is highly sensitive to seawater oxygen levels, redox (Holland, 1999). For the same reason, some well oxygenated soils can suffer vanadium loss (Holland, 1999). However, vanadium sorption onto goethite (if present) will prevent vanadium loss irrespective of soil redox (Peacock & Sherman, 2004). A co-variance of 0.929 between vanadium and iron in the Timahoe dark silica-clays suggests vanadium sorption onto goethite. Vanadium in the Timahoe weathering profile cannot be used to comment on past oxygen levels nor can it be compared with the MSGS database. However, the elements Ce, Cr, La, Sc, Sr, Th and Zr appear to correlate well with the MSGS database in particular (Table 2.2).

2.8.3 Nature of the siliceous clasts

Initially, the white siliceous clasts were a mystery (figure 2.8); they were in turn thought to be rhyolite, quartzite, sandstone or silcrete (Adrian Phillips, pers. comm., 2003). They are bleached, microporous and some have a distinctly low density and can be scratched by finger nail, presumbly because they are microporous.

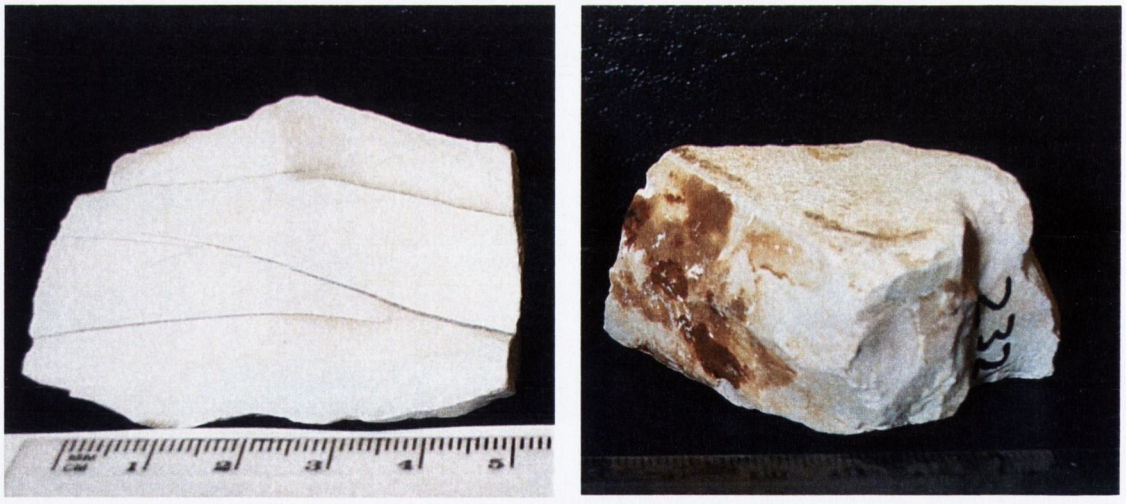

Fig. 2.8: A cut and polished rotted chert clast with thin quartz veins and a clast that preserves original bedded contacts.

Two forms of silcrete may occur in soils, pedogenic silcrete and magadiite chert. Pedogenic silcrete is a hard white siliceous precipitate that can form in intensely weathered soils in desert or semi-desert climates. However, silcrete will form at most a few layers in such soil profiles (Thiry & Simon-Coinçon, 1996). At Timahoe, siliceous clasts formed dozens of discrete layers or lenses and such was their abundance, they acted to scaffold the silica-clays and prevented the drill hole collapsing in on itself (David Ball, pers. comm., 2003).

Magadiite chert forms from magadiite (figure 2.9), a sodium rich silicate mineral that may precipitate at alkaline warm springs and lakes (Sebag *et al.*, 2001). The Dublin-Timahoe area is noted for tepid springs (Cunningham, 2000). Perhaps Timahoe was the site of an alkaline warm spring where magadiite and ferricrete precipitated, and that magadiite chert formed following the removal of sodium (Eugster, 1968).

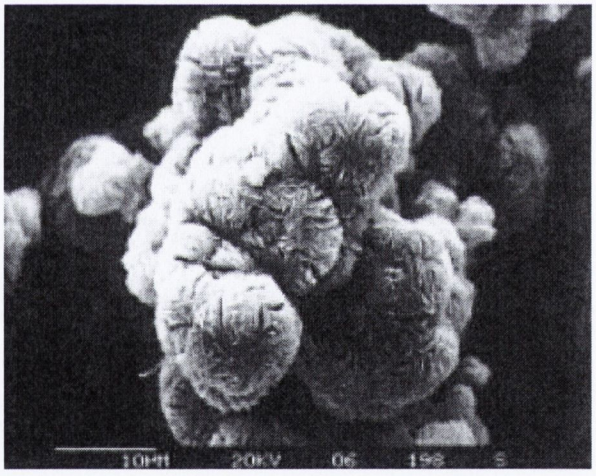

Fig. 2.9: Electron microscope view of spherical aggregates of magadiite crystals (from Eugster, 1968).

However, the formation of magadiite chert occurs via sodium loss that results in a volume decrease of *c.* 10 %, resulting in the formation of distinctive polygonal shrinkage cracks. Also, magadiite chert often contains microscopic pseudomorphs after spherical magadiite crystal "flowers" (figure 2.9). Instead, faint parallel banding is present in some hand samples and was noted in thin section. Gradually, it was appreciated that the siliceous clasts at Timahoe are Carboniferous cherts subjected to various levels of de-silicification and are the "rotted" cherts common to pocket deposits.

The interpretation as altered Carboniferous chert is further supported by these following points:

- The quartz crystallinity index (QCI) for a Carboniferous black chert and a Timahoe white siliceous clast was measured according to the procedure of Murata & Norman (1976). Both clasts have similar QCI, 2.2 for black chert and 2.75 for the white siliceous clast.

- A number of thin sections of the white and black siliceous clasts were inspected and a small number of sponge spicules were identified in both (George Sevastopulo, pers. comm., 2003).

- Several brown-grey siliceous clasts exhibit festoon texture (a millimetre scale rhythmic overlapping dark and light brown bands) a texture unique to Carboniferous chert (George Sevastopulo, pers. comm., 2003).

Thus, the siliceous clasts are interpreted as weathered Carboniferous chert i.e. "rotted" cherts. The abuntant clay sized quartz detected by XRD may have been derived from the weathering of chert, an interpretation previously made by Beese *et al.* (1983).

2.8.3.1 Formation of decomposed cherts

Rotted cherts indicate considerable silica dissolution. Silica is normally only solubile in highly alkaline conditions (pH >9) (Azaroual *et al.*, 1997; Rimstidt, 1997). However, a resolution may be found in Rodgers *et al.* (2004) who carefully studied the stepwise transformation (maturation) of geothermal sinters in New Zealand. The sinters which were originally composed of opal-A, gradually transformed in a stepwise manner to increasingly stable silica phases, ultimately forming α-quartz after several thousand years (Rodgers *et al.*, 2004). Rodgers *et al.* (2004) coined the term "mobility by metastability" to explain the phenomena. "Mobility by metastability" states that a less crystalline silica phase seeks thermodynamic equilibrium by transforming to a more stable highly crystalline phase (Rodgers *et al.*, 2004).

Importantly, during phase transformation the amount of silica in solution will remain low and silica phase change can proceed under conditions normally suppressant to silica solution e.g. over saturated conditions, neutral to acidic pH (Rodgers *et al.*, 2004). According to Rodgers *et al.* (2004), "no special geological or geochemical conditions are needed for Landmesser's model to operate". All that is required is a source and a sink that provide sufficient chemical potential to cause silica phase transformation. The dissolution of the less crystalline phase is balanced by the precipitation of the more crystalline phase (Rodgers *et al.*, 2004).

Thus, if chert has a lower crystallinity than α-quartz, chert can transform to the more stable silica phase. A rotted chert clast from the Timahoe weathering profile was measured with a CI 2.75, a slightly higher crystallinity then an unweathered chert clast - CI 2.2. The silica phase transformation may account for the clay sized quartz in the Timahoe silica-clays, silica mobilised and precipitated from chert. Finally, Rodgers *et al.* (2004) noted that carbonate can increase the rate of silica phase transformation by more than 10 fold.

2.9 Gravity Modelling and Past Palaeodrainage Studies

A basic 2-dimensional gravity simulation of the Timahoe weathering profile was produced using Gravcad for Windows® (figure 2.10). A simulated density of 2.2 and 2.0 g/cm^3 was used for pocket deposit silica-clays and 2.65 g/cm^3 for limestone, a similar density to the silica-clays of the Dunshaughlin pocket deposit, County Meath (Reynolds, 1974). The simulated pocket deposit dimensions were 300 metres wide and 130 meters deep. The aim is to model the gravity low associated with the Timahoe weathering profile, and compare the predicted gravity low with the linear gravity lows identified in Dublin Institute of Advanced Studies (DIAS) gravity data for Ireland (Readman *et al.*, 1997) that Pasquali (2002) interpreted by as possible palaeorivers.

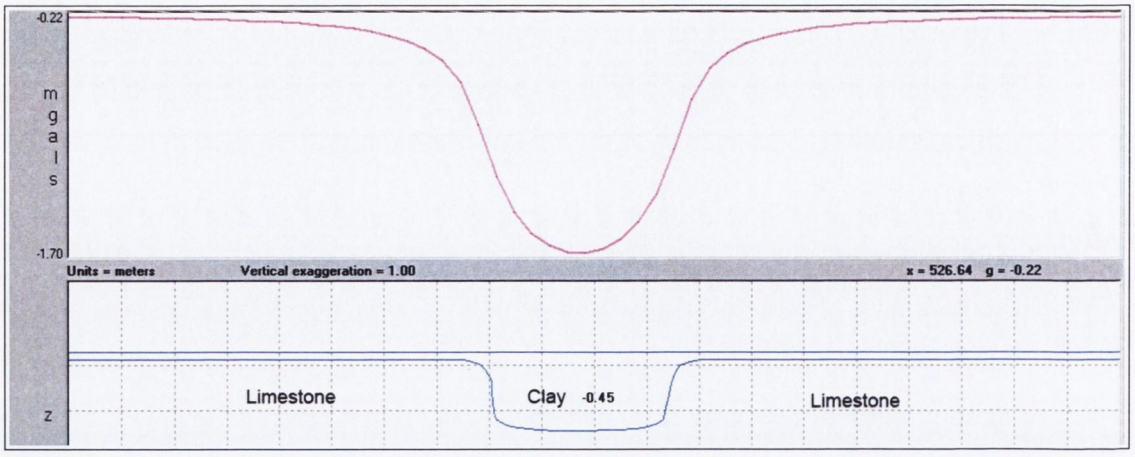

Fig. 2.10: A gravity model of the Timahoe weathering profile assuming a density of 2.2 g/cm3 for the weathering profile. The upper graph shows the predicted gravity gradient and the lower diagram is a simplified density model for the Timahoe weathering profile, that is 0.45 g/cm3 less dense then the surrounding limestone. The model predicts a maximum negative gravity anomaly of -1.7 milligals.

Gravity modelling of the Timahoe weathering profile predicts a gravity low *c.* 350 metres wide, with a maximum gravity low of -1.7 or -2.48 milligals over the centre-line of the pocket deposit, for a silica-clay density of 2.2 or 2.0 g/cm^3 respectively. Detailed gravity surveying was not carried out over the Timahoe weathering profile and the regional DIAS gravity survey uses a grid spacing that is too coarse to detect the Timahoe weathering profile's gravity anomaly. Nevertheless, the kilometre scale gravity lows seen in the Midlands of Ireland, interpreted by Pasquali (2002) as possible palaeorivers, may be larger pocket deposits on the scale of the kilometre scale Dunshaughlin pocket deposit but aligned along fault lines or lithological contrasts.

2.9.1 Relation to palaeodrainage studies

Pasquali (2002) proposed that deep depth to bedrock values in the Midlands of Ireland, particularly above lithologies typically resistant to karstification, are early-Tertiary palaeorivers. However, Pasquali (2002) did not acknowledge non-traditional mechanisms of karstification *i.e.* that pyrite oxidation may generate sulphuric acid that may be capable of dissolving impure limestones that are normally resistant to karstification such as clay rich Calp limestone and calciferous shales, a process that is described in section 2.10 below.

Pasquali (2002) delineated several linear deep depth to bedrock anomalies in the Midlands of Ireland, namely the Portarlington, Kinnegad and Kilcormac anomalies that are up to 2.6 km wide. With the aid of gravity surveying, computer modelling of predicted and actual gravity field, resistivity surveying and drilling of the anomalies in question, the three anomalies were interpreted as Tertiary palaeoriver channels rather than deeply karstified limestone. While it is agreed that Pasquali (2002) may have correctly interpreted the Kilcormac anomaly as a pre-glacial palaeoriver with a palaeo-watershed somewhere in north County Wicklow, the Portarlington "channel" appears to possess several attributes in common with the Timahoe weathering profile. In particular, the hard red clay lenses in brown/orange stiff clays found in boreholes D8 and D9 drilled in the Portarlington "channel", may be the equivalent of the orange iron-rich banded clays with ferricrete of the Timahoe weathering profile. Two pictures of iron rich banded clays from the Portarlington "channel" are included in Pasquali (2002) on page 119 of his thesis. However, one of the images is just 18 mm in width and second is only a little larger. Nonetheless, the pictures and the description of the materials encountered in boreholes D8 and D9 on Portarlington "channel" are similar to the materials collected from the Timahoe weathering profile.

Additionally, XRD analysis revealed that the clays of borehole D8 (from 26, 34, 39 and 49 metres), are mineralogically similar to the Timahoe dark clays, except for the presence of minor calcite; both contain illite/smectite (*sic.* illite), kaolin, micron sized quartz and goethite. The presence of calcite in the Portarlington "channel" clays suggests that the dissolution of limestone was incomplete.

2.10 Discussion of Pocket Deposit Formation

It will be suggested here that the Timahoe weathering profile was formed when pyrite decay caused acid dissolution of calcite (de-calcification), leaving behind an inert residuum of silica-clays.

2.10.1 Previous interpretations

Walsh *et al.* (1972) carried out 2-dimensional sandbox experiments and concluded that pocket deposits cannot form via collapse of cavern roofs, as many pocket deposits are too big. Instead, Walsh *et al.* (1972) proposed that pocket deposits form by even dissolution of limestone by laterally flowing groundwater charged with carbonic acid, at the base of a subsidence structure, in a process they termed "Basal Sapping". According to Walsh *et al.* (1972), pocket deposits form via a bottom up process whereby limestone that is gradually dissolved at depth, causes the mass of limestone above to gradually collapse into a growing depression. Walsh *et al.* (1972) suggested that pocket deposit formation requires landscape uplift, river incision and lateral ground water flow. However, the mechanism does not explain why pocket deposits are often associated with the Namurian Millstone Grits and inter-bedded Namurian sandstones and shales (Walsh *et al.*, 1972). This suggests that the causal mechanism of pocket deposit formation is not situated below a pocket deposit but above it, in the Namurian Millstone Grits, sandstones and shales.

Reynolds (1974) described the Dunshaughlin pocket deposit near Dunshaughlin, County Meath. It is a large 2 km x 0.75 km pocket deposit containing silica-clays located in limestone. The study was largely concerned with gravity surveying of the deposit. Reynolds (1974) postulated that the deposit was formed along a feather-edge. A contact between impermeable Namurian shales and limestone was envisaged were surface run-off from the Namurian shales, unbuffered by carbonate was especially enriched with CO_2 and caused focused karstification. Alternatively, Reynolds (1974) speculated that pyrite, which is common in the Namurian shales surrounding the Dunshaughlin deposit, could have oxidised and generated sulphuric acid that

accelerated karstification. This proposal was put forward by Reynolds (1974) after he observed that limestone treated with acetic acid formed clays very similar to the clays in the Dunshaughlin pocket deposit. The Namurian shales of county Meath were first described by G. Du Noyer in 1859 but since then little further work has been carried out, and their extent is poorly constrained (McConnell & Philcox, 1994). However, it is known that because of their pyrite content they weather easily and are thus identifiable by their iron oxide covered exposures (McConnell & Philcox, 1994).

Intriguingly, Chigira & Oyama (1999) described four pyritic weathering horizons in Miocene to Pliocene mudstones and sandstones in Japan, with a 1.1 to 2.2% pyrite content. In these weathering profiles, pyrite oxidation generated sulphuric acid that dissolved susceptible minerals generating an oxidised zone, an acid dissolved zone below and a dissolution front above fresh rock (Figure 2.11). At one of the profiles Chigira & Oyama (1999), the oxidised zone was 34 metres thick and the dissolved zone was 16 metres thick, giving a total weathering profile of *c.* 50 metres thick. Chigira & Oyama (1999) also stated that the clear separation between the oxidised zone and the dissolved zone can only develop in mountainous terrains with high rainfall, a situation that encourages vertical groundwater flow.

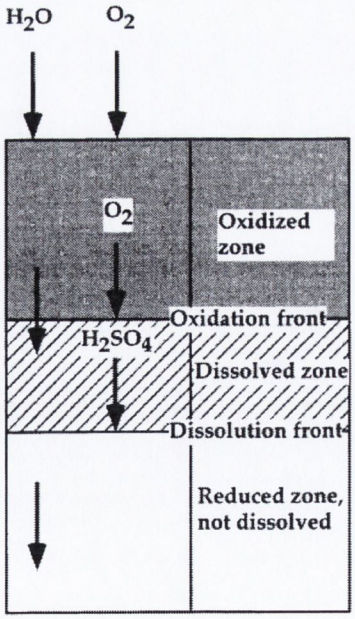

Fig. 2.11: A schematic diagram that explains the development of a pyritic weathering profile, from Chigira & Oyama (1999). Downward percolating oxygenated meteoric waters oxidise pyrite in the oxidised zone and the sulphuric acid generated dissolves rock in the dissolved zone below it.

2.10.2 Summary of formation mechanism

The proposed mechanism of pocket deposit formation herein is an extension of Chigira & Oyama's (1999) work and Reynold's (1974) suggestion that pyrite oxidation can cause calcite dissolution. In an ideal example, the oxidation of pyritic lithology at or close to the Earth's surface will generate sulphuric acid and downward percolating acidified ground waters will subsequently dissolve a soluble lithology below. The dissolution process will form a weathering profile containing minerals that are resistant to acid dissolution, encompassing an oxidised zone that contained pyrite and a dissolved zone that was pyrite free below, bounded by a sharp dissolution front (Chigira & Oyama, 1999). Acid dissolution would explain several unusual features in the Timahoe weathering profile. The iron rich dark silica-clays may have been a pyritic lithology (the oxidised zone) and pale clays that are iron poor would be a dissolved pyrite free lithology.

2.10.3 The pre-weathered state

For the reason outlined above, it is likely that the Timahoe weathering profile developed in a well drained possibly hilly landscape that encouraged vertical ground water flow. Geochemistry suggests that the oxidised zone was Calp Limestone or Namurian shale, and the identity of the dissolved zone is likely to be the Boston Hill Formation. The dark silica clays contain *c.* 8% more iron then the pale clays below, and so the extra iron may be accounted for by former pyrite. The linearity of the Timahoe deposit suggests that faulting may be involved. A similar scenario was proposed for the Ballygaddy pocket deposit, County Offaly (Beese *et al.*, 1983).

2.10.3.1 Acid dissolution and the pH attained

Geochemical analysis of the Timahoe weathering profile silica-clays indicates that sulphur and selenium (selenium is chemically similar to sulphur) might increase towards the base of the weathering profile (table 2.2). In addition, several gypsum crystals ($CaSO_4{\cdot}2H_2O$) were found in the pale silica-clays towards the end of drilling. There is little chance that these were introduced by contamination. Hammarstrom *et*

al. (2003) describe the development of $Fe(OH)_3$ and gypsum coatings on limestone grains in contact with Acid Mine Drainage (AMD) at the Friendship Hill National Monument Site, Pennsylvania, USA, indicating sulphate saturation and pH increase at the limestone grain boundaries (Hammarstrom *et al.*, 2003). Geochemistry and gypsum crystals in the Timahoe weathering profile, indicate that acid dissolution occurred down to the bottom of the pale clay section.

In regard to pH attained, the ferricrete corona sample, that is likely to come from the dark clay section, is identical in mineraology and structure to the iron oxide coated carbonate grains described by Hammarstrom *et al.* (2003). The coatings they observed only developed within a very narrow pH range of 2 to 3 (Hammarstrom *et al.*, 2003); the AMD at the Friendship Hill National Monument has a pH of 2.9 (Hammarstrom *et al.*, 2003). The Timahoe ferricrete corona suggests that local conditions, at least, were highly acidic with a pH between 2 to 3. If the corona sample is indicative of the conditions throughout the oxidised zone, then this zone probably once contained abundant pyrite and had little acid buffering carbonate.

2.10.4 The formation process

The processes involved in the production of Acid Mine Drainage (AMD) provides a clue to the possible events that created the Timahoe weathering profile. AMD involves the oxidation of sulphides, usually pyrite, that produces mine waters rich in toxic sulphuric acid and heavy metals. AMD is a major environmental concern, and accordinly it is the subject of extensive research.

The findings of Rose & Cravotta (1998) in particular are useful in reconstructing the possible events that formed the Timahoe weathering profile. In addition, Cravotta *et al.* (1999) present the pH measurements of more than 1000 coal mine AMD sites that illustrate a bimodal pH distribution of 3-3.5 and 6-6.5, an important clue to the process that causes AMD and the Timahoe weathering profile. Cravotta *et al.* (1999) describe three stages of AMD formation, they include:

Stage I

Initially, at slightly acidic or near neutral pH, pyrite oxidation proceeds via a slow, mostly inorganic and minor bacterial mediated reaction (1.1). Generated Fe(III) oxides are almost insoluble at circum neutral pH and they tend to form inhibitory coatings on pyrite that slows further oxidation. However, the habitat of *Thiobacillus ferrooxidans* and *Acidithiobacillus ferrooxidans* is limited to acidic pyrite surfaces, and these microorganisms convert insoluble Fe(III) to soluble Fe(II), permitting continued pyrite oxidation (Mielke *et al.*, 2003).

$$FeS_2 + 3.5\ O_2 + H_2O \rightarrow Fe(II) + 2\ SO_4^{2-} + 2H^+ \quad (1.1)$$

Stage II

Gradually, as generated sulphuric acid reduces the pH to 3 to 4.5, conditions that promote the growth of *Thiobacillus ferrooxidans* and *Acidithiobacillus ferrooxidans* are met. Both bacteria convert Fe(II) to Fe(III) via reaction 1.2. Fe(II) more soluble than Fe(III) (Robertson *et al.*, 2002). Fe(II) is also a strong oxidising agent that promotes further oxidisation of pyrite, reaction 1.3, even in anoxic conditions.

$$Fe(II) + 0.25\ H_2O + H^+ \rightarrow Fe(III) + 0.5\ H_2O \quad (1.2)$$

Stage III

At stage III, reaction 1.3 becomes dominant and pyrite oxidation becomes very rapid and exothermic.

$$FeS_2 + 14\ Fe(III) + 8\ H_2O \rightarrow 15\ Fe(II) + 2\ SO_4^{2-} + 16\ H^+ \quad (1.3)$$

The oxidisation of 1 mole of pyrite (120 grams) to Fe(III) releases 1546 kJ of heat (Rohwerder *et al.*, 1998). Heating of the pyritic lithology may occur (Cravotta *et al.*, 1999) and can cause thermal circulation of ground waters that facilitates further pyrite

oxidation at depth (Rose & Cravotta, 1998). The corona sample, described earlier, indicates that, at least locally, a low pH was indicative of stage III. Stage III is only attained if there is no acid neutralising carbonate (Rose & Cravotta, 1998). If carbonate is present the pH will remain above pH 4.5, insoluble Fe oxides will coat pyrite in a self-inhibitory reaction and the process of pyrite weathering will be greatly slowed (Kamei & Ohmoto, 2000)

On the other hand, stage III is self limiting. *Thiobacillus ferrooxidans* that aids pyrite oxidation is killed above 60°C (Rose & Cravotta, 1998). Only under unusual circumstances, self heating can occur to the point of combustion *e.g.* well oxygenated highly pyritic weathering profiles rich in organic materials (Cravotta *et al.*, 1999).

2.11 Conclusions

It is possible that the Timahoe weathering profile formed when oxidation of pyrite in Namurian Shale or Calp Limestone generated sulphuric acid that dissolved limestone below. The well partitioned dark silica-clays and pale silica-clays may be an oxidised and dissolved zone. If so this indicates that the Timahoe weathering profile witnessed strong vertical groundwater flow in a well drained hilly landscape. The age of the Timahoe weathering profiles is unknown, but a pre-glacial age is very likely. An age could be obtained by (U-Th)/He dating of goethite, a promising isotopic dating technique that can determine the age of goethite if it contains sufficient uranium (Shuster *et al.*, 2005).

2.11.1 Implications for landscape evolution studies

Missing section above a pocket deposit is commonly reconstructed to the Namurian level. This procedure is based on observations regarding well studied pocket deposits such as; the Bees Nest pocket deposit Derbyshire, Rhes-y-cae pocket deposit North Wales and the Ballygaddy pocket deposit County Offaly (Walsh *et al.*, 1972; Walsh *et al.*, 1999). However, some express concern that reconstructing the missing section to the Namurian level appears arbitrary and unjustified (Pete Coxon, pers. comm., 2004).

If it can be shown that a clay filled karst feature formed via acid dissolution, it could support reconstructing the lost stratigraphic section to a potential or known pyritic lithology. In the case of the Hollymount pocket deposit, the addition of *c.* 140 metres of missing section to the potentially pyritic Namurian aged Luggacurren Shale Formation may be warranted (McConnell & Philcox, 1994). Thus, the proposed level of the late-Miocene Hollymount palaeosurface by Walsh *et al.* (1999) near 210 metres OD, may be correct.

2.11.2 Implications for palaeodrainage studies

The Timahoe weathering profile was originally mistaken for a Tertiary palaeoriver (O'Connor, 2003). However, the linearity of the Timahoe weathering profile may be due to faulting or narrowly spaced parallel fractures that focused the ingress of oxygenated groundwater that facilitated deep weathering. In support of this position, faulting was similarly invoked to explain the elongated development of the Ballygaddy weathering profile (Beese *et al.*, 1983).

This study supports the view of Murphy (1966), Reynolds (1974) and Beese *et al.* (1983), that linear gravity lows in the limestone dominated Midlands of Ireland may be karstic features aligned along fault and fracture systems.

Chapter 3 – Lineament Analysis

3.1 Summary of Chapter

This chapter presents the results of lineaments analysis for the study area. Twidale (2004) stated that "Lineaments are straight or gently arcuate structural lines (faults, cleavage, folds) which, being zones of weakness find expression in the landscape". Rivers often exploit such zones of weakness and drainage patterns developed may be an excellent aid in elucidating geological structure (Hills, 1963, p. 439).

Lineaments are usually identified using subjective judgement. At best, topographic data is enhanced using a technique that accentuates linear features, then an operator hand traces features that look like lineaments. Subjectivity carries a number of serious drawbacks. Significantly there is a lack of repeatability, and no two operators will create an identical lineament map from the same topography. Thus there is a need to develop an objective method of identifying lineaments, a method that minimises subjectivity and operator error. A simple work-flow incorporating Feature Network Extraction (FNE) is developed. This is a method that automatically detects topographic lineaments. Topographic data from the Shuttle Radar Topography Mission (SRTM) and Ordnance Survey of Ireland are analysed using FNE.

It is shown that drainage patterns underlain by granite highlight faults and fracture systems, whereas areas underlain by metamorphic and sedimentary lithologies drainage patterns highlight schistosity and bedding in addition to faults and fractures. Also, two new major lineaments were discovered using FNE, namely the Billy Byrne's Gap Lineament and the Woodenbridge Lineament. The Shankill Fracture Zone, that is located close to the Billy Byrne's Gap Lineament, was visited in the field and will be described in Chapter 4 – The Cloghleagh Iron Mine.

3.2 Previous Work

Previous lineament studies of south east Ireland used Landsat® satellite imagery and aerial photographs that were examined by eye for lineaments, a subjective process (Brück & O'Connor, 1982). Over areas of impoverished outcrop, that typifies the Leinster Mountain chain, bedrock lineaments may be difficult to spot and artificial features e.g. roads, tracks and large drainage ditches, may mimic lineaments. Despite these drawbacks, Brück & O'Connor (1982) identified a number of lineaments using Landsat® satellite imagery and aerial photographs. The lineaments trend north west across the Leinster Mountains and are expressed as prominent valleys e.g. Glencullen River, the Sally Gap, Glendasan-Kings River and the Glenmalure lineaments. Brück & O'Connor (1982) proposed that the fractures were formed by tectonic stress and circulating hydrothermal fluids shortly after the final crystallisation of the Leinster Granite, concurrent with the formation of base metal vein veins. They noted that the fractures are spatially associated with hydrothermal alteration, including haematisation of microcline in pegmatites, K-metasomatism, carbonatisation of plagioclase and chloritisation of biotite (Kennan, 1978). Brück & O'Connor (1982) also indicated that the fracture system might have been reactivated during the Cenozoic.

3.3 Lineament analysis, methods and materials

An objective method of lineament detection was developed using the following data and software.

Data & Software	*Description*
SRTM-90 and OSI-50	90 and 50 m resolution Digital elevation Model (DEM)
OSI Shapefiles	Vector data from the Ordnance Survey of Ireland
ArcView 3.2a	Processing and viewing GIS data
Landserf 2.2	Feature Network Extraction of topography
Global Mapper 7	DEM viewing and (re-)projection of data
3DEM 18.7	Viewing, merging and reprojection of topographic data
GMI's batch conversion	Splits shapefiles into individual layers
Projection Utility	Datum conversion of shapefiles

3.3.1 Data quality issues in Digital Elevation Models

Digital Elevation Models (DEMs) also called Digital Terrain Models (DTMs) or Grids, are computer based representations of topography defined by a 3-dimensional array of elevation values X, Y and Z. This study used two separate elevation data sets, OSI-50 and SRTM-90. This allows the results to be cross-referenced and helps rule out inherent data artefacts. OSI-50 was provided as 20 metre resolution contour lines in DXF format by the Ordnance Survey of Ireland (OSI) in TM65 (National Grid datum) (Michael Cunningham, pers. comm., 2000) and was converted into a 50-metre resolution DEM using Topogrid (Hutchinson, 1989). OSI-50 covers most of the southern portion of Ireland.

Topogrid assumes the landscape was moulded by fluvial erosion and it accordingly attempts to create a hydrogeologically correct DEM (Hutchinson, 1989). In a hydrogeologically correct DEM, water courses find an unhindered path to rivers, ponds and lakes. This assumption may fail in glaciated terrains that are not moulded by fluvial erosion and as a result, the generated DEM may not match true topography.

SRTM-90 was acquired by the Shuttle Radar Topography Mission (STS-99) in Feb 2000 using the X-SAR instrument, a synthetic aperture synthesis Radar (Rabus *et al.*, 2003). A total of 9.8 Terabytes of mission data were received and processed, culminating in a near global DEM covering the Earth from 60° north and to 57° south. The quality of SRTM data was tested over central Asia by comparison with the Shuttle Laser Altimeter-02 (SLA-02) data and field observations (Sun *et al.*, 2003). Errors in relative vertical accuracy are more of a concern then errors of absolute vertical accuracy. Relative vertical errors are caused by thermal noise in the X-SAR receiver system and because relative vertical errors are random, they cannot be removed (Rabus *et al.*, 2003). However, relative vertical error in SRTM-90, revealed as surface roughness over the Irish Sea east of the study area, varies by +/- 4 metres. This is well within mission guidelines (Rabus *et al.*, 2003).

Another source of error in SRTM data is forest cover. Sun *et al.* (2003) compared SRTM and Shuttle Laser Altimeter-02 data, and they found that over mature Taiga forest in central Asia, SRTM data measures height at the tree canopy rather then ground level. To test for this source of error, SRTM-90 was subtracted from OSI-50 in ArcView using Map Calculator. Forested areas were identified using a Landsat®-7 image taken in the year 2000. The greatest difference in height was found in areas of high slope rather then forested areas. Sun *et al.* (2003) found a similar disparity in areas of high slope between SRTM and SLA-02 data. They attributed the error to poor performance of SLA-02; Acute laser incidence angles caused poor laser returns (Sun *et al.*, 2003). It follows that the errors in areas of high slope reside in OSI-50, not SRTM-90. If this were not the case then STRM-90 would be well outside mission guidelines.

SRTM-90 exceeds mission objectives of an absolute vertical accuracy of ±16 metres and relative vertical accuracy of ±6 metres in the study area. In addition, SRTM-90 appears to reflect true topography better then OSI-50 and it is especially detailed in areas of low relief where there are few contours for DEM construction using Topogrid. However, OSI-50 advantage resides in its superior spatial resolution. It has good detail in areas of moderate to high relief, but OSI-50 may not reflect topography accurately in restricted areas of high slope e.g. steep valley sides and cliffs.

3.3.2 SRTM and OSI-50 DEM preparation

SRTM data was obtained from a NASA website in twenty-four tiles, each tile covering 1 x 1 degree. SRTM files are in unprojected decimal degrees with height values expressed relative to WGS-84 datum. Twenty-four tiles were merged using 3DEM 18.9, forming a continuous coverage for all of Ireland. The topographic data was saved from 3DEM 18.9 as a United States Geological Survey DEM in Universal Transverse Mercator (UTM) coordinates, a popular map projection in WGS-84 datum that expresses horizontal distances in metres; file name SRTM-90.DEM. Additionally, a subset of two tiles covering only south east Ireland were merged and saved in UTM coordinates; file name SRTM-90-SE.DEM.

All the tiles that comprise Ireland are listed below, with the two tiles that cover only the study area of south east Ireland underlined:

N51W008.hgt N52W007.hgt N53W007.hgt N54W007.hgt N55W006.hgt
N51W009.hgt N52W008.hgt N53W008.hgt N54W008.hgt N55W007.hgt
N51W010.hgt N52W009.hgt N53W009.hgt N54W009.hgt N55W008.hgt
N51W011.hgt N52W010.hgt N53W010.hgt N54W010.hgt N55W009.hgt
N51W012.hgt N52W011.hgt N53W011.hgt N54W011.hgt

Additionally, OSI-50 (and all vector data) was re-projected from National Grid (NG) datum to (UTM) coordinates, so that rivers and the results of FNE could be compared simultaneously in ArcView 3.2a. The reprojection of OSI-50 from NG to (UTM) coordinates was carried out as follows:

- OSI-50 was loaded into ArcView and made active. The NG coordinates of 13 Grid Control Points (GCP), representing 13 corner edges of the DEM, were found using the identify tool and their positions were recorded; the more GCPs the more accurate re-projection.

- The GCPs were converted from NG datum to UTM coordinates using Grid InQuest 6.0 conversion utility.

- OSI-50 was then loaded into Global Mapper 7. Using the re-rectify tool, the 13 converted ground control points in NG datum were replaced with new UTM coordinates. OSI-50 was then reprojected from NG datum to UTM coordinates using Triangulation and Bilinear interpolation.

- The reprojected OSI-50 was saved as a USGS DEM in UTM coordinates using WGS-84 datum. The quality of the reprojection was tested in ArcView 3.2 by over laying SRTM-90 above OSI-50. They coincided to within 50 meters.

The reprojection of vector data in ArcView shapefile format, which includes rivers, roads, lakes, county boundaries etc., was a straightforward process. These data were re-projected using ArcView's Projection Utility. Shapefiles were reprojected to the Geographical coordinate system, GCS_WGS_84 [4326], with distance units in decimal degrees. ArcView 3.2a cannot properly handle vector data in Projected UTM coordinates.

For map construction, all elevation and vector data were projected in ArcView3.2a using the Ordnance Survey of Ireland's prescribed Irish Transverse Mercator (ITM) map projection (Bray *et al.*, 2001), whose parameters are as follows:

Projection:	Transverse Mercator
Reference Ellipsoid:	GRS80
Central Meridian:	-8° (West)
Scale on CM:	0.999 820
True Origin:	Latitude (Φ) 53° 30'
	North Longitude (λ) 8° 00' West
False Origin (metres):	600 000 W 750 000 S

GRS80 is based on WGS-84, they are coincident to the meter level (Bray *et al.*, 2001).

3.4 FNE of topographic lineaments

Feature Network Extraction (FNE) is used to identify topographic lineaments. It is a computer based approach. Rather than identifying lineaments by eye, FNE identifies lineaments automatically and objectively. FNE was developed by Fisher *et al.* (2003) and is practically applied in the topographic analysis software, Landserf 2.2. FNE builds upon more than a century of work on topographic and surface network analysis, beginning with Maxwell's (1870) seminal observations regarding the universal properties exhibited by topography, that include:

Number of Peaks = number of passes + 1
Number of Pits = number of bars + 1
Peaks are local surface maxima, they are connected to passes via ridges
Pits are local surface minima, they are connected to bars by channels

Surface Networks are a set of visual statements that describe the connections between various surface features and the nature of the lines that connect them Fisher *et al.* (2003). According to Fisher *et al.* (2003), FNE in Landserf 2.2 is biased towards identifying Surface Networks with greater linearity. Thus, FNE is particularly adept at identifying lineaments.

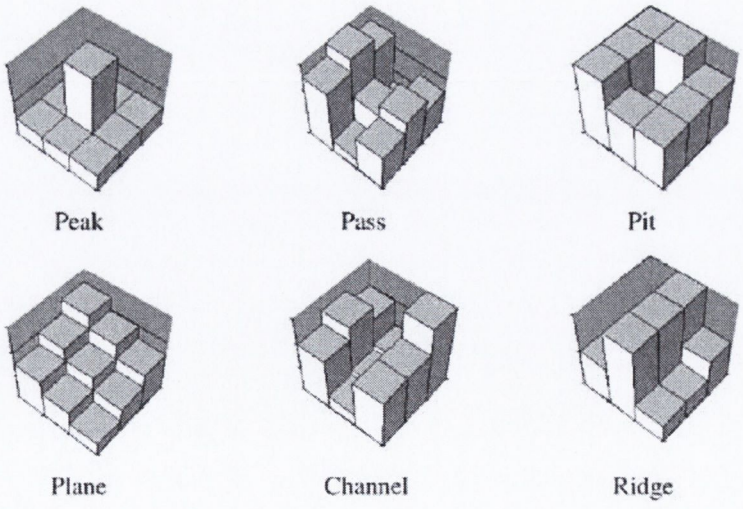

Fig. 3.1: A visual explanation of various surface features, from Fisher *et al.* (2004).

3.4.1 Feature Network Extraction in Landserf 2.2

Procedure of feature network extraction implemented in Landserf 2.2 is as follows:

Create a quadratic surface representation of the DEM

- Features of Digital Elevation Model initially identified by shape
- Fit a bivariate quadratic surface through local patch [kernel] using least squares
  - Differentiate quadratic function to identify features
  - Pits and peaks are elliptic conic sections
  - Passes are hyperbolic conic sections
- Ridges and channels are parabolic conic sections
- The size of the patch can be varied according to landscape complexity (default 3x3)

Surface Rules

- All networks have at least one pass
- A surface with one pass must have two peaks and two pits (an elementary surface)
- The entire network is assumed to be an island, bounded by a global minimum
- Any pits connected to a global minimum are a universal pit
- Pits + peaks – passes = 2

Network Generation Algorithm

- Identify morphometric pass
- Follow channel down from the pass until an edge or pit is reached
  Terminate at each pit
- Follow ridges up from pass until a pass or peak is reached
  Terminate at each peak
- Repeat for all passes
- Identify universal nodes
- Identify strongly connected nodes
- Correct all intersecting edges

3.4.2 Landserf methods

Both OSI-50 and SRTM-90 were imported separately into Landserf 2.2 as USGS DEMs. From the Configure menu, window scales of 5, 7 and 9 were tested with a distance decay of 0. A smaller values detects more features, whereas a larger value detects fewer larger features, a window scale of 5 was found to give the best resolution. From the Analyse menu, Feature Network Extraction was selected via the command Analyse Surface Parameter. After about a minute of computation, FNE results were displayed (figures 3.2 & 3.3) with the following feature types, colour and their corresponding numerical values:

Channels are Blue – 2
Pits are Green – 3
Ridges are Yellow – 4
Peaks are red – 5
Remaining surface is grey – 6

In Landserf 2.2, the values of all features except the Channels were transformed to a value of zero, using the command Raster Values under the menu heading Transform. Additionally, Channel values were transformed to a value of 20 using the same command. The modified FNE raster, containing only Channels with a value of 20, was saved as an ArcGIS text raster, file extension .grd. Global Mapper 7 was then used to convert the ArcGIS text raster to a USGS DEM; file names were OSI-50-FNE.dem and SRTM-90-FNE.dem. The files were imported into ArcView 3.2a as USGS DEMs.

The command Set Grid Value(s) to Null, provided by the United States Geological Survey GridPig ArcView extension, was used to set all the zero values in OSI-50-FNE and SRTM-90-FNE to null values. Null values are empty data and null values were set to transparent. Finally, the Convert to Shapefile command was used to convert both OSI-50-FNE and SRTM-90-FNE grids, to shapefiles. Recall that shapefiles are primarily used to store, manipulate and analyse vector data.

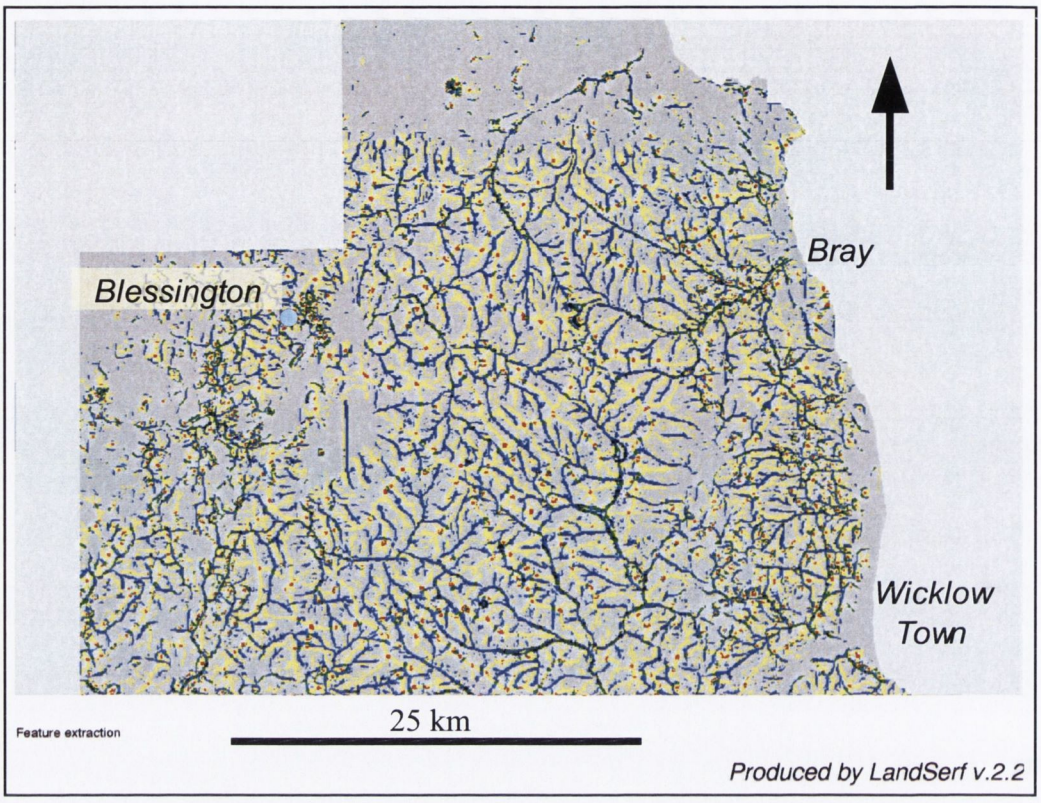

Fig. 3.2: The result of FNE on OSI-50 with a window size of 5. The Blue areas are Channels, Yellow are Ridges, Red are Peaks, Green are Passes and Back are Pits.

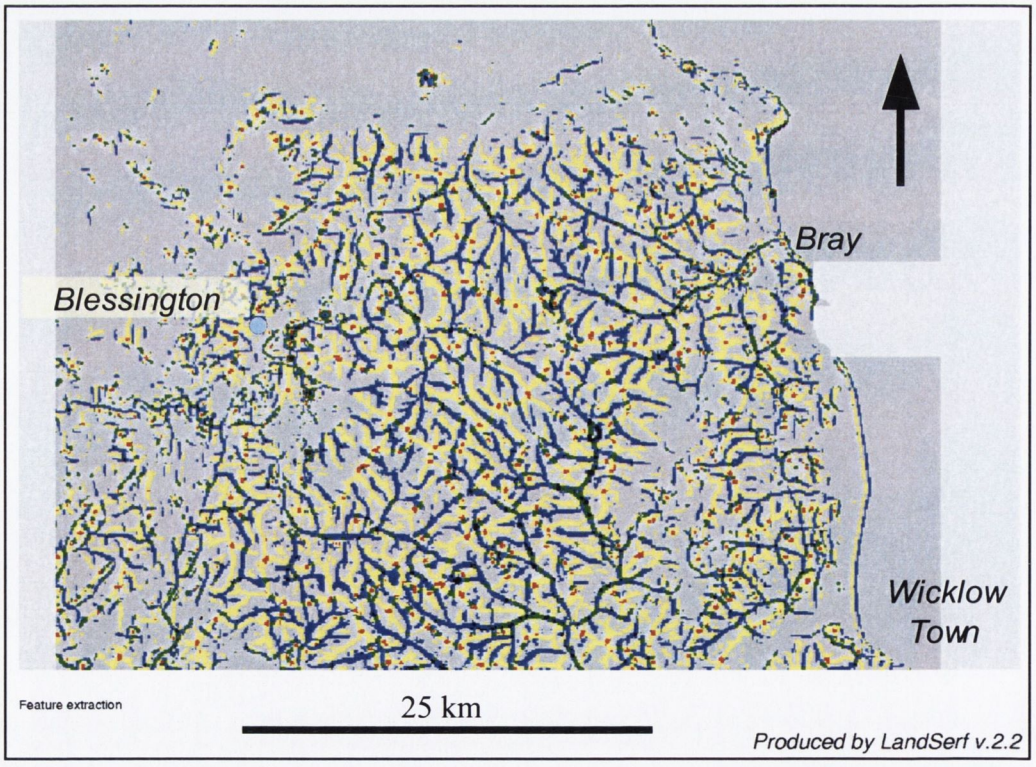

Fig. 3.3: The result of FNE on SRTM-90 with a window size of 5. There is close agreement between OSI-50 and SRTM-90. The most obvious difference is the larger (90 metre) cell size seen in SRTM-90.

3.5 Results of FNE

Feature network extraction aided the detection of two new major lineaments, henceforth referred to as the Billy Byrne's Gap Lineament and the Woodenbridge Lineament.

3.5.1 The Billy Byrne's Gap Lineament

The first lineament is a *c.* 15 km long, arcuate, convex to the east lineament (figure 3.4). It begins near The Lamb at NGR 306194 213910 and it then continues along the River Liffey and then Ballydonnel Brook. The lineament then passes through Billy Byrne's Gap at NGR 305483 207349 and it then proceeds south along the Ballinagee River. The lineament ends its journey at the Kings River, near NGR 303483 201880.

The northern extremity of the lineament coincides with the Slade Valley Fault, a major normal fault. The Slade Valley Fault parallels the Shankill Fracture Zone, *c.* 1.5 to its east (figure 3.4). The Shankill Fracture Zone (SFZ) is a hydrothermally mineralised normal fault that is up to 30 metres wide and at least 5 km long, that cuts the Leinster Granite batholith and bordering lower Palaeozoic meta-sediments (Brindley, 1971). Beginning at its northern extremity, the SFZ is first expressed as a *c.* 2 km long linear topographic anomaly extending to the granite-schist junction; drag folds in mica schist bordering the SFZ near the granite-schist junction record top down to the east motion (Brindley 1971). South of the granite-schist junction, the SFZ is expressed as a 3 km long Fe and Mn oxide mineralised quartz vein. The mineralisation was exploited by the Cloghleagh Iron Mine near NGR 305450 217115; the Cloghleagh Iron Mine will be described in detail in chapter 4. The nearby Slade Valley Fault / Billy Byrne's Gap lineament may have also channelled hydrothermal fluids. If so, the lineament may find expression in the landscape due to hydrothermal wall-rock alteration that is easily eroded.

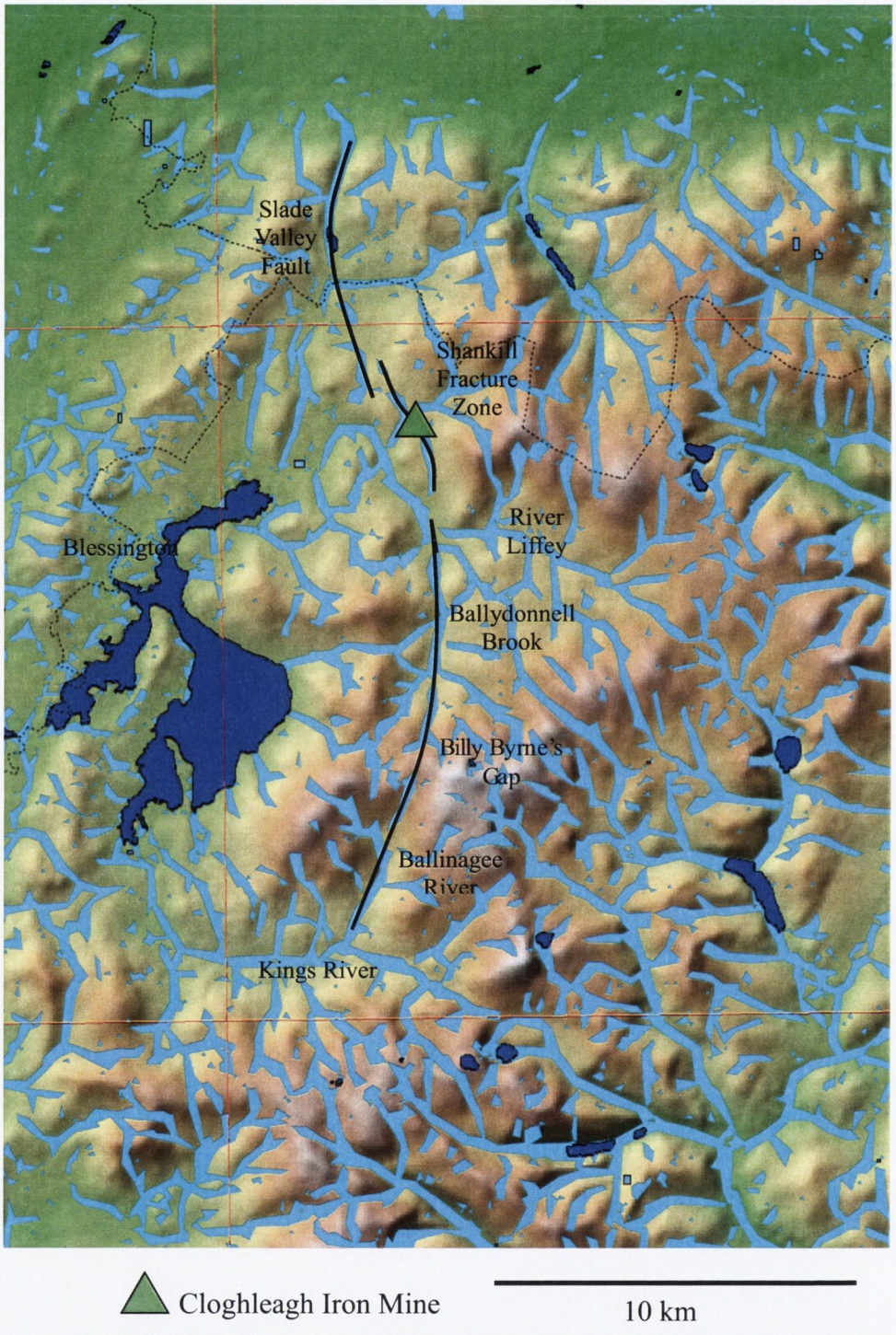

Fig. 3.4: OSI-50-FNE projected over the topography of north west Wicklow. The proximity of the SFZ and SFV to the Billy Byrne's Gap Lineament, suggests that the Billy Byrne's Gap Lineament may be an extension of the SFZ or SFV and it may find expression in the landscape due to fault hosted hydrothermal activity.

3.5.2 The Woodenbridge Lineament

The second lineament is *c.* 20 km long and also appears to coincide in part with a mapped fault, in this case the Kilmacrea Fault (figure 3.5). The lineament is also slightly arcuate, convex to the east and its northern section appears to coincide with the southern mapped extent of the Kilmacrea Fault, near NGR 323650 185386. The lineament then proceeds SSE along the Avoca River and then along the eastern slopes of Croghan Mountain. The lineament then reappears along the upper reaches of the Bann River near NGR 314019 171960 and ends at Annagh Hill. The Annagh Fault is a major NW-SE fault that trends through the Wicklow Gap in County Wexford, at NGR 310680 168962 (figure 3.5) (Mitchell, 1980).

The Woodenbridge Lineament demarcates an important drainage boundary; it separates an interior drainage area to its west from a parallel coastal drainage area to its east that flows directly to the sea. Active faulting often influences drainage pattern development; in particular normal faulting can produce parallel drainage that flows away from an active scarp front. Accordingly, the Woodenbridge Lineament may have witnessed normal faulting that produced a fault scarp with an associated parallel drainage that flowed towards the sea.

The unusual drainage of the Avoca River was discussed by Mitchell (1980). While most major rivers in the region trend NW-SE, following lineaments that trend orthogonal to the Caledonian grain, the Avoca River flows NNE-SSW and is at the centre of a centripetal drainage that developed on the Rathdrum Surface (Mitchell, 1985). The Avoca River follows the trace of the Woodenbridge Lineament, which may be a normal fault and an extension of the Kilmacrea Fault. Accordingly, the Avoca River may have initiated as a river that flowed along the foot of a fault scarp.

Fig. 3.5: OSI-50-FNE projected over the topography of south east Wicklow and north Wexford. The Woodenbridge Lineament demarcates a drainage boundary between an area of coastal parallel drainage and one of interior trellis drainage. The boundary may have originated due to tectonic activity influencing drainage development.

3.5.3 Similarity to drainage patterns

Finally, rivers of the region were placed over the FNE shapefile. The FNE was found to be in close agreement with the drainage pattern of the region (figure 3.6). However there are several notable exceptions.

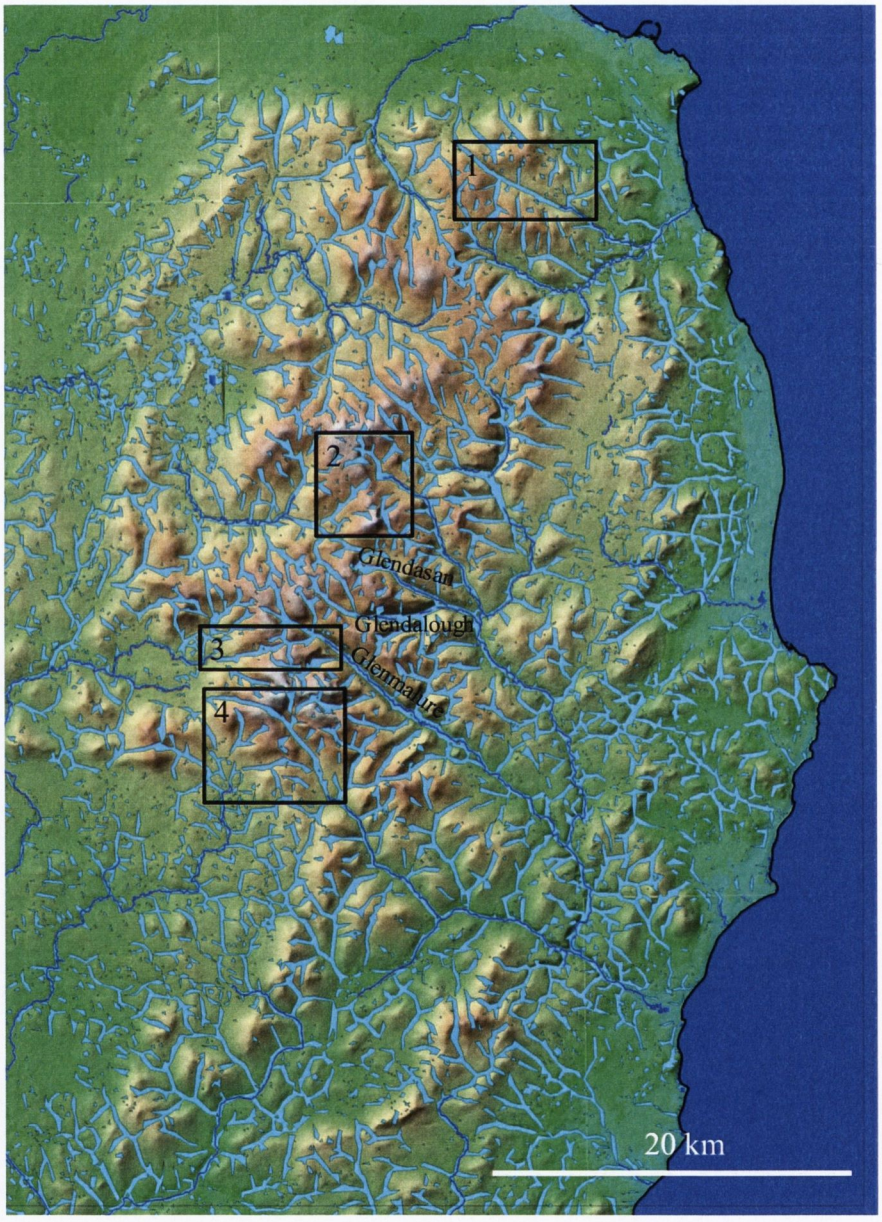

Fig. 3.6: Drainage patterns shapefile superimposed over results of FNE for SRTM-90. There is a close agreement between the region's drainage pattern and the results of FNE. Exceptions include (1) Glencullen Fracture (2) Schist Septum trending north east to south west (3) Lugnaquilla Fracture (4) Ow River Fracture, that are not occupied by drainage or contain minor streams.

Drainage patterns underlain by granite highlight faults and fracture systems that generally trend NW-SE. They are typically expressed as major fracture-controlled valleys e.g. Glencullen Valley, Glendalough, Glenmalure Valley. In areas underlain by metamorphic and sedimentary lithologies, drainage patterns seem to highlight schistosity and bedding in addition to faults and fractures.

The lineament in box 1 that tends NW-SE is the Glencullen Fracture, a fault that displays a *c.* 250 metre sinistral displacement. The valley may have formed when fluvial and glacial erosion eroded hydrothermally altered granite beside the Glencullen Fracture (Brück & O'Connor, 1982). The lineament that trends NE-SW in box 2 coincides with a *c.* 100-200 metre wide schist septum that separates the Northern Pluton from the Lugnaquilla Pluton of the Leinster Granite batholith. It is a positive topographic anomaly that stands *c.* 20-30 metres above the surrounding landscape. The lineament in box 3 that trends ENE-WSW cuts the Lugnaquilla Pluton. Here named the Lugnaquilla Fracture, it may be an unmapped fault rather then a lithological contrast. Finally, the prominent lineament in box 4 coincides with the Ow River Fracture, a fault with an unknown displacement. Brück & O'Connor (1982) expressed the view, as with the other fractures in the region, that the Ow River Fracture finds expression in the landscape due to hydrothermal wall rock alteration that was eroded by fluvial and glacial erosion.

3.6 Conclusions

There is close agreement between FNE results for OSI-50 and SRTM-90. The only exception was a slight shift in grid positions, which is an artefact of re-projection from National Grid datum to UTM coordinates. FNE automatically detects lineaments, it removes subjective bias and operator error. Also, the technique could be used by novices, because an operator does not need prior experience in lineament identification. Significantly, once the work flow is applied correctly two independent operators could each create an identical lineament map from the same topography.

FNE aided the detection of numerous lineaments in the study area. These lineaments include two previously unknown major lineaments, here named the Billy Byrne's Gap Lineament and the Woodenbridge Lineament. It is hypothesised that these and other lineaments in the study area find expression in the landscape due to fault hosted hydrothermal fluids that caused chemical alteration of wall-rocks. This hypothesis is tested in Chapter 4 – The Cloghleagh Iron Mine.

Finally, FNE largely coincides with the drainage patterns of the region, as expected. Rivers often exploit zones of weakness (Hill, 1963, p. 439). But there are several lineaments that are not occupied by drainage. One of these is a schist septum that is expressed as a positive topographic anomaly.

Chapter 4 – The Cloghleagh Iron Mine

4.1 Introduction and Chapter Summary

In the previous chapter, it was hypothesised that the faults and fractures in the study area, which control topographic and fluvial development, channelled hydrothermal fluids that caused wall-rock alteration that is liable to erosion.

This chapter describes just such a hydrothermally altered and mineralised lineament. The Shankill Fracture Zone (SFZ) is a major normal fault that cuts the Upper Liffey Valley pluton of the Leinster Granite Batholith and bordering Lower Palaeozoic meta-sediments in northwest County Wicklow. The 19th century Cloghleagh Iron Mine lies along a mineralised section of the SFZ and allows excellent access to the fault. A genetic model describing the formation of the mineralisation at the Cloghleagh Iron Mine is constructed, and is compared with similar mineral deposits abroad. Evidence shows that the Shankill Fracture Zone hosted mineralising hydrothermal fluids.

4.2 Overview of the Cloghleagh Iron Mine

The Cloghleagh Iron Mine is situated between the townlands of Knockatillane and Cloghleagh in northwest County Wicklow at 305450 217115 275m OD, some 20 km southwest of Dublin (figure 4.1). The mine is sited *c.* 30 metres from the south bank of the Shankill River. The Cloghleagh Iron Mine formerly consisted of underground workings and two open cast pits that were operated jointly by Illingworth between 1862-1868 and the Dean of Clogher between 1862-1866 (Cole, 1922).

According to Cole (1922) the ore was brown haematite (a synonym for limonite and goethite) and psilomelane (cryptomelane-hollandite) in a quartz vein cutting the Leinster Granite. The mine was not successful because the ore quickly ran out at depth (Hone *et al.*, 2002). It is likely that the ore was a superficial supergene gossan that formed by the weathering of hypogene Mn/Fe oxide mineralisation.

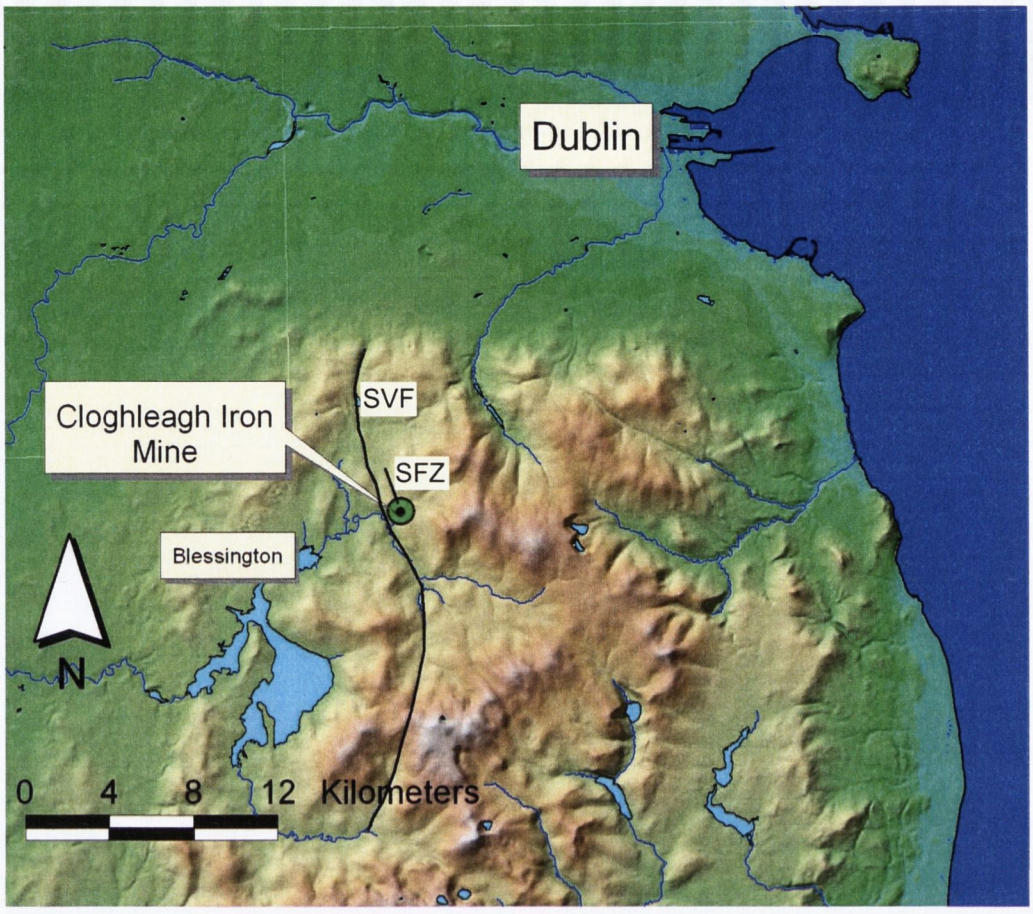

Fig. 4.1: Location map of the Cloghleagh Iron Mine (green circle). The Cloghleagh Iron Mine lies on the Shankill Fracture Zone (SFZ), which may be a splay of the longer Slade Valley Fault (SVF) *c.* 3 km to its west.

A rich pod of ore consisting of supergene fibrous and stalactitic goethite with minor cryptomelane was found in a 2 m long, 1 m deep, 0.75m wide trench, *c.* 5 metres right of the Cloghleagh Iron Mine adit (Figure 4.3). The trench was cut with a diamond wheeled petrol-powered Stihl® saw in the spring of 2004 (Stephen Morton, pers. comm., 2004). The trench allowed an excellent view of a minor fault that cuts the supergene mineralisation.

4.3 Regional Geology

The Cloghleagh Iron Mine is located in the northern part of the Upper Liffey Valley pluton on a mineralised section of the Shankill Fracture Zone (figure 4.2) (Brindley, 1971). The Upper Liffey Valley pluton is one of 5 plutons of the 1500 km^2, 405 ± 2 Ma

Leinster Granite Batholith (O'Connor *et al.*, 1989). The Leinster Granite Batholith was intruded in a series of sinistrally emplaced en echelon plutons, concurrent with folding, D2 sinistral shearing and metamorphism of surrounding abyssal flyschoid muds, slates and quartzites of the Cambro-Ordovician Ribband Group (McConnell & Philcox, 1994). The event locally marks the culmination of the Caledonian Orogeny (McKerrow *et al.*, 2000). The Cambro-Ordovician Ribband Group is divided into five formations that include - the Maulin Formation, Aghferrell Formation, Conlanstown Formation, Glencullen River Formation and the Ballylane & Oaklands Formations (undifferentiated) (McConnell & Philcox, 1994).

4.3.1 Geology of the Upper Liffey Valley pluton

The Upper Liffey Valley pluton is composed of two granite varieties - Type I and II. Type I is a fine grained granodiorite variety that is scattered throughout the pluton and is most common along the margins and its eastern flank (Brindley, 1971). An occurrence Type I granodiorite lies along the Shankill stream (Brindley, 1971) near the Cloghleagh Iron Mine. Type II variety is most common and it comprises the majority of the northern part of the Liffey Valley pluton (Brindley, 1971). It is a medium grained biotite adamellite distinguished by occasionally conspicuous K-feldspar phenocrysts (Brindley, 1971; McConnell & Philcox, 1994). Mica includes biotite and muscovite, which occasionally form small aligned phenocrysts (Brindley, 1971).

The age relationship between the two varieties is unclear, Type I appears older or younger than Type II from outcrop to outcrop (Brindley, 1971). Aplitisation is widespread over much of the Upper Liffey Valley pluton (Brindley, 1971). It involves the indiscriminate late stage alteration of Type I and II granite that overprints earlier gneissose texture, causing the loss of biotite and recrystallisation of the groundmass; the result is a paler and texturally indistinct rock (Brindley, 1971). Brindley's (1971) description is suggestive of the potassium metasomatite - episyenite, that was seen elsewhere in the study area by Kennan (1978). O'Reilly (1992) described extensive episyenite formation in South Mountain batholith of Nova Scotia, Canada, that is spatially associated with the granite hosted New Ross manganese veins.

O'Reilly (1992) proposed that K-metasomatism caused the breakdown of biotite which released manganese and iron that was precipitated in the nearby New Ross manganese veins.

Leinster Granite clasts are found in Upper Devonian clastics of the Comeragh Mountains (Capewell, 1956) and in Lower Carboniferous limestones of south County Dublin, indicating that emplacement, cooling and original unroofing of the Leinster Granite Batholith took place in less then 40 My.

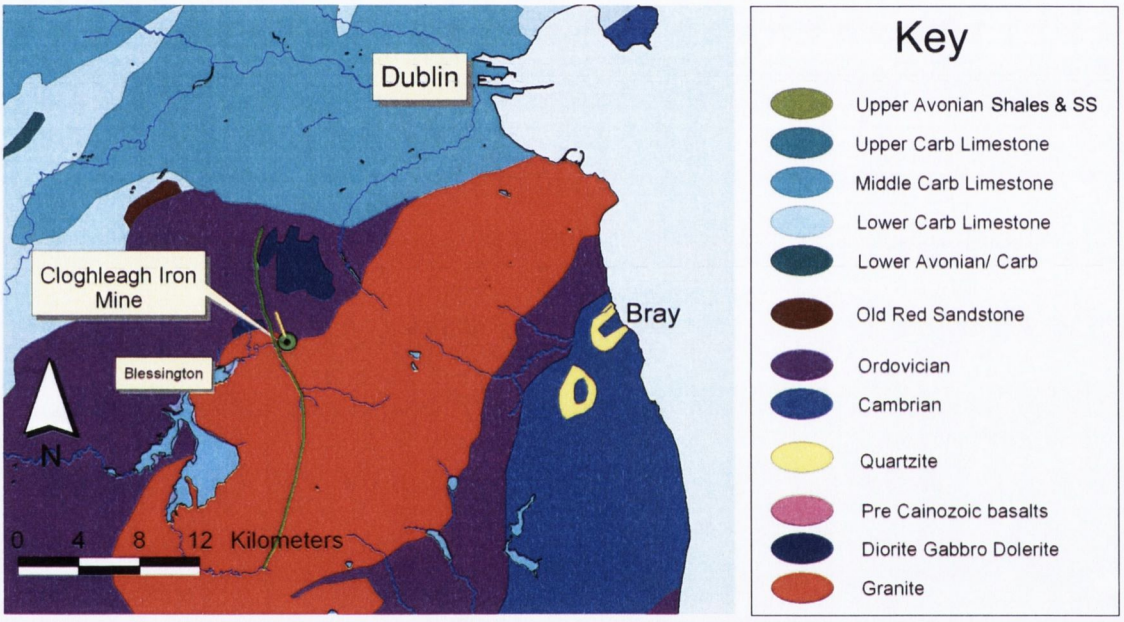

Fig. 4.2: A geological map showing the location of the Cloghleagh Iron Mine. The Shankill Fracture Zone is highlighted yellow, whilst the Slade Valley Fault and its lineament extension, is green

4.3.2 Coticule

Coticule is found in the Maulin Formation to the east and the Butter Mountain Formation to the west of the Leinster Granite Batholith. It is a quartz-mica layered psammite that is often chaotically folded, perhaps due to synsedimentary slumping or rheological contrast between layers during orogenic folding (Mühlhaus *et al.*, 2002). Coticule is distinguished by an abundance of small (*c.* 1mm) spessartine garnet [$Mn_3Al_2(SiO_4)_3$]. Occasionally the garnets form rings and these are thought to represent ghosts of deep-sea manganese nodules (Kennan, 1972).

Coticule is less abundant on the west side of the Leinster Granite Batholith, where is it occasionally found in the Butter Mountain Formation (McConnel & Philcox, 1994). For this reason, the Butter Mountain Formation is believed to be the western continuation of the Maulin Formation; its name is kept for historical reasons (McConnell & Philcox, 1994). Coticule may be the source of the manganese found in the SFZ.

4.3.3 Pb-Zn-Cu sulphide mineralisation

The eastern boundary of the Leinster Granite Batholith and its adjacent aureole rocks, contain Pb-Zn-Cu sulphide vein mineralisation that was mined for lead and zinc from the early 1800's to1953. Kennan (1978) favoured an age of 240-280 Ma for sulphide mineralisation, based on Moorbath's (1962) galena Pb isotope ages. However, Moorbath (1962) used the Holmes-Houtermans Pb isotope model that assumed a closed system with a single step derivation from primordial mantle, the U bearing source; according to Dickin (1997) "the galena method is largely discredited as a dating tool". An internet search failed to find any peer reviewed articles that used the Holmes-Houtermans Pb isotope model after 1980.

Kennan (1978) noted that the eastern aureole contains abundant coticule and speculated that metals found in the sulphide veins may have been leached from the coticule by inward, batholith directed fluid flow, during late stage cooling of the Leinster Granite Batholith. These assertions were based on stable oxygen isotope studies on granites in other countries and the spatial association between sulphide mineralisation and hydrothermal alteration within the Leinster Granite Batholith, which includes chloritisation, haematisation (the reddening of K-feldspars in pegmatites), argillisation, carbonation and episyenite generation (Kennan, 1978). Haematisation is usually restricted to the boundary of the Leinster Granite except for granite exposures along fault controlled valleys, where reddened K-feldspars in pegmatites are found, suggesting that fracture confined fluid flow pathways were centred along major valleys.

Finally, Kennan (1978) briefly mentioned the Cloghleagh Iron Mine, noting that it was the only mined mineral deposit on the western side of the Leinster Granite Batholith and he suggested that a deficiency of coticule in the western aureole could explain the lack of sulphide veins there. However, as earlier noted, coticule occurs in the Butter Mountain Formation.

4.4 Geology of the Cloghleagh Iron Mine

The Cloghleagh Iron Mine is a Mn/Fe oxide mineralised section of the Shankill Fracture Zone (SFZ) that cuts the Upper Liffey Valley pluton (Brindley, 1971). The SFZ appears to be a splay of the Slade Valley Fault (SVF), which it parallels. The southern part of the SVF connects with a major lineament, the Billy Byrne's Gap lineament, *c.* 15 km long, identified using Feature Network Extraction (FNE) in the preceding chapter. Drag folds in mica schist bordering the SFZ at the granite-schist junction record top down to the east motion (Brindley 1971). Also, the SVF sinistrally offsets the Slade Valley – Hollywood Shear Zone (SV-HSZ), a major sinistral shear zone (Max *et al.*, 1990) that just pre-dates the intrusion of the 405 ± 2 Ma Leinster Granite Batholith, in agreement with Brindley's (1971) drag fold kinematics.

Brindley's (1971) observations suggest that the SFZ near the Cloghleagh Iron Mine is a sinistral dip-slip fault or normal fault. Such fault kinematics can result in local fault dilation, fluid flow and mineralisation (Mitcham, 1974; Sibson, 1987; Sibson, 2000). There are numerous examples of hydrothermal mineralisation found along dilational sections of normal faults e.g. the Comstock Lode, Nevada, U.S.A., where the highest ore grades occur along dilational zones of curvilinear normal faults (Vikre, 1994). In addition, Brindley (1971) indicated that the SFZ right steps near the Cloghleagh Iron Mine, which could represent a dilatational fault jog. A fault jog can result in fault dilation and fluid flow (Sibson, 2000).

The Shankill Fracture Zone (SFZ), at the Cloghleagh Iron Mine (figure 4.3), is a *c.* 20 metres wide mineralised quartz reef that dips 60 to 70 degrees to the north east. The SFZ is zoned (figure 4.5) and quartz textures represented are typical of epithermal

mineralisation (figure 4.4). They include from the foot wall to the hanging wall, *c.* 10 metres of crustiform, zonal, colloform, cockade and pseudo-acicular quartz (Dong *et al.*, 1995) followed by *c.* 10 metres of manganese free and then manganese oxide rich breccias on the hanging wall side of the fault (figures 4.3 and 4.4). According to Dong *et al.* (1995) pseudo-acicular quartz forms via the pseudomorphous replacement of fibrous calcite by quartz. The crustiform, colloform and cockade quartz display rhythmic banding alternating between white and yellow/brown, perhaps due to iron oxides (figure 4.4).

The Mn poor breccia contains matrix supported clasts up to 5 cm, in a very fine grained flinty quartz matrix. The dark Mn rich breccia (figure 4.4) exhibits the same variety of textures as in the main quartz vein. The matrix of the Mn rich breccia is intriguing; bulk powder XRD and XRF identified hollandite-cryptomelane $Ba(Mn^{3+},Mn^{2+})_8O_{16} - K(Mn^{3+},Mn^{2+})_8O_{16}$ surrounding euhedral quartz crystals (0.1 mm to 3 mm). The euhedral quartz crystals "float" in the fine grained Mn oxide host; the quartz crystals do not touch each other (figure 4.6). It appears that Mn oxides precipitated rapidly from a supersaturated solution, trapping quartz crystals and other suspended materials in situ. Rapid precipitation would explain why the crystals and clasts did not settle and are matrix supported. It is interpreted as a hydrothermal breccia, formed by co-seismic explosive boiling of hydrothermal fluids in an epithermal mineral deposit (Jébrak, 1997; Sibson, 2000).

Above the adit entrance there is a manganese oxide rich breccia with subangular to subrounded clasts, indicating a degree of transport and abrasion. A loose boulder with sharply angular clasts up to 5 cm in size in a brown manganese-iron oxide host was found amongst opencast workings, c. 200 south east of the adit entrance. The sharp angularity of the clasts indicates a brief period of explosive violence and the the clasts remained close to their source (see figure 1 in Browne & Lawless, 2001).

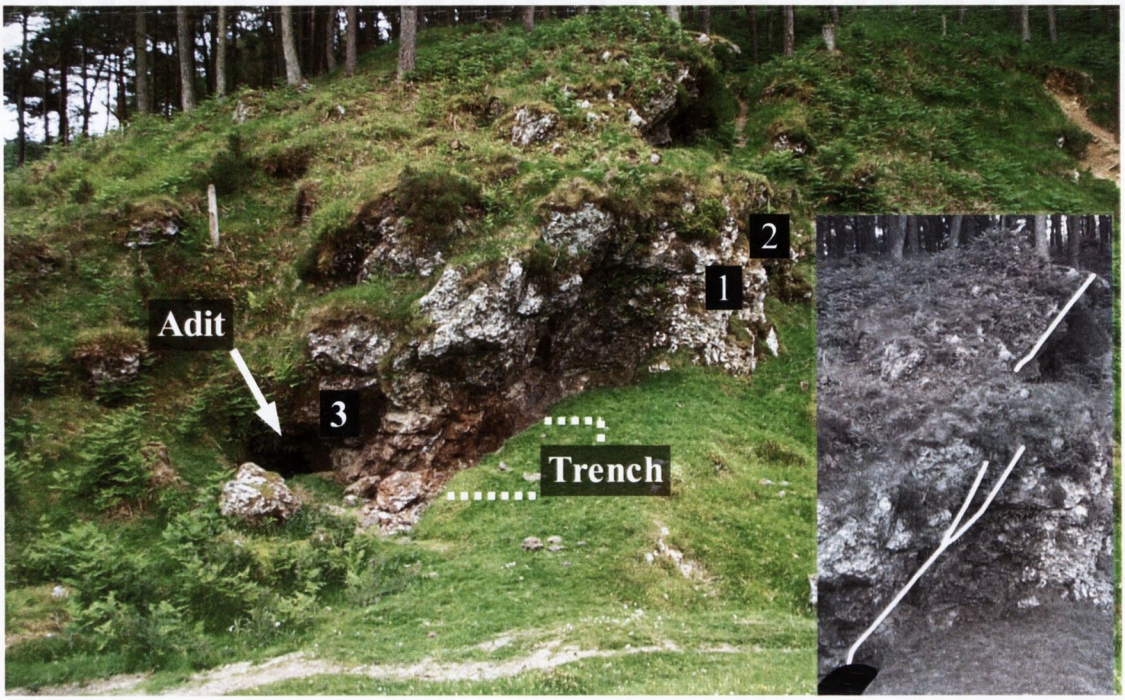

Fig. 4.3: The Cloghleagh Iron Mine looking to the south east, numbers refer to figure 4.4. A late normal fault that cuts both supergene weathering and the quartz vein is highlighted in the inset.

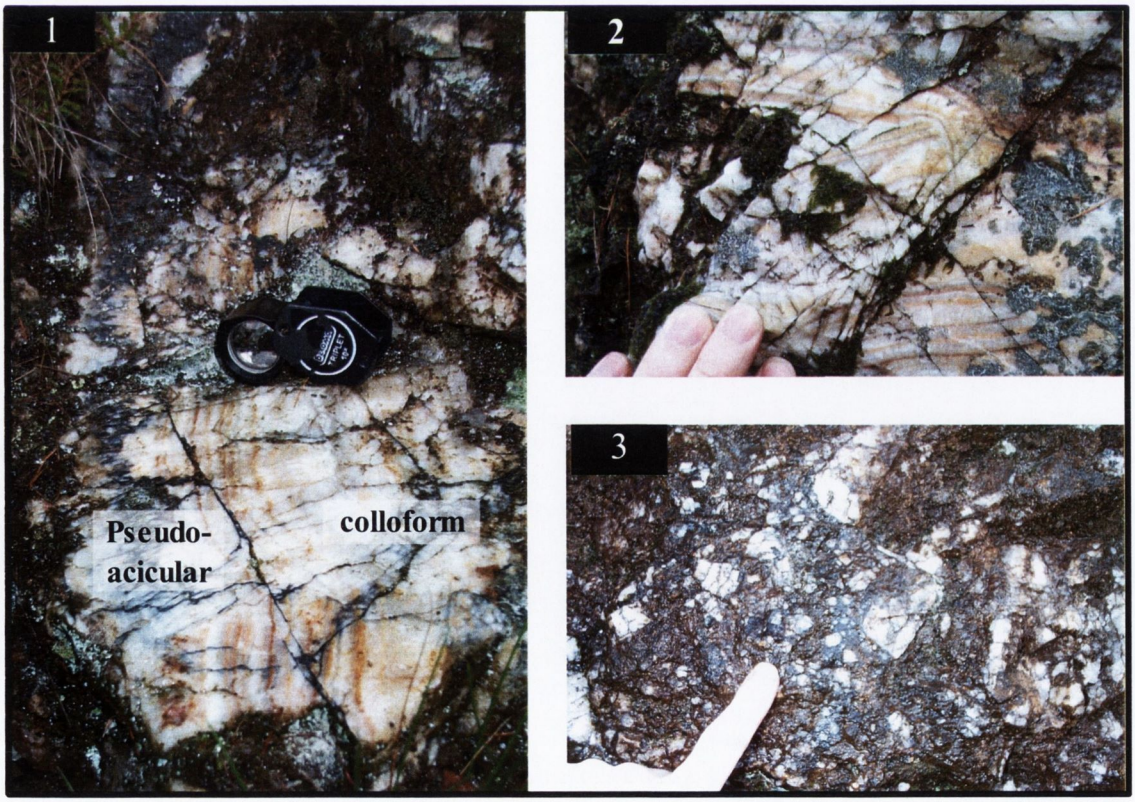

Fig. 4.4: Pseudo-acicular and colloform (1), rhythmic layered cockade breccia, note that later brittle fractures offset the mineral layering (2) and the manganese rich breccia (3). Mineralisation styles are indicative of epithermal processes (Dong *et al.*, 1995).

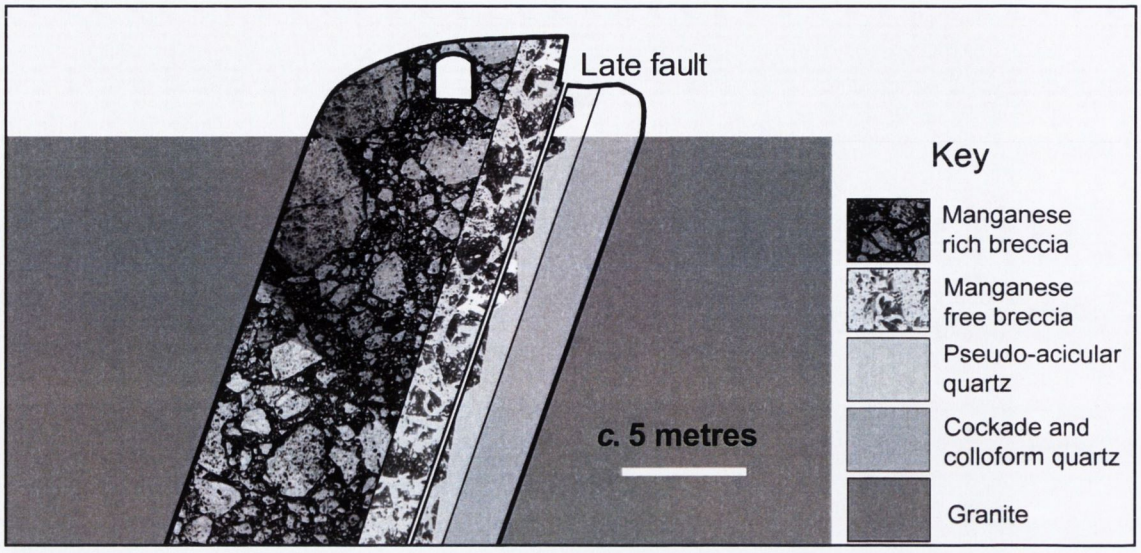

Fig. 4.5: A cross-section schematic of the SFZ at the Cloghleagh Iron Mine looking to the south east. The *c*. 20 metre wide vein is zoned - from right to left cockade, colloform, pseudo-acicular quartz, manganese free and manganese rich breccias. Note that the breccias are restricted to the hanging wall side of the fault.

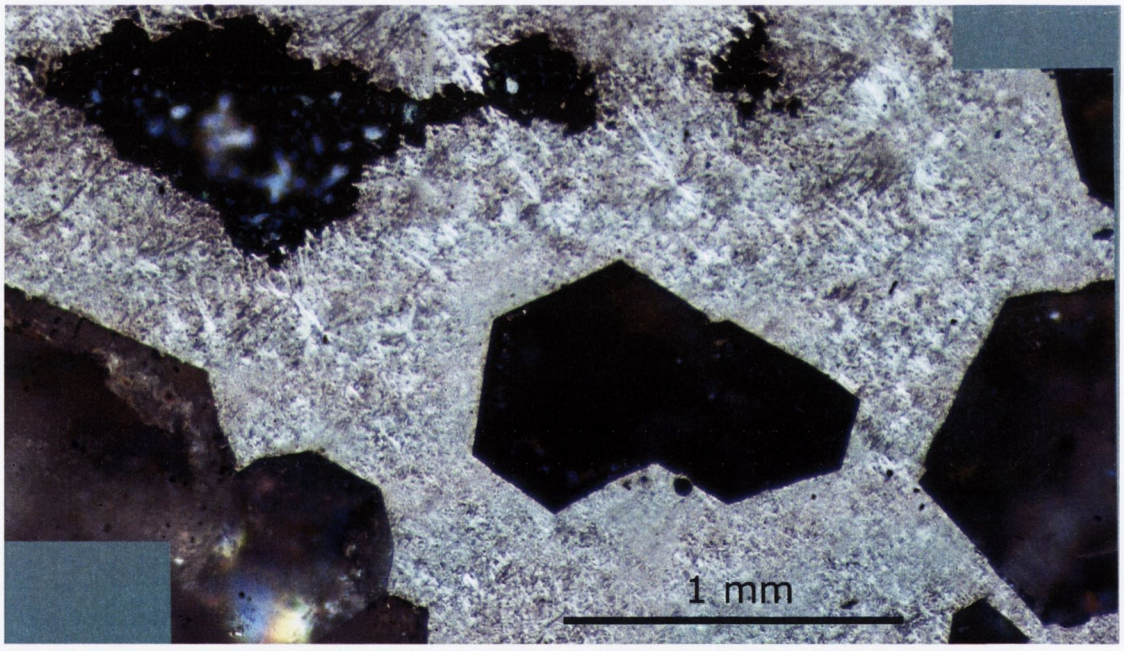

Fig. 4.6: Euhedral quartz crystals set in a acicular matrix of hollandite-cryptomelane. It appears that hollandite-cryptomelane suddenly precipitated from a saturated solution trapping the quartz crystals in situ.

The SFZ was detected on a geophysical survey (VLF-EM) *c*.1 km to the south east of the mine, where it apparently broadens into three segments; the SFZ does not die out, rather the anomaly becomes stronger (George Reynolds pers. comm., 2006).

4.5 Similar Deposits Elsewhere

The Cloghleagh Iron Mine is a vein type manganese deposit hosted in granite. After extensive collaborative investigation (Pablo Leal pers. comm., 2004), it appears that such granite hosted vein type manganese oxide deposits are very rare; only two other similar deposits were identified, namely:

- The New Ross Mn deposits, Lunenberg County, Nova Scotia, Canada (O'Reilly, 1992)
- The Sierras Pampeanas deposits, Córdoba and Santiago del Estero districts, Argentina (Leal, 2004)

Also, there are several Mn oxide mineral deposits hosted in granite in Germany and France that may be similar but a lack of information prevents a definitive judgement. In addition, there are two deposits that share a similar mineralisation style but they are hosted in quartzite or sedimentary lithologies rather than granite:

- The Romanèche Mn deposit, Rhône-Alpes, France (Hautmann & Lippolt, 2000)
- The Eisenbach district, Black Forest, Germany (Hautmann & Lippolt, 2000)
- Mn-Fe oxide veins of Arndilly, Banffshire, Scotland (Nicholson, 1986)
- The detachment fault hosted Mn oxide-barite mineralisation of the Artillery Range, Arizona, U.S.A. (Spencer & Welty , 1986)

The only English description of the Romanèche and the Eisenbach manganese deposits are two brief paragraphs of text in Hautmann & Lippolt (2000). Romanèche deposits consist of Mn-Fe-Fluorite-Barite-Quartz veins cutting the "granite des Morvan". Eisenbach manganese deposits are base metal sulphide and manganese oxide veins cutting granite. The Arndilly Mn-Fe vein (Nicholson, 1986) appears similar to the Cloghleagh Iron Mine manganese deposit, but it is hosted in a Dalradian quartzite breccia just outside the domain of a granite pluton. Nicholson (1986) proposed, based on geochemical evidence, that the Arndilly deposit is a Dubhite, a Mn oxide equivalent of a Fe-oxide gossan.

The Mn oxide-barite mineralisation of the Artillery Range, Arizona, U.S.A is hosted in detachment faults cutting sedimentary lithologies (figure 4.7) (Spencer & Welty, 1986). It is believed that the mineralisation was formed when down-welling basin brines caused K-metasomatism (episyenite generation) of basement granitic rocks along shear-zone, resulting in the release of base-metals. As hydrothermal fluids ascended along the detachment faults, sulphides were first precipitated and then at more oxidising conditions closer to the surface, Fe oxides then Mn oxides were precipitated.

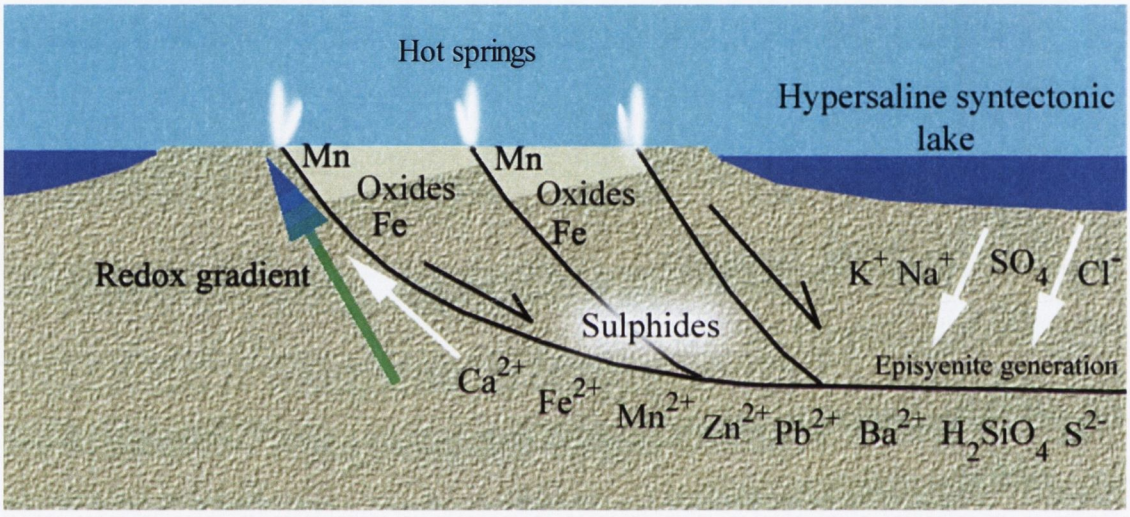

Fig. 4.7: The hypothesised mechanism regarding detachment fault mineralisation (adapted from Spencer & Welty, 1986). Mn oxides precipitate last, closest to the Earth's surface at higher oxygen fugacity.

4.6 Proposed Genetic Model

It is proposed, based on the quartz textures, the hydrothermal breccia and the presence of adularia in quartz, that the Cloghleagh Iron Mine is a low-sulphidation epithermal mineral deposit i.e. neutral pH conditions that were changing to mildly alkaline conditions due to a loss of volatiles, especially CO_2, from conditions favouring illite stability to adularia stability (Dreher *et al.*, 1998). A predominance area diagram for manganese at 200°C and 10 bar was created using the geochemical modelling software, Medusa (figure 4.8). Most probably, increased Eh (oxygen potential) was facilitated by the sudden ingress of well oxygenate meteoric water during boiling.

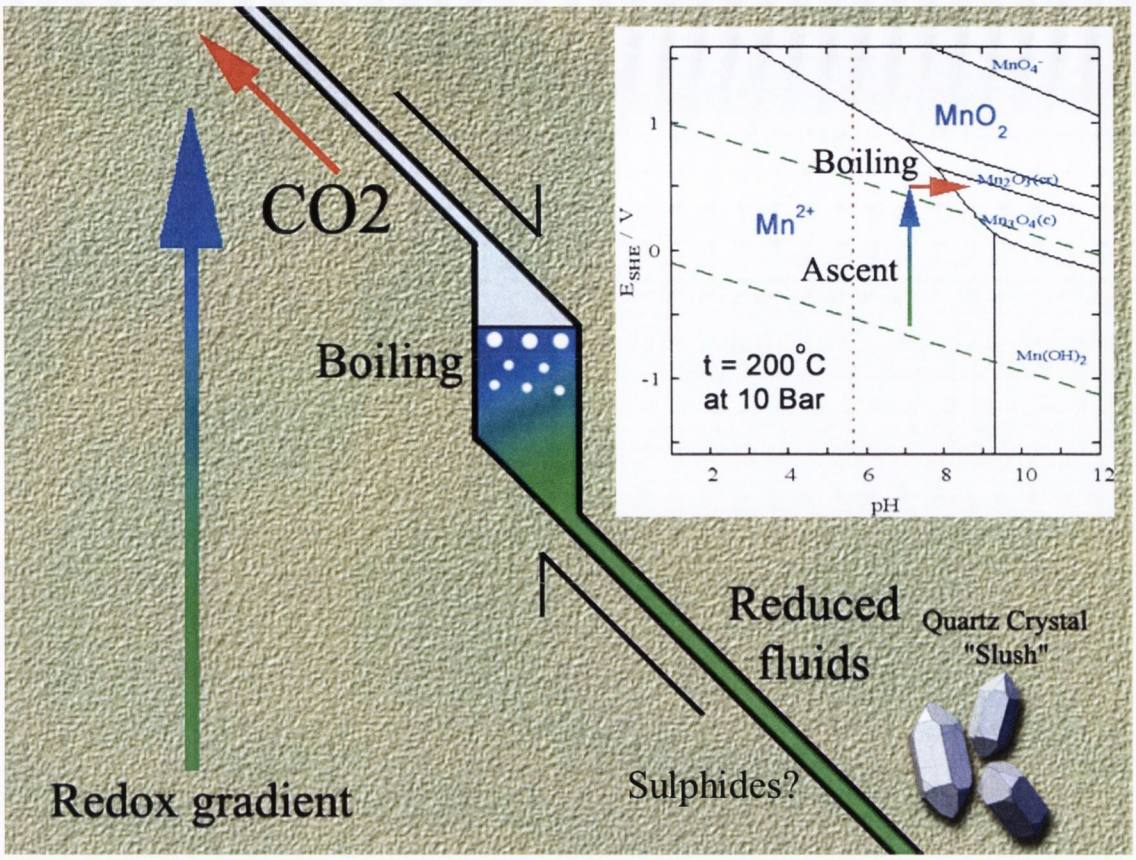

Fig. 4.8 : Illustration of the proposed scenario explaining the mineralisation of the manganese breccia. The Eh-pH predominance area diagram was generated by Medusa.

Due to seismic activity, a conduit was opened to the surface that allowed the pressure of the hydrothermal reservoir to decrease, resulting in violent boiling and brecciation within the fault zone (Figure 4.8) (Mitcham, 1974; Sibson, 2000; Browne & Lawless, 2001). Due to CO_2 loss during boiling, manganese rapidly shifts from a soluble phase to an insoluble oxide phase. This would explain the presence of euhedral phenocrysts of quartz floating in hollandite-cryptomelane; the phenocrysts were tapped from a reservoir below the dilatational fault zone, during seismic motion, and trapped in a hollandite-cryptomelane matrix that rapidly precipitated.

It is also proposed that manganese and iron were derived from the K-metasomatism of granite, not the coticule. This would agree with the observations of O'Reilly (1992) regarding the New Ross manganese deposits, which are closely associated with areas of K-metasomatism in the granite there. K-metasomatism is similarly suggested to be responsible for the generation of detachment fault hosted manganese oxides (Roddy *et*

al., 1988). It is believed that in this case, the ingress of playa lake brines into hot shear zone (*c.* 290-330°C) caused K-metasomatism of basement granite and gneiss (Roddy *et al.*, 1988).

Detachment fault hosted mineralisation, the favoured analogous model, predicts that at depth below the Cloghleagh Iron Mine there would be an increase in iron oxides, with base metal sulphide mineralisation at even greater depth. It is thus suggested, that the mineralisation at the Cloghleagh Iron Mine was contemporaneous with base metal mineralisation.

Structure, mineralisation style and analogous mineralisation, suggests that the Cloghleagh Iron Mine was formed during a period of regional crustal extension. Also, judging from vein mineralisation style and the Bissig *et al.* (2002) study of the El Indio-Pascua epithermal veins of Chile and Argentina, it is likely that mineralisation proceeded with concurrent landscape lowering. In this case, as is commonly seen in other epithermal deposits, the epithermal veins are "telescoped" and mineralisation styles belonging to different depths overlap as the boiling front is lowered. Thus, it is suggested that during mineralisation at the Cloghleagh Iron Mine the landscape was undergoing uplift and erosion. Indeed, it is thought that efficient epithermal mineralisation requires landscape lowering (Bissig *et al.*, 2002). Epithermal mineral deposits are typically restricted to the upper 1 km of the brittle crust (Sibson, 2000).

It is also likely, given the requirement for well oxygenated meteoric waters, that dry land existed above the Cloghleagh Iron Mine during mineralisation. This would agree with the requirement for contemporaneous uplift and erosion, causing the descent of the boiling front and egress of meteoric waters promoting epithermal mineralisation. In this light, it is significant that Leinster Granite pebbles and cobbles are found in the Calp Limestone of south County Dublin (Ball, 1888), suggesting that the northern part of Leinster Batholith was land and it was being eroded at this time, a period that also included the formation of base metal mineralisation in the Carboniferous limestones of Ireland (Symons *et al.*, 2002). Thus, the Cloghleagh Iron Mine may have formed concurrently with Carboniferous base metal mineralisation.

Additionally, Berner (1999) indicated that the oxygen content of the Carboniferous atmosphere may have been as high as 35%. Such high oxygen levels could have created ideal conditions for the generation of well oxygenated groundwater that aided the formation of manganese mineralisation at the Cloghleagh Iron Mine. Equally, high atmospheric oxygen levels could also explain the haematisation of the Leinster Granite (see addendum below).

4.7 Conclusions

The Cloghleagh Iron Mine is interpreted as an epithermal vein type manganese oxide deposit hosted in granite, that formed in an active fault zone <1km beneath a landscape that was above sea-level. Large quantities of hydrothermal fluids circulated throughout the Leinster Granite Batholith along the SFZ. These fluids may have also caused K-metasomatism of granite causing the release of Fe, Mn and other metals at depth. Oxygenated meteoric fluids that entered from a land-surface above aided mineralisation nearer the surface. It will be seen in Chapter 7, that platy calcite (Etoh *et al.*, 2002) and hydrothermal breccia were found amongst the Pb-Zn sulphide mine spoil heaps of Glendasan, County Wicklow, and the nearby base metal sulphide veins may be contemporaneous.

These observations agree with the hypothesis that the faults and fractures in the study area, which control topographic and fluvial development, channelled hydrothermal fluids that caused wall-rock alteration that is liable to erosion.

Addendum: Please consult enclosure at the rear of this thesis. A peer reviewed paper co-published by the author, shortly after submission of this thesis for examination, describes the Ar-Ar dating of potassium rich manganese oxides from the hydrothermal breccia that revealed a mineralisation age of 12.1±1.6 Ma (2σ). Accordingly, the Shankill Fracture Zone was seismically active during the Miocene.

Chapter 5 – The Cloghleagh Iron Mine's Filamentous Microstructures

5.1 Introduction and Chapter Summary

This chapter describes and discusses intriguing filamentous structures found in fault rock from a narrow fault that cuts hypogene breccia and younger supergene weathering at the Cloghleagh Iron Mine, County Wicklow (henceforth referred to as the late fault). The structures consist of microscopic iron-oxide coated branched filamentous inclusions in polygonal quartz. In some instances, structures resembling cells and cellular chains occur. The filaments resemble fossilised microbial life. However, the growth process known as Viscous Fingering (King, 1987), a process that generates Diffusion Limited Aggregation (DLA)-like growth (Sander, 2000), can generate inorganic structures that look remarkably like the biomorphs in question. In this chapter, both organic and inorganic origins are considered and evaluated. The criteria of Hoffman & Farmer (2000) are used to assist interpretation.

5.2 Location and Description of Sample Site

The filamentous structures were discovered in a late fault at Cloghleagh Bridge Iron Mine at NGR 305450 217115, 275m O.D.. The late fault zone is composed of an orange-brown porcelainous fault rock, *c.* 10 to 15 cm thick, that cuts both hypogene hydrothermal fault breccia and later supergene weathering that is composed of goethite and minor cryptomelane-hollandite (figures 5.1 & 5.2). Two strike and dip measurements taken along the late fault were 158/62NE and 132/55 NE (figure 5.3). A sample from the late fault was collected with the intention of finding kinematic indicators e.g. rotated survivor grains, A-C fabric, etc. Ultimately, no kinematics indicators were found in the sample from the late fault zone. However, the fault was re-examined and three slickensides were found with slicken fibres that yielded a consistent down to the northeast trend and plunge (figure 5.3), indicating that the late-fault is a normal fault.

Fig. 5.1: The Cloghleagh Iron Mine looking to the south east. The upper arrow indicates the sample location and the lower arrow indicates the trench dug by Stephen Morton.

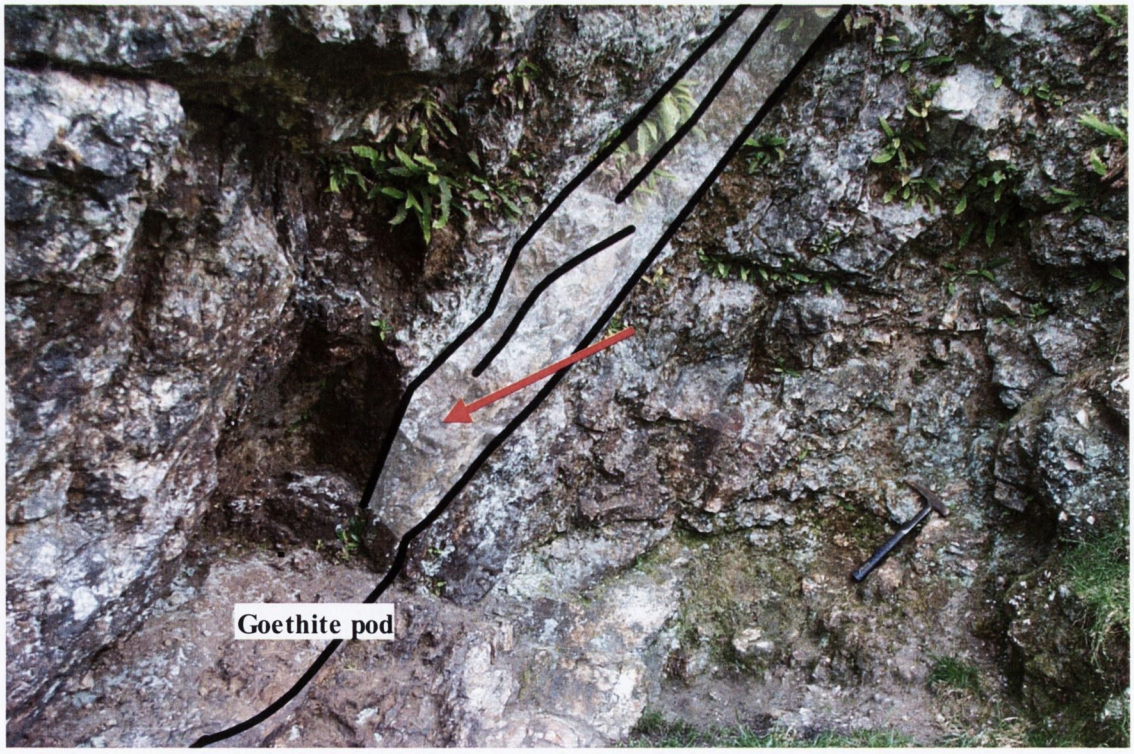

Fig. 5.2: Interpretation of the late fault. The sample was taken from the centre-line of the late fault (note the hammer to the right for scale). The trench is immediately to the lower left of the fault that cuts the goethite pod.

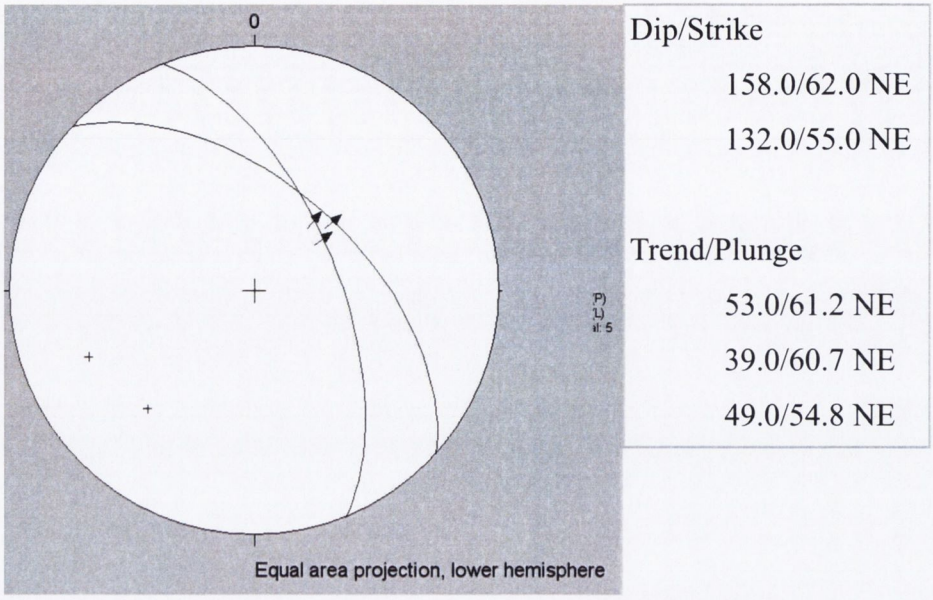

Fig. 5.3: Stereo-net diagram for the late fault, indicating normal fault motion.

5.2.1 Description of macroscopic sample

The collected sample was a 6 x 10 x 4 cm orange-brown hard porcelainous fragment of fault rock taken from the centre section of the late fault (figure 5.2). The density of the sample appears to be lower then the average for crustal rocks of 2.65 g/cm^3. The gouge may be filled with minute voids. There are occasional white fragments to *c.* 1 x 0.5 mm in matrix. Thin section analysis indicates that the white fragments may be quartz and chalcedony. Thin section analysis also indicates that the fault material is composed of quartz and Fe^{III} oxides, with iron perhaps derived from the adjacent goethite rich supergene weathering. If so, the late fault may post-date the supergene weathering as well as the hydrothermal breccias or the late fault may coincide with an episode of supergene weathering. If the latter is the case, late faulting may have developed rich pods of secondary minerals by causing brecciation of the main outcrop and opening voids via dilation.

Although the fault gouge is cohesive, it is likely, for reasons to be detailed later, that it was originally composed of silica gel (an amorphous silica rich fluid) that rapidly transformed to solid opal and eventually quartz (Rodgers *et al.*, 2004). It is not necessary to invoke burial and heating. The collected gouge sample was cut into 3 pieces and 3 thin sections were made from these.

5.2.2 Thin section description

The first thin section was over-thick, at 100-150 μm. The initial view under plane-polarised light at low power was of a nondescript turbid orange-brown matrix with occasional black opaque sub-circular "grains" 25 to 100 μm in diameter with fretted outlines, possibly made of manganese oxides or haematite (figure 5.4). Occasional non-strained transparent polygonal quartz and rarer fragments of finely granular chalcedony up to 100 μm in diameter, possessing a sharp outline set against matrix, are dispersed throughout the slide. Judging from the colour of the thin section and the association with goethite rich supergene weathering, the orange-brown matrix may be composed of colloidal iron oxyhydroxide, possibly goethite. Notably, in *c.* 20 separate areas of the thin section, enigmatic filamentous structures were found. Most of these form dense networks of dark brown, 2 to 10 μm in diameter branched and unbranched filaments set in transparent un-strained quartz.

The finest examples are found towards the edge of the thin section covers *c.* 0.33 x 0.2 mm; these filaments are 2 to 4 μm in diameter (see section 5.4). Two more thin sections were made to the standard thickness of 30 μm. Although these thin-sections were too thin to conveniently observe the filamentous structures in 3-dimensions, they were useful for mineral identification. Other than very fine colloidal, orange-brown limonite/goethite that colours the bulk of the matrix, the only other minerals present appear to be quartz, rarer chalcedony fragments and subrounded fretted-edged opaque grains, that may be manganese oxide or haematite (figure 5.4). The opaque grains are bluish and submetallic in reflected light and are seen in hand sample with a hand lens. Gugger & Hoffman (2004) reported similar opaque grains in the samples they examined from the TAG submarine hydrothermal field near the central mid-Atlantic, that they interpreted as opaque manganese oxides. On the other hand, the opaque grains may be haematite derived from frictional heating and dehydration of goethite (Gualtieri & Venturelli, 1999; Catling & Moore, 2003).

5.3 The Filamentous Microstructures

Loose to densely anastomosed and branched networks of iron oxide coated filaments are set in coarse polygonal quartz. The filaments are about 2 to 4 μm in diameter and are coloured amber to brown; the thicker filaments are darker. The filaments are not restricted to quartz grain boundaries but are true inclusions within quartz. Many filaments ignore quartz grain boundaries and pass unhindered from one grain to the next. Clearly the filaments are antecedent to the quartz. In some areas, the filaments appear to be roughly aligned, seemingly in response to a former flow direction. On careful observation, the filaments maintain full development within the amorphous orange-brown matrix. Filament diameter measurements are presented in section 5.5. Most filaments appear to be coated with a thin layer of brown-orange Fe-oxides that at high magnification appear to form a rough textured, frilled coating.

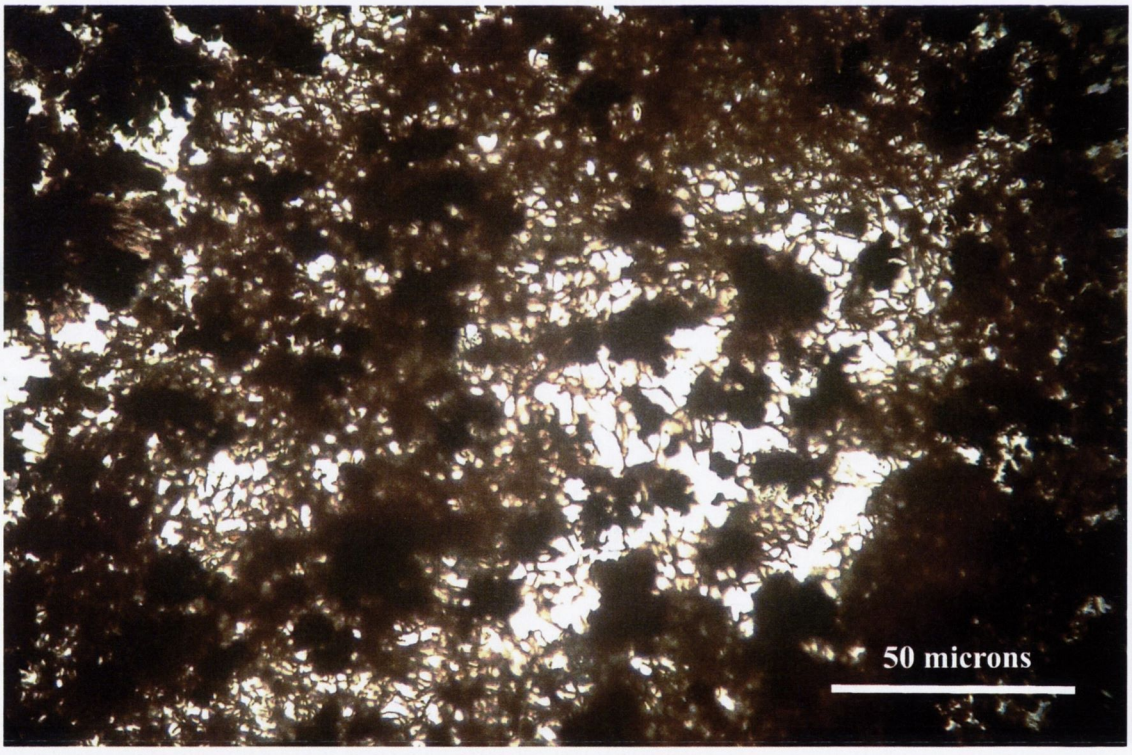

Fig. 5.4: Thin section view in plane polarised light at medium magnification showing anastomosed filaments in quartz, interspersed with sub-rounded grains of opaque oxides.

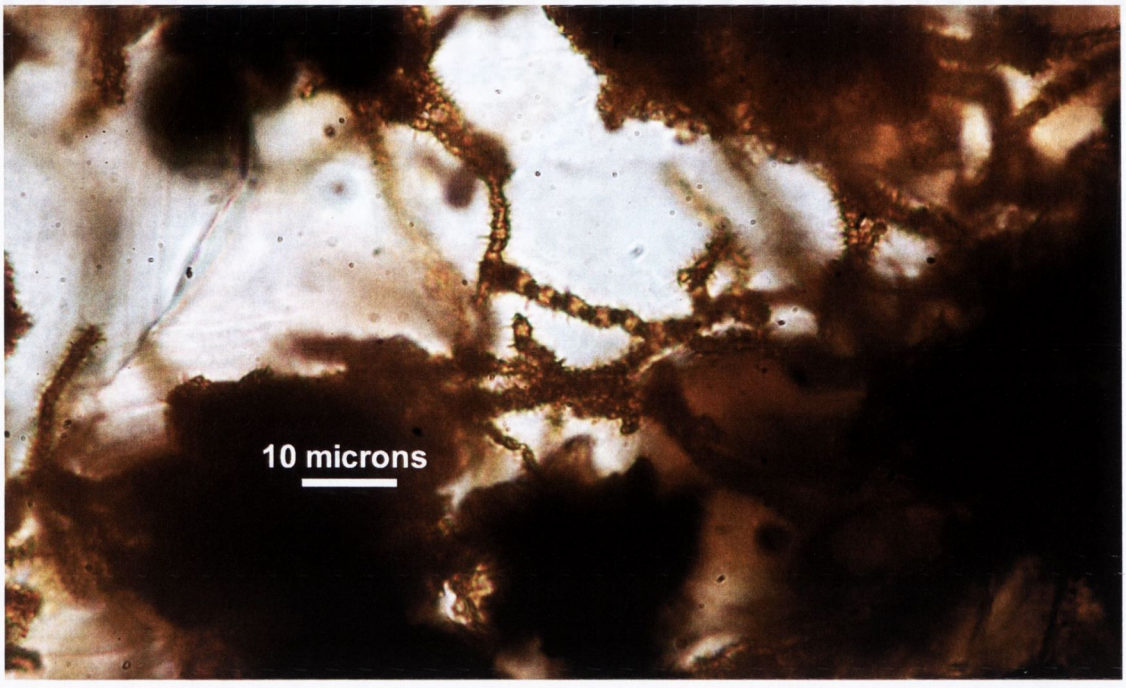

Fig. 5.5: A thin section view in plane polarised light at high magnification showing branched and interconnected filaments, showing a variable branching angle.

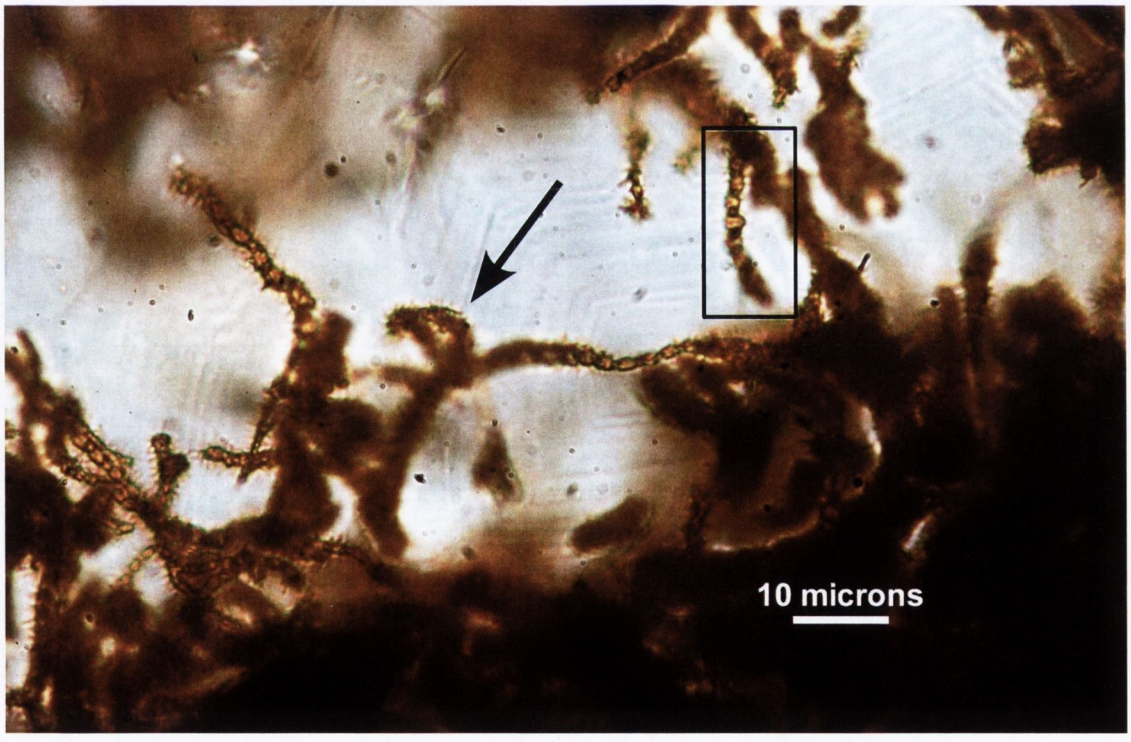

Fig. 5.6: A thin section view in plane polarised light at high magnification showing filaments that appear to be formed from chains of coccoid to bacilli shaped "cells", three secondary branches arrowed. The box highlights the filament modelled in figure 5.7.

A small minority of filaments are un-coated and these appear to consist of alternating large (1 to 1.2 μm) and small "cells" (*c.* 0.5 μm), forming a beaded appearance (figures 5.4, 5.5 and 5.6). Many filaments are interconnected to other filaments at a variable branching angle (figure 5.6). Some filaments have smaller side branches along their length and these side branches tend to branch *c.* 90° from the primary filament (figure 5.7). A few filaments bifurcate near 30° producing a Y appearance.

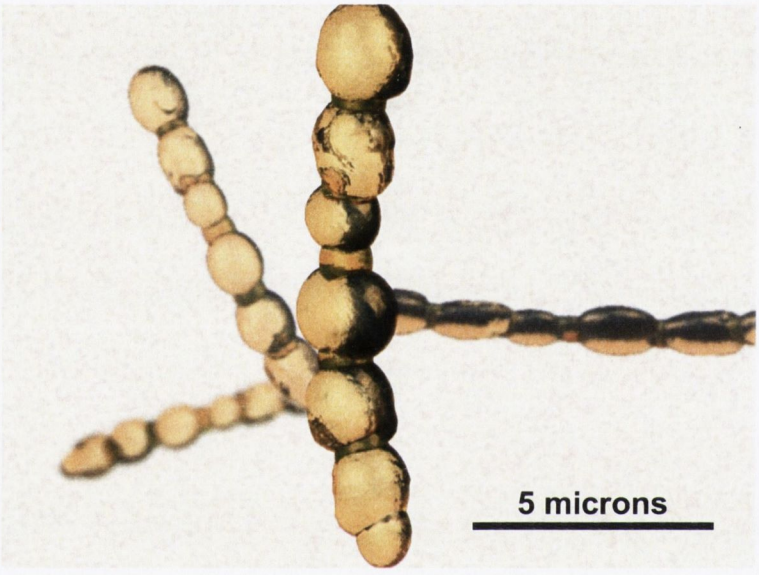

Fig. 5.7: 3D model of a "cellular" filament outlined by box in figure 5.6. Note the alternating large and small "cells".

5.4 Origin of Filaments

Both organic and inorganic processes are capable of generating filamentous forms. Here organic and inorganic origins are carefully considered and evaluated.

5.4.1 An organic origin

Here an organic hypothesis is considered and the criteria of Hoffman & Farmer (2000) are used to assist interpretation.

5.4.1.1 The cyanobacteria

Cyanobacteria are a type of prokaryotic chlorophyll producing bacteria that obtain their energy via photosynthesis, using water as an electron donor and generating oxygen as a by-product (Whitten & Potts, 2000). Most cyanobacteria die in just 2 to 3 hours in dark anoxic conditions (Whitten & Potts, 2000). However, a few mat forming varieties may survive, but not multiply, in darkness for several days by fermenting of stored sugars (Stal, 2000). Cyanobacteria tolerate mildly acidic to mildly alkaline waters, pH 5.6 to 10 (Ward & Castenholz, 2000) and most require well oxygenated conditions; a few are anaerobes (Stal, 2000). Cyanobacteria may be the first organisms preserved in the fossil record, with alleged examples from 3.5 Ga (Schopf *et al.*, 2002; Golubic & Seong-Joo, 1999) that are becoming increasingly controversial (Brasier *et al.*, 2002). Nonetheless, non-marine terrestrial cyanobacteria are rare in the fossil record (Dörfelt *et al.*, 2000). Most terrestrial fossil cyanobacteria are preserved in hot spring sinter deposits. *Calothrix*, *Oscillatoria*, *Synechococcus* and *Fischerella* are common in hot springs and are easily fossilised (Ward & Castenholz, 2000). The processes involved in the silicification of *Calothrix* and *Fisherella* are well understood. Coatings form passively (Konhauser *et al.*, 2001; Konhauser *et al.*, 2004) but rates of silicification may be enhanced by a "primer coating" of electrically charged iron^{III} oxides (Phoenix *et al.*, 2001; Yee *et al.*, 2003). Phoenix *et al.* (2000) demonstrated that *Calothrix* can continue to photosynthesise despite almost total envelopment by silica, as the precipitated silica is restricted to the protective outer skin of the organism, the extracellular sheath.

Rapid silicification ensures the preservation of the organisms to the cellular level. The true-branching cyanobacteria are morphologically similar to the Cloghleagh Iron Mine filaments, especially the species *Fisherella*, *Westiellopsis* and *Nostochopsis sp.* (Gugger & Hoffmann, 2004). However, there are two notable differences. Firstly, the Cloghleagh Iron Mine filaments average 2.333 μm in diameter, less then half the diameter of the true-branching cyanobacteria. Secondly, the cyclic repetition between large and small "cells" exhibited by the Cloghleagh Iron Mine filaments is unusual. When some filamentous cyanobacteria species experience nitrogen starvation (nitrogen is needed to make chlorophyll) some vegetative cells will transform to large thick walled heterocysts. But no more than one in 10 vegetative cells will transform to a heterocyst (Adams, 2000). The similarity between the Cloghleagh Iron Mine filamentous forms and the true-branching cyanobacteria is tempting. Nonetheless, the organisms photosynthetic requirements make it unlikely that large and intact cyanobacteria colonies survived descent underground and fossilisation in a fault gouge. Also, there are a number of unique characteristics exhibited by the Cloghleagh Iron Mine filaments but not repeated by known cyanobacteria species.

5.4.1.2 The sheathed bacteria

The Cloghleagh Iron Mine filaments also look like the sheathed bacteria (Schmidt & Schäfer, 2005). Of these, the iron-manganese oxidising bacteria *Leptothrix* and *Sphaerotilus* are the most common extant species (Waggoner, 1996). They are found in nutrient poor waters, often enriched in dissolved iron (van Veen *et al.*, 1978). They require roughly neutral conditions of pH 6.5-8.5, are obligate aerobes and live between 15 and 40°C (van Veen *et al.*, 1978). They oxidise dissolved Fe^{II} and Mn^{II} compounds and in doing so they accumulate FeOOH and manganese oxide coatings on their sticky oligosaccharide rich cell membranes (Chan *et al.*, 2004). Oxidation causes the pH of the microenvironment surrounding the bacteria to decrease to the organism's preferred level (Chan *et al.*, 2004). Schmidt & Schäfer (2005) describe fossilised sheathed bacteria, *Leptotrichites resinatus* in alpine Cretaceous amber from Schliersee, Bavaria, southern Germany. They provide a useful table detailing the morphological characteristics of extant *Leptothrix* species (table 5.1).

Cells	Cloghleagh Iron Mine Filaments	*Schliersee Leptothrix resinatus*	*L. cholodnii*	*L. discophora*	*L. lopholea*	*L. mobilis*	*L. ochracea*
Diameter	1 and 0.5(?)	0.9 to 1.3	0.7 to 1.3	0.6 to 0.8	1.0 to 1.4	0.6 to 0.8	1
Length	1 and 0.5(?)	1.5 to 3.5	2 to 15	2.5 to 12	3 to 7	1.5 to 12	2 to 4
Large cells?		+		–	+	–	+
Flagella							
Monotrichous polar	–	?	+	+	–	+	+
Polytrichous subpolar	–	?	–	–	+	–	–
Sheath							
Diameter	2 to 4	4 to 12	2 to 10	8 to 12	1.5	–	0.8 to 3.0
Rough surface	+(?)	+	+	+	(+)	–	(+)
Granulation	+(?)		+	+	(+)	–	(+)
Empty sheaths	?	+	(+)	+	(+)	–	+
Fe accumulation	+	+	–	+	+	+	+
Mn accumulation	–	–	+	+	+	?	–
Branching	common	+	–	(+)	(+)	–	–

Table 5.1: The Cloghleagh Iron Mine Filaments compared with extant Leptothrix species. Key: +, feature present; –, feature absent; (+), feature rarely seen. Table adapted from Schmidt & Schäfer (2005).

The bacilli of the sheathed bacteria are elongated, with an aspect ratio between 1:1.5 to 1:4. However, the Cloghleagh Iron Mine filaments possess round to slightly elongated coccoid "cells". Thus, in balance, the Cloghleagh Iron Mine filaments do not appear to be sheathed bacteria.

5.4.1.3 The actinomycetales

The actinomycetales are a diverse family of bacteria that are common in soils and are important decomposers of plant matter (Garrity & Boone, 2001). Many species of actinomycetales form branched filamentous colonies like the Cloghleagh Iron Mine filaments. Images of *Nocardiopsis dassonvillei*, a sub-species of *Nocardiopsis* in volume IV of Bergey's Manual of Determinative Bacteriology (McCarthy, 1989) look strikingly similar to Cloghleagh Iron Mine filaments (Figures 5.8 and 5.9). *Nocardiopsis* and its sub-species are common soil bacteria and live in aerobic conditions between 4 to 45 °C at circum neutral pH (McCarthy, 1989). However, unlike *Nocardiopsis dassonvillei*, and the other actinomycetales, the Cloghleagh Iron Mine filmaments display alternating large and small "cells".

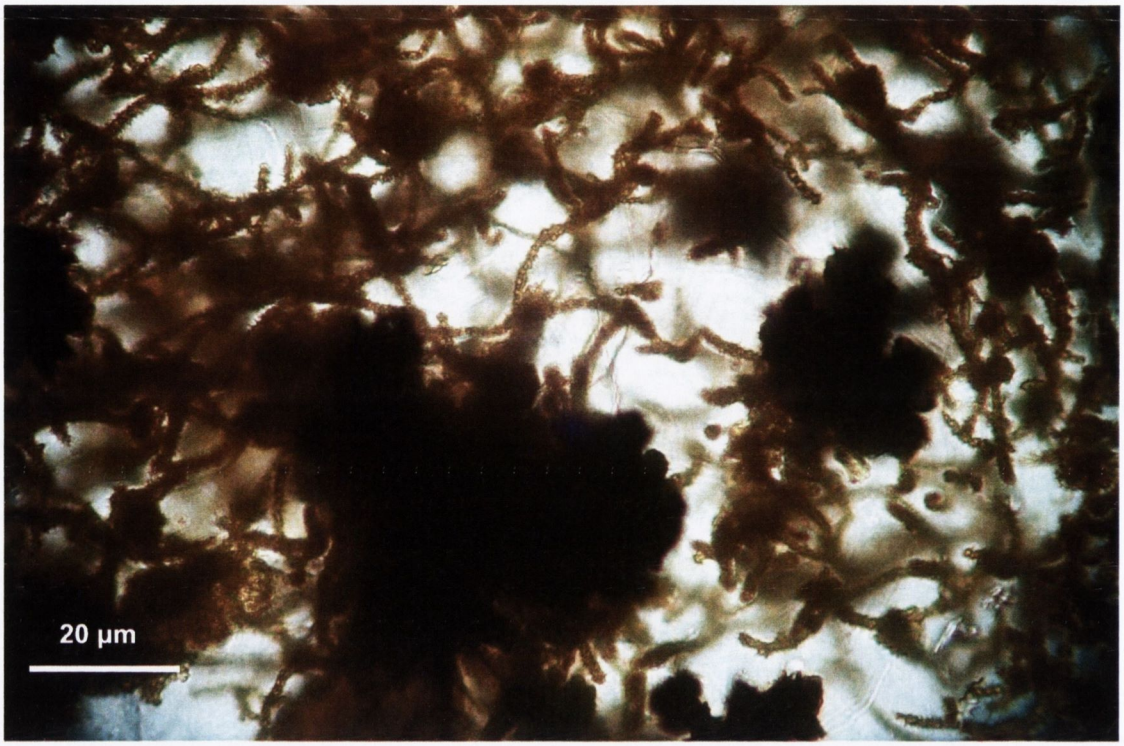

Fig. 5.8: A thin section view in plane polarised light at high magnification of Cloghleagh Iron Mine filaments with interspersed sub-rounded grains of opaque Fe^{III} or manganese oxides.

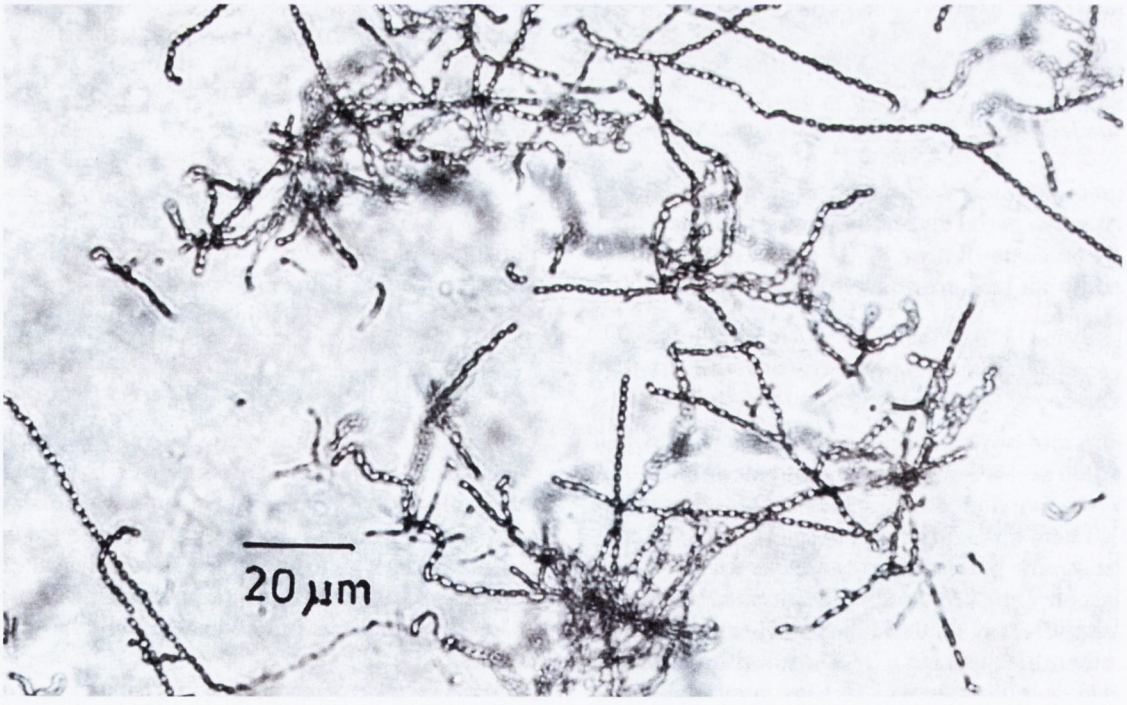

Fig. 5.9: Image of *Nocardiopsis dassonvillei* ATTC 23219, from page 2566 in volume IV of Bergey's Manual of Determinative Bacteriology (McCarthy, 1989). Images are at a similar scale.

5.4.1.4 Discussion

Of the cyanobacteria and bacteria considered, the actinomycetales look most like the Cloghleagh Iron Mine filaments, especially *Nocardiopsis dassonvillei*, a soil bacterium. However, the alternating large and small "cells" exhibited by the Cloghleagh Iron Mine filaments remains an outstanding difference. Most examples of fossilised cyanobacteria and bacteria are preserved in chert, sinter and amber (Schmidt & Schäfer, 2005). Rapid fossilisation is required to preserve bacteria. In the case of the Cloghleagh Iron mine filaments, rapid fossilisation could have been achieved by entrainment and preservation in an active fault zone composed of silica gel undergoing gelation, a rapid phase change from liquid to solid silica gel (Cipelletti *et al.*, 2000; Cipelletti & Ramos, 2005). Following the cessation of fault movement, rapid gelation of silica gel would ensure fossilisation of entrapped bacteria.

However, the lack of widespread filament alignment suggests that the filaments developed in the fault after fault motion ceased, and that they were not entrained in a moving fault. In this case, it is hard to understand how rapid fossilisation could have taken place.

5.5 Filament Diameter Measurements

Hofmann & Farmer (2000) described macroscopic and microscopic filamentous structures they attributed to fossilised microbial life in oxidised ore bodies, hydrothermally altered volcanic rocks and other low temperature mineral assemblages from more than 140 localities worldwide. The preservation process they propose involve encrusting microbial filaments with iron oxides, silica or various zeolite group minerals. Although mineral coatings tend to obliterate salient features required for species or even genera identification, Hofmann & Farmer (2000) suggested that in oxidised ore bodies, the filamentous structures may be the fossilised iron oxidising bacteria *Galionella sp.* and *Leptothrix discophora.*

Several criteria were set out by Hofmann & Farmer (2000) to support biogenicity for the biomorphs they observed: -

- Tubular construction with an inner hollow core of 1 to 2 μm in diameter.
- Coalesced filaments that form mat like structures.
- Apparent gravity draping of microscopic and coalesced macroscopic filaments that attests to former flexibility.
- Restriction to low temperature mineral assemblages.
- Similar morphology to microbiota preserved in modern hot spring sinters.

The Cloghleagh Iron Mine biomorphs exhibit many of these qualities; they are filamentous, are coalesced into anastomosed mats, a few filaments appear to follow an apparent flow direction, they are in a low temperature mineral assemblage (goethite begins to transform to hematite at 200°C; Gualtieri & Venturelli, 1999; Catling & Moore, 2003) and they are similar in morphology to the soil bacteria *Nocardiopsis dassonvillei* (McCarthy, 1989) and other actinomycetales. Additionally, Hofmann & Farmer (2000) proposed that a restricted filament diameter supports a biogenic origin.

Accordingly, the diameters of 30 filaments were measured. Filaments were chosen at random and included some coated filaments. Their diameters were measured with an eyepiece graticule graduated in microns, at the highest magnification (chart 5.1).

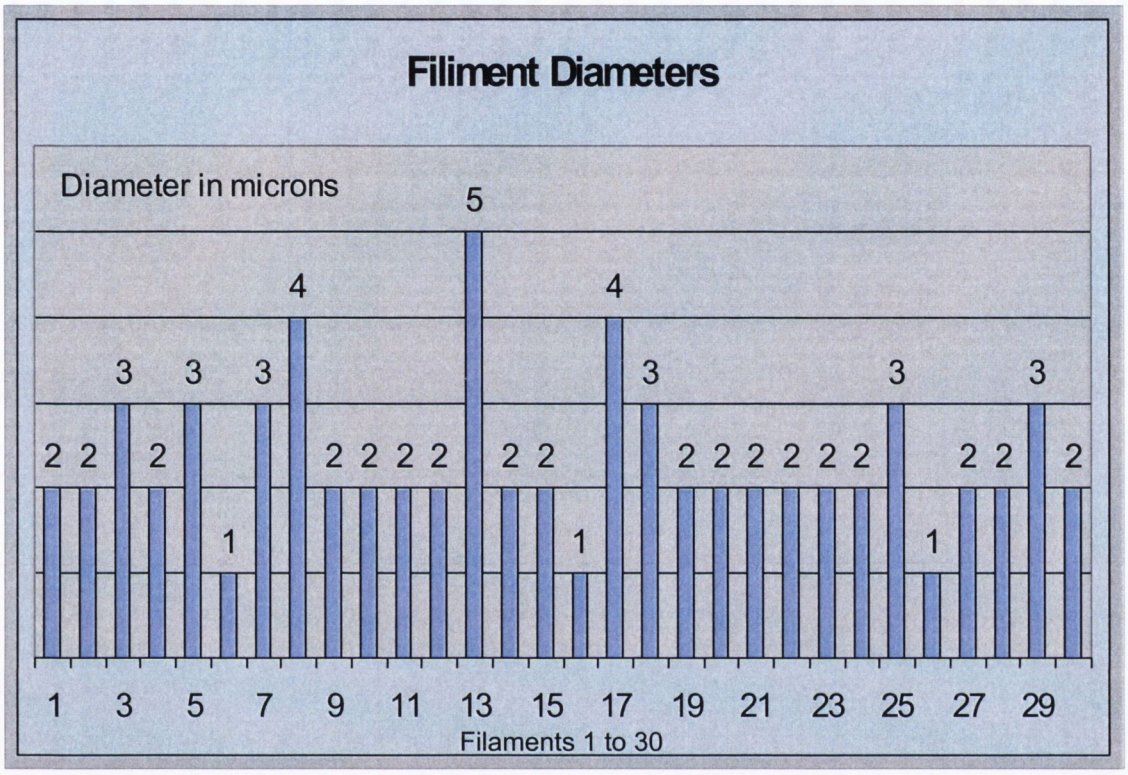

Table 5.2: This chart plots the diameters of 30 filaments in microns. The consistent diameter of the filaments, suggests that they are biogenic.

The Cloghleagh Iron Mine filaments have a consistent filament diameter, averaging 2.333 μm with a standard deviation of 0.884. According to Hofmann & Farmer's (2000) criteria, the Cloghleagh Iron Mine filaments are fossilised bacteria. However, Hofmann & Farmer (2000) were unaware of the abiotic processes capable of creating filaments that will be discussed next.

5.6 An Inorganic Origin

When the Cloghleagh Iron Mine filaments where first observed, their similarity to Diffusion Limited Aggregation (DLA) was noticed (Sander, 2000). Hopkinson *et al.* (1998) observed DLA-like growth in similar Fe^{II} rich filaments from the TAG hydrothermal field in the central Mid-Atlantic. DLA is a computer simulation method developed by Witten & Sander (1981) that generates branched fractal forms. The process of DLA can be imagined as follows:

- A particle is released into a 2-dimensional simulated space, far from a fixed particle that is placed at the middle of the simulation area
- The path of the free particle is random, its movement simulates chaotic Brownian motion
- The released particle eventually collides with the stationary seed particle at the centre of the simulation and it immediately adheres, at a random point
- Another particle is released and the process is repeated thousands of times

Structures built by DLA (figure 5.10) look like various natural dendritic structures e.g. manganese dendrites (Potter & Rossman, 1979), Viscous Fingering (King, 1987), electrochemical deposition, dielectric breakdown, blood vesicles and the growth of certain bacteria and fungal colonies (Daccord *et al.*, 1986; Sander, 2000).

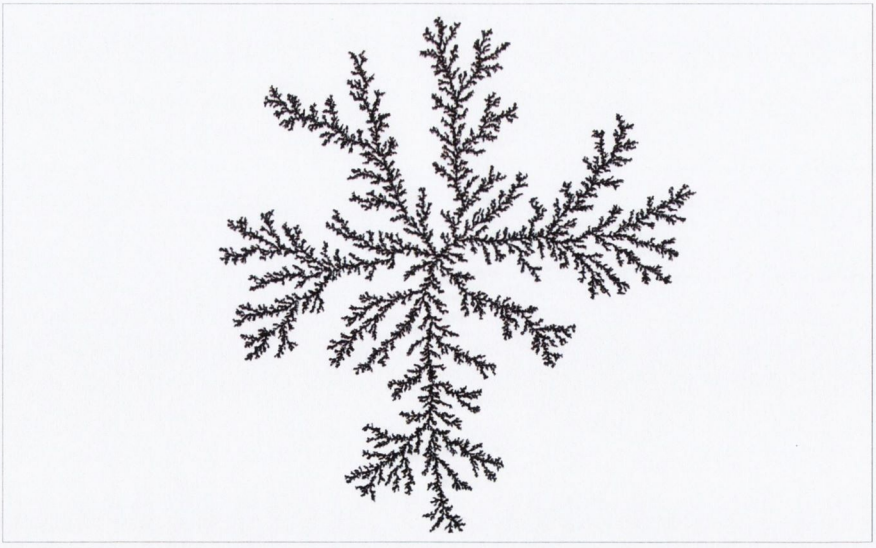

Fig. 5.10: A 2-dimensional DLA dendritic structure generated with 155,000 particle collisions, using the program TillbergDLA written by Dan Tillberg.

Of the natural processes that DLA can simulate, Viscous Fingering (a form of Saffman-Taylor instability) can generate branched 3-dimensional structures similar to the Cloghleagh Iron Mine filaments. Viscous Fingering occurs when an inviscous fluid is injected into a viscous fluid (Daccord *et al.*, 1986; King, 1987). The interface between the two immiscible fluids can form a highly convoluted 3-dimensional filamentous morphology, if the viscosity contrast between the two fluids is very high (King, 1987). King (1987), who used a variation of computational DLA with simulated viscosity ratios up to 1000, produced branched filamentous structures strikingly similar to the Cloghleagh Iron Mine filaments. Zhang & Liu (1998) demonstrated the close similarity between simulated and analogue models of Viscous Fingering, for a viscosity ratio of 1 to 10,000. One should note that, the viscosity contrast between the two fluids does not denote intrinsic viscosity. Instead, an apparent viscosity contrast is often generated by the mechanical stiffness of the membrane (or surface tension) separating the two fluids (Ben Amar *et al.,* 1993). Buka *et al.* (1986) and Ben Amar *et al.* (1993) include excellent images of analogue experiments of Viscous Fingering (Figure 5.11).

Fig. 5.11: Viscous Fingering produced by injecting silicon oil into a meshed nylon cloth held between two glass plates. From Ben Amar *et al.* (1993).

The morphology of the Cloghleagh Iron Mine filaments indicates that they could have formed when an inviscous fluid was injected into a more viscous medium, generating a morphology typical of Viscous Fingering. It is a kind of "Chemical Garden" that involves the injection of a fluid into a medium from which it is separated by a semi-permeable boundary.

5.6.1 The chemical garden

The Chemical Garden (or Silica Garden) phenomena was first described by the Renaissance alchemist Johann Rudolf Glauber (1604-1670) in 1646 (Cartwright *et al.*, 2002). In its original form, the Chemical Garden involved the introduction of ferrous chloride ($FeCl_2$) crystals into a solution of potassium silicate (K_2SiO_3, water glass) (Glauber, 1651). A rapid chemical reaction ensues, generating an elastic semi-permeable membrane of colloidal iron silicate that envelops the $FeCl_2$ crystals, via the reaction 6.1:

$$FeCl_{2(aq)} + K_2SiO_{3(aq)} \longrightarrow FeSiO_{3\downarrow} + 2KCl_{(aq)} \qquad \text{(rec. 6.1)}$$

The membrane permits the flow of solvent (water) but blocks the flow of solute - Fe^{2+}, Cl^-, K^+, SiO_3^{2-} ions etc. As a result, osmosis causes the fluid pressure within the membrane to increase, causing membrane growth (Cartwright *et al.*, 2002; Stone & Goldstein, 2004). A wide variety of chemicals besides ferrous chloride and potassium silicate can generate a Chemical Garden. Sodium carbonate may be used in place of potassium silicate, while $FeCl_2$ can be replaced by various water soluble aluminates, sulphates, dichromates and carbonates (Cartwright *et al.*, 2002; Maselko & Strizhak, 2004). Balköse *et al.* (2002) describe the chemical and physical properties of various silica based Chemical Gardens. A wide variety of structures can grow in minutes to hours (figure 5.12). The following passage from Thomas Mann's novel, *Doktor Faustus*, illustrates the surprising appearance of a growing Chemical Garden:

> I will never forget the sight. The crystallization vessel in which this transpired (the chemical garden) was filled to three-quarters with a slightly mucilaginous water, diluted water glass to be precise, and from the sandy bottom up rose a grotesque miniature landscape of differently coloured growths–a muddle of vegetation, sprouting blue, green, and brown and reminiscent of algae, fungi, rooted polyps, of mosses, too, but also of mussels, fleshy flower spikes, tiny trees or twigs, and here and there even of human limbs–the most remarkable thing my eyes had ever beheld, remarkable not so much because of their very odd and perplexing appearance, however, but because of their deeply melancholy nature (Mann, 1999).

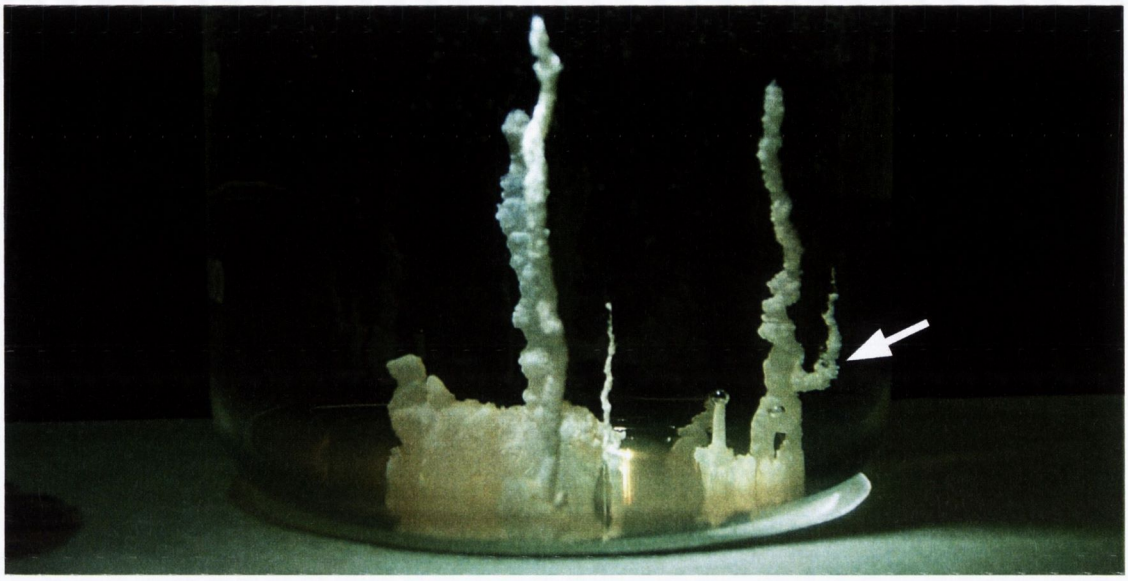

Fig. 5.12: A Chemical Garden grown by the author. $MnCl_2$ crystals were added to a 1.5 molar solution of $Na_2CO_3{\cdot}6H_2O$. Arrow highlights a branch. The photograph was taken *c.* 25 minutes after the addition of the $MnCl_2$ crystals.

The van't Hoff equation (eqn. 5.1 & 5.2) can be used to estimate the osmotic pressure generated inside a Chemical Garden. In this case for a 0.1 molar solution of $FeCl_2$.

$$\pi = M(i)RT \quad \text{(eqn. 5.1)}$$

Where M are moles of solute, R is the ideal gas constant at 0.08206 L · atm · mol^{-1} · K^{-1}, T is the temperature in Kelvins and π is the osmotic pressure in atmospheres. In addition, because $FeCl_2$ is an ionic compound that contains 3 atoms, the van't Hoff factor (i) must be used. In this case the value of i is 3.

0.1 moles (3) x 0.083144 L · atm · mol^{-1} · K^{-1} x 293.14 K = 7.31 atm (eqn. 5.2)

According to the van't Hoff equation (eqn. 5.2), osmotic pressure (π) inside the chemical garden will be 7.31 atmospheres. In reality, it is difficult to predict the osmotic pressure accurately, however, for concentrated solutions the osmotic pressure is generally greater then predicted. Osmotic pressure will cause the precipitated flexible membrane to grow via plastic extension and/or episodic rupture-sealing, usually at a filament tip (Cartwright *et al.*, 2002; Thouvenel-Romans & Steinbock, 2003). Branching can also occur (figure 5.12) (Jones & Walter, 1998).

Significantly, the effects of zero-gravity on Chemical Garden growth was investigated in 1993 on mission STS-55 of the Shuttle Columbia (Jones, 2002). In the absence of gravity, the Chemical Garden formed a branched morphology similar to the Cloghleagh Iron Mine filaments. The branching style in zero gravity was interpreted by Jones & Walter (1998) as Laplacian-growth, a form of Viscous Fingering/Saffman-Taylor instability.

As for the beaded morphology exhibited by the Cloghleagh Iron Mine filaments, Thouvenel-Romans & Steinbock (2002) studied episodic growth in Chemical Gardens. They state that, episodic growth is caused by the same mechanism that causes a water tap to drip. The smallest and narrowest stems with the lowest fluid-flow rate, extend via "drip tip extension" i.e. episodic rupture, fluid escape and resealing (Thouvenel-Romans & Steinbock, 2002). Leduc (1911) grew a number of Chemical Garden filaments that grew via "drip tip extension". Leduc's (1911) last stem in particular, is strikingly similar to the beaded Cloghleagh Iron Mine filaments (figures 5.13 & 5.14).

It is proposed that the Cloghleagh Iron Mine filaments are a natural iron-based Silica Garden, a type of Chemical Garden. It is proposed that the filaments are formed in iron oxide rich silica gel. They are not fossilised bacteria. In response to Hofmann & Farmer's (2000) question, "*Filamentous microfabrics in low temperature mineral assemblages: are they fossil biomarkers?*", the answer may be no; some filamentous microfabrics may be Chemical Gardens.

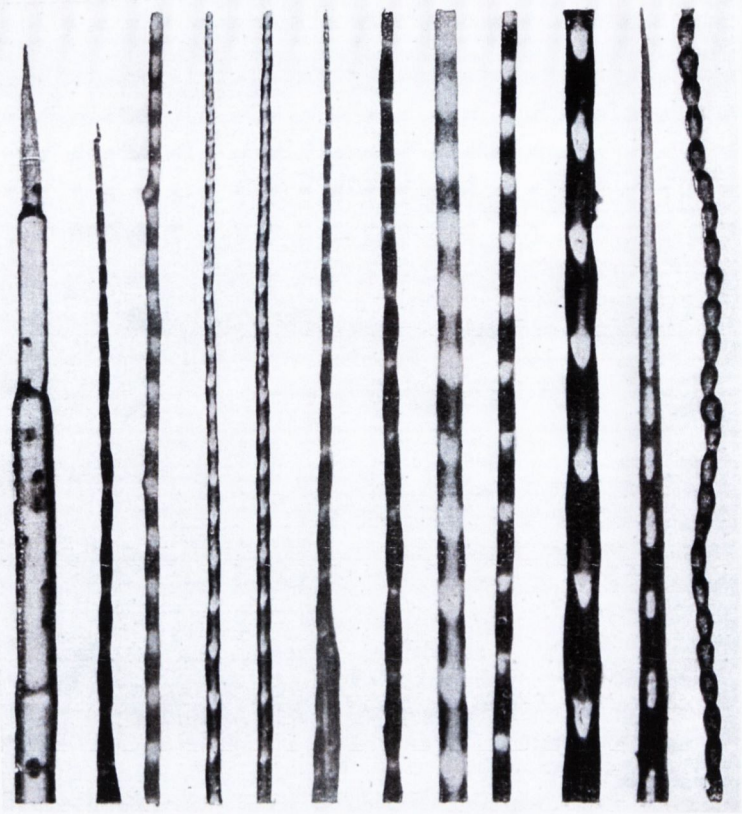

Fig. 5.13: This is figure 56 from Leduc (1911) with the title, "*Fig. 56. - Microphotograph showing the structure of osmotic stems. (Magnified 40 diameters.)*". The similarity of the last stem in particular to the Cloghleagh Iron Mine filaments, is striking.

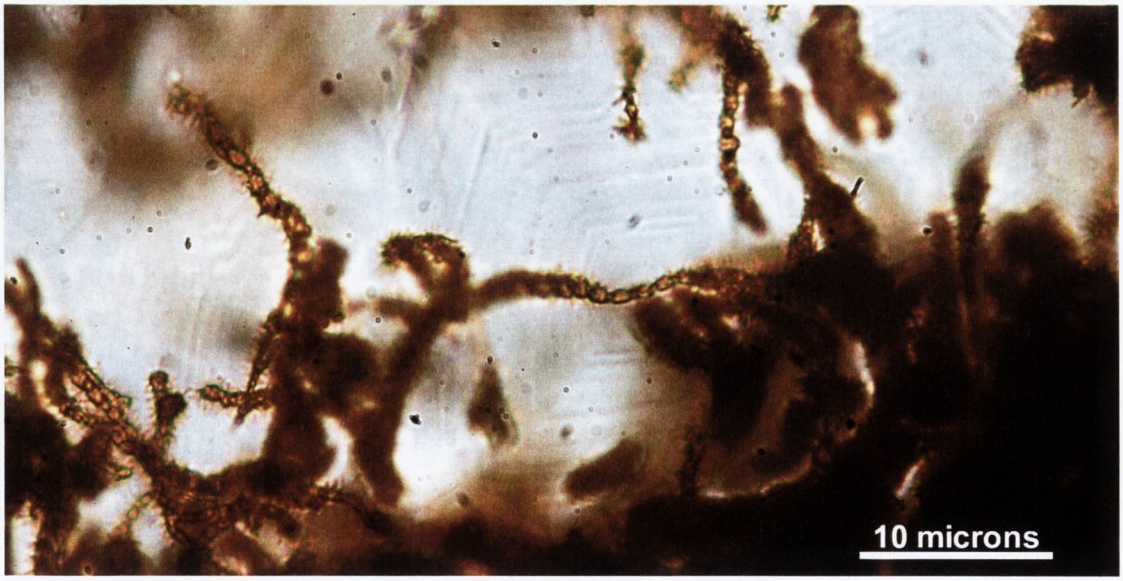

Fig. 5.14: Some of the Cloghleagh Iron Mine filaments appear to form beaded chains similar in morphology to the last stem in Leduc's (1911) figure 56. In particular, note the elongation of some of the beads in the Cloghleagh Iron Mine filaments.

5.7 Other Examples

Select examples of supposed fossil bacteria will now be reassessed with the Chemical Garden phenomenon in mind.

5.7.1 The alleged biota of deep-sea hydrothermal vent sites

Little *et al.* (2004) describe bacteriogenic iron oxide precipitation in deep sea hydrothermal vents from the Ordovician to the present day (figure 5.15). The filaments are interpreted by Little *et al.* (2004) as iron-oxide coated fossil bacteria. Many examples (e.g. filaments from the *c.* 190 Ma Figueroa jasper of California, USA) exhibit a branching style typical of Viscous Fingering. Three examples are included in figure 5.15 and are compared to computational DLA. Half the filamentous structures depicted in Little *et al.* (2004) exhibit such branching and may be Chemical Gardens.

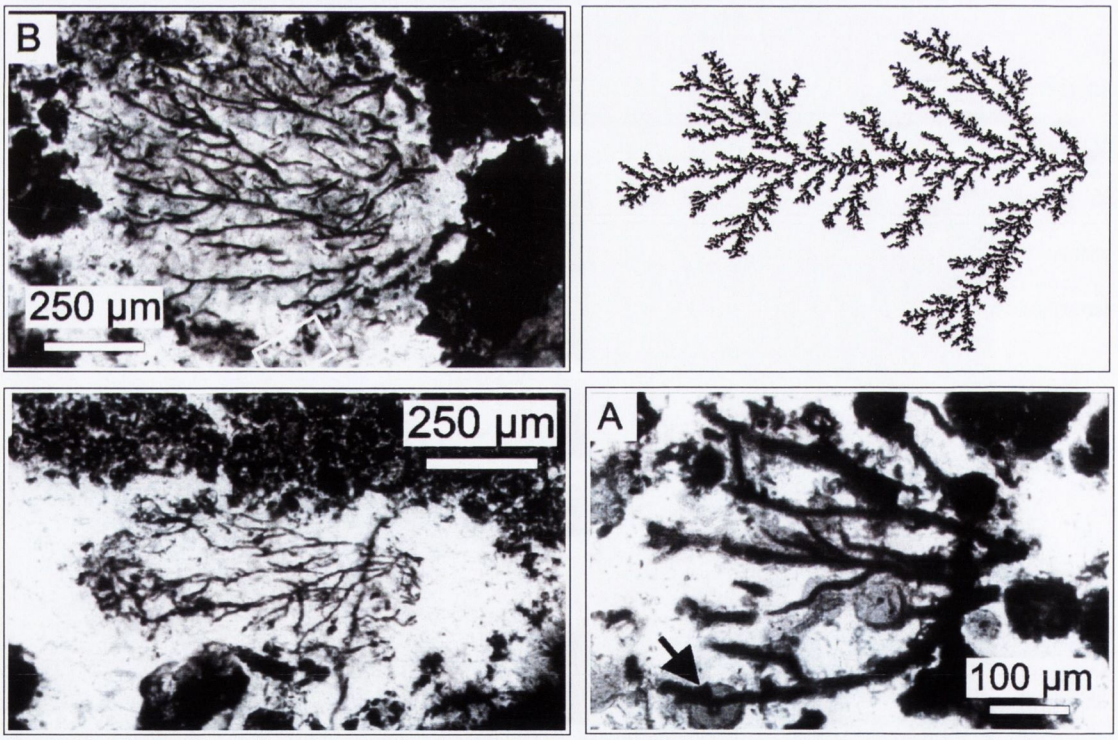

Fig. 5.15: Three alleged bacteria fossils from Little *et al.* (2004) compared to computation DLA, upper right. DLA like dendritic branching is suggestive of Viscous Fingering, produced by the Chemical Garden process. Upper left titled – *Sparsely branched dendrite growing from a discrete point, Figueroa jasper;* Lower left titled – *Dendritic filaments in quartz domain, Figueroa jasper;* Lower right titled – *Sparsely branched dendrite growing from a discrete point, Figueroa jasper.*

Little *et al.* (2004) also described branched filamentous networks from the Trans-Atlantic Geotraverse (TAG) hydrothermal field in the central Mid-Atlantic. They suggest that the filaments are fossilised true branching or false branching filamentous bacteria e.g. *Gallionella* spp. or sheaths from *Sphaerotilus natans*.

In contrast, Hopkinson *et al.* (1998) stated that the TAG filaments are abiotic and explained their formation via a rather awkward mechanism, involving DLA-like self-organised competitive particle growth via episodic Ostwald-Liesegang cycles in a cooling and oxidising Fe^{II} rich hydrothermal silica gel. In support of abiotic DLA-like growth, Hopkinson *et al.* (1998) measured the fractal dimension (D_f) (Theiler, 1990) of two planer filamentous networks, at 1.72 and 1.78. The D_f for DLA is *c.* 1.7 (Witten & Sander, 1983).

Some TAG filaments are not enveloped by quartz and grow into sea water (Crispin Little, pers. comm., 2005). These are extremely brittle and attempts to preserve them for microscopic examination failed (Crispin Little, pers. comm., 2005). Additionally, many Figueroa filaments are hollow (Little *et al.*, 2004). It is for this reason that Little *et al.* (2004) suggest that the Figueroa filaments were occupied by bacteria. However, Laser Raman spectroscopy failed to detect any organic materials in the Figueroa filaments (Little *et al.*, 2004). Nevertheless, according to Little *et al.* (2004) in the absence of an abiotic mechanism that explains the development of the hollow filaments, a bacterial explanation is considered more likely. However, a Chemical Garden origin would predict the development of hollow filaments, they were originally filled with fluid.

Thus it is suggested that, some of the filamentous microstructures from ancient and modern deep sea hydrothermal vents depicted in Little *et al.* (2004) are Chemical Gardens, in particular those filaments that display DLA-like growth.

5.8 The Chemical Garden and Origin of Life

Given the cell like properties (Strizhak & Maselko, 2004) of the Chemical Garden and its occurrence in deep-sea hydrothermal springs that are proposed by many as the birthplace of life (Reysenbach & Cady, 2001), it is attractive to speculate that the iron-based Chemical Garden was involved in the emergence of cellular life.

5.8.1 The iron-sulphur world

Theories concerning the origin of life on Earth fall into two general categories. The "cells first" scenario that involves a pre-biotic "stew" containing accumulations of increasingly complex biomolecules, proteins and lipid vesicles that self-assembled to form primitive cellular life (Nisbet & Sleep, 2001). RNA is thought to have been the original replicative molecule, for example the Ribosome that copies the DNA of cells contains RNA at its heart, thus RNA preceded DNA (Bartel & Unrau, 1999).

More recently, a "metabolism first" iron-sulphur origin of life has gained attention (Wächtershäuser, 1990). The iron-sulphur world proposes that cell-less, metabolism first life, arose along redox-pH fronts associated with Archean deep sea hydrothermal vents that contained iron sulphides (Russell, 2003). The metabolism first iron-sulphur world hypothesis is supported by several lines of evidence, including pyruvic acid synthesis by FeS under hydrothermal conditions (Cody *et al.*, 2000), phylogenetic analysis that illustrates the antiquity of hyperthermophiles (Reysenbach & Cady, 2001; Schwartzman & Lineweaver, 2004) and ancient metabolic pathways catalysed by iron-sulphur centres e.g. acetyl-CoA/Pyruvate Dehydrogenase (Russell & Martin, 2004).

Martin & Russell (2003), who extended Wächtershäuser's (1990) arguments, proposed that life arose in proto-cellular bubbles composed of iron-nickel monosulphide (greigite & mackinawite) in Archean deep-sea hot springs. Recently, Russell (2003) and Russell & Arndt (2005) concede that a hot origin of life may be flawed, since essential biomolecules are thermolabile (Levy & Miller, 1998; Bada & Lazcano, 2002) and they now favour warm alkaline deep-sea hydrothermal springs as the birthplace of life. Also experiments show that RNA is rapidly destroyed by free radicals that are

generated on pyrite surfaces (Cohn *et al.*, 2004). Furthermore, at present day Black Smoker vent sites, seawater close to freezing point is found within metres of hot hydrothermal fluids up to 350°C. Thus, Russell & Arndt (2005) need not restrict the birthplace of life to a low temperature vent or in iron-nickel monosulphide bubbles. Nevertheless, it is significant that iron oxide Chemical Gardens, with their conspicuous cell-like properties, grow at redox-pH fronts at present day Black Smoker vent sites (Hopkinson *et al.*, 1998). Perhaps life developed within a proto-cellular iron oxide-silica gel Chemical Garden, at moderate temperatures beside a Black Smoker "fire" that provided organic compounds and pH, Eh, thermal and other kinds of potential energy.

5.8.2 Lipid world versus the chemical garden

Most workers believed that the first living cell developed when a replicative molecule such as RNA, hijacked an empty lipid vesicle (Segré *et al*, 2001). However, Fenchel (2002) points out several difficulties with this cell first scenario:

- It has proven difficult to synthesize lipids under conditions likely to have existed on the early Earth (Russell, 2003)
- It has proven difficult to explain the growth and division of simple lipid vesicles
- The additional cell wall of bacteria is unexplained
- It is difficult to explain how a simple energy metabolism could be established as charged molecules cannot pass through a basic lipid membrane
- The current lipid membrane is vastly more complicated then a simple lipid membrane

Additionally, the dissimilar membrane lipids of the Archaea and Bacteria, Ether linked versus Ester linked (Wächtershäuser, 2003), indicates that the last common ancestor (LCA) had a membrane that was compositionally radically different (Peretó *et al.*, 2005) or the ancestor lacked a lipid membrane. If the latter was the case, the LCA may have had an inorganic Chemical Garden boundary that was gradually replaced by the evolution of the lipid cell membrane.

5.8.3 Composition of the chemical garden

Due to the oxygen free reducing conditions in the Archean oceans (Holland, 1999), it is likely that double layered hydroxide (DLH) minerals precipitated in place of Fe^{III} oxides and oxyhydroxides (Génin *et al.*, 2005). Thus, an Archean Chemical Garden may have been composed of DLH e.g. fougerite rather then goethite. Due to the predicted widespread occurrence of DLH minerals during the Archean, their biopoetic capacity is the subject of research (see Arrhenius (2003) and references therein). Significantly, DLHs are surface active minerals that strongly concentrate and select specific organic compounds, including amino acids (Arrhenius, 2003). Their interlayers can accommodate inorganic molecules that promote reactions such as phosphorylation (Arrhenius, 2003), an important element in cellular energy metabolism (Deamer, 1997). DLHs can also form membranous compartments that can provide accommodation for organic compounds that gain access through selective diffusion (Arrhenius, 2003). Finally, Génin *et al.* (2001) discuss fougerite's ability to neutralise certain types of pollution (Figure 5.16 includes several redox reactions promoted by fougerite). Therefore, an Archean Chemical Garden composed of fougerite or other DLH minerals, could concentrate, select and perhaps generate useful organic compounds.

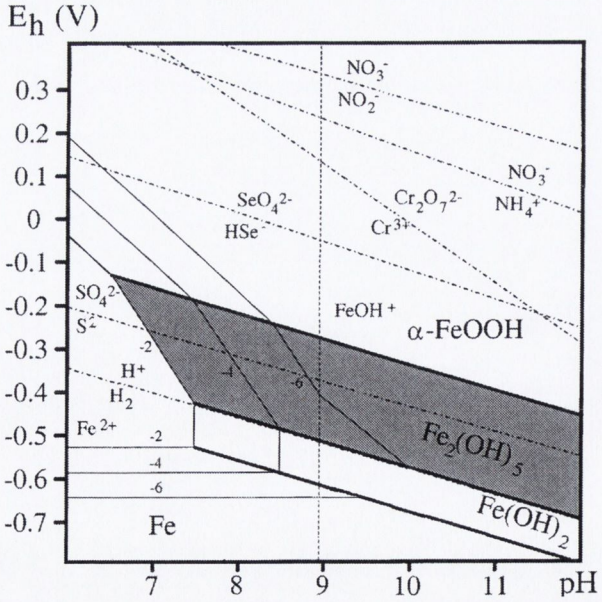

Fig. 5.16: E_h-pH stability diagram for the Fe-O-H, Fougerite represented by $Fe_2(OH)_5$. Redox reactions induced by Fougerite are depicted by dashed lines. Adapted from Génin *et al.* (2001).

5.8.4 The iron hydroxide chemical garden hypothesis

As filaments grow, they change their structure and chemical state, particularly in the case of drip-tip growth where each division could represent a separate biochemical and evolutionary experiment i.e. variably of traits. Also, the Chemical Garden possesses a semi-permeable boundary that experiences pH, Eh and ion gradients, similar to the modern cell membrane. But in contrast to the basic lipid membrane, the Chemical Garden's membrane allows the flow of ions (Maeselko & Strizhak, 2003). Thus an energy potential across the membrane could be established, an important element of basic cellular metabolism (Deamer, 1997). In addition, the membrane could prevent the entry of unwanted chemicals, the escape of reaction intermediates and protect fragile molecules such as RNA from decomposition. Lastly, if a Chemical Garden contains DLH minerals, it could concentrate and even generate novel biochemicals useful for the development of a replicating molecule e.g. RNA (Arrhenius, 2003). Finally, if a growing Chemical Garden competes for limited resources, nutrients, energy and space i.e. selective stress, Darwinian natural selection may initiate if the following points are satisfied:

1. If there are organisms that reproduce, and
2. If offspring inherit traits from their parents(s), and
3. If there is variability of traits, and
4. If the environment limits the size of natural populations,
5. Then those members of the population with maladaptive traits (as determined by the environment) will die out or reproduce less, and
6. Then those members with adaptive traits (as determined by the environment) will survive to reproduction or reproduce more.

From Darwin (1995)

Thus, the path towards life may hinge on the origin of a mutually symbiotic relationship between a Chemical Garden and a heritable molecule e.g. RNA. If the heritable molecule promotes faster growth, for example, the faster growing Chemical Garden would be chosen via Darwinian natural selection over those Chemical Garden's that are slower (less fit) growing and the path towards life may commence.

5.8.4.1 Experimental support

Crucial experimental support for exceedingly simple competitive growth, coupled with Darwinian natural selection, was found by Chen *et al.* (2004). They observed that the simple presence of RNA in lipid vesicles causes increased osmotic pressure and vesicle growth, at the expense of RNA free vesicles that shrink. Osmotic stress is caused by a form of anabolism, the creation of fewer larger molecules of RNA from many precursor amino acids (recall the van't Hoff factor (i) in eqn. 5.2). The polymerisation of amino acids within the lipid vesicles results in a decrease in the number of free amino acid molecules, causing an increase in osmotic stress and vesicle growth.

Chen *et al.* (2004) proposed that the fastest growing vesicles, containing the most efficiently polymerising and replicating RNA, would be selected over slower growing vesicles through Darwinian natural selection. Accordingly, RNA would increase in abundance as vesicles survive and grow. To conclude, the establishment of a symbiotic relationship between a heritable molecule and a growing membrane seems to be far simpler then imagined.

5.8.5 Conclusion

Early cellular life may have emerged due to abiotic stress in Archean Chemical Gardens, associated with deep sea hydrothermal springs. The lipid membrane may be a gradually evolved replacement of a previously inorganic boundary.

5.9 Silica Gel Generation and Fault Weakening

An outstanding problem in geophysics is the determination of the frictional resistance (μ) along faults during earthquakes. Currently faults appear much weaker than expected (Marone, 2004). Knowing the value of the coefficient of friction μ is critical in predicting the damage potential of fault zones. The lower the value of μ, the more energy will be released as damaging seismic waves; energy otherwise absorbed by frictional heating (Di Toro *et al.*, 2004).

The coefficient of friction μ for crustal rocks obtained from laboratory and theoretical work is constantly high, varying from μ 0.6 to 0.85 (Byerlee, 1978). These high friction values predict more friction generated heat flow from fault zones than is observed (Scholz, 2000; Saffer *et al.*, 2000). For example, the observed heat flow from the San Andreas fault in California supports to a coefficient of friction μ of only 0.1 to 0.2 (Parsons, 2002). There are two main schools of thought; either the fault zone materials for have a lower coefficient of friction than expected during slip (Sibson, 2000; Parsons, 2002) or fluid pressure in the slip zone rises during motion and reduces friction by pushing the walls of the fault zone apart (Wibberley & Shimamoto, 2005).

Until recently, experimental limitations prevented workers from combining the high slip velocities, displacements and pressures required to investigate possible mechanisms responsible for the dynamic weakening of natural fault zones (Di Toro *et al.*, 2004). However, an innovative test bed developed by Di Toro *et al.* (2004) that simulates a fault zone by holding two disks of Arkansas novaculite (a quartz rich sedimentary rock) together at a high pressure and subject to rotary shear, attained near real world values for slip velocity, slip length and confining pressures of 30 mm s^{-1}, *c.* 4.5 metres and 5 Mpa. Initially, at a low slip velocity of 1 μm s^{-1}, coefficient of friction μ was 0.7-0.8, a typical value for crustal rocks in past studies (Di Toro *et al.*, 2004). However, when the slip velocity increased to 30 mm s^{-1}, coefficient of friction μ reduced to only 0.2. After returning to a low slip velocity of 1 μm s^{-1}, coefficient of friction μ gradually reverted to 0.7 after about 100 seconds (Di Toro *et al.*, 2004). A temperature of *c.* 100°C measured near the sliding interface precluded friction melting and freezing.

Di Toro *et al.* (2004) propose that the low μ value is due to lubrication by thixotropic silica gel, generated by a combination of atmospheric humidity and ultra-comminuted quartz. Delayed strength recovery may be due to gelation of silica gel, the gradual growth of a 3-dimensional network of colloidal silica microspheres (Cipelletti *et al.*, 2000; Cipelletti & Ramos, 2005). More recently, the same team attained a slip velocity of 0.1 m s^{-1} and μ of just 0.1 (Roig Silva *et al.*, 2004). They further predict that friction will tend to zero as slip velocity approaches 1 m s^{-1} (Roig Silva *et al.*, 2004). Accordingly, Di Toro *et al.* (2004) propose that fault weakening in moist quartz rich rocks may be due to the generation of lubricating silica gel. All that is needed is field evidence (Marone, 2004).

Amorphous silica gel quickly forms opal-A, a far from equilibrium solid (Cipelletti & Ramos, 2005). It will quickly transform from opal-A through opal-A/CT, opal-CT, opal-C and finally to crystalline quartz (Rodgers *et al.*, 2004; Lynne, 2005). A complete transformation can take place in as little at 1900 years at surface conditions (Lynne *et al.*, 2005) and is faster at depth where higher temperatures and pressures prevail (Oehler, 1976). Such a transformation would normally obliterate any prior indications that a fault zone was originally composed of silica gel. However, the interpretations advanced here regarding the abiotic genesis of the Cloghleagh Iron Mine filaments, supports Di Toro *et al.* (2004) and other proposals that fault weakening in moist quartz rich rocks may be related to silica gel lubrication.

5.10 Discussion and Conclusion

The presence of cells and the satisfaction of Hoffman & Farmer's (2000) criteria appears to support a biogenic origin for the filaments from the Cloghleagh Iron Mine fault zone. In particular, some Cloghleagh Iron Mine filaments look like certain species of actinomycetal bacteria, especially *Nocardiopsis dassonvillei*, a soil bacterium. However, an unlikely sequence of events are required to ensure fossilisation of bacteria in a fault zone. Rather, it is proposed that the filaments are a natural analogue of the celebrated Chemical Garden phenomenon, and that the filaments formed in a fault zone that was composed of solidifying iron-oxyhydroxide rich silica gel. Proposals by Di Toro *et al.* (2004) that fault weakening in quartz rich rocks may be related to silica gel lubrication, would be supported by the interpretations advanced here.

In light of these proposals, other examples of claimed microbial fossils should be reassessed with the Chemical Garden phenomenon in mind. Already, a number of filamentous structures interpreted by Little *et al.* (2004) as bacteria, were reinterpreted as Chemical Gardens. The pantheon of supposed microbial fossils of the Archean, for which evidence of biogenicity is sometimes based only on morphology, would be threatened by these observations.

It is also suggested that that an iron based Chemical Garden may have played a key role in the emergence of cellular life, and that the lipid membrane is a result of a gradually evolved replacement of an earlier inorganic boundary. Darwinian natural selection could have identified and promoted a symbiotic relationship between a heritable molecule and Chemical Garden growth, thus initiating the path towards replicative cellular life. This hypothesis is supported by experimental evidence (Chen *et al.*, 2004).

Chapter 6 – Saprolites and Hydrothermal Alteration

6.1 Chapter Summary

This chapter describes a chemically altered granite at a site overlooking Lough Tay, County Wicklow. The chemically altered granite, which is associated with a tepid spring, was initially thought to be a clay rich saprolite (the product of surficial chemical weathering in a humid tropical to warm temperate climate). However, hydrothermal mineralisation can cause chemical alteration superficially similar to saprolitic weathering. A gossan containing abundant supergene cerussite ($PbCO_3$) after hypogene galena (PbS) is associated with the chemically altered granite.

It will be shown that the chemically altered granite is a product of low temperature hydrothermal activity that occurred less than *c.* 200 metres underground, know as argillic alteration. The implications of these findings are discussed in relation to the Cloghleagh Iron Mine and other base metal veins in the study area.

6.2 Grus and Clay Rich Saprolite

Grus, which is also called arène, is a weakly weathered gravelly saprolite typical of granite landscapes. Grus often preserves primary igneous minerals, magmatic textures, veining (Figure 6.2) and mineral alignment. Grus is formed following the initial weathering of biotite and plagioclase (Hall & Sugden 1987; Migon & Thomas, 2002). Biotite weathers along its basal (001) cleavage plane (figure 6.1) forming hydrobiotite, vermiculite and eventually kaolinite, causing volumetric expansion along the mineral's c-axis (Aoudjit *et al.*, 1996). The expansion of biotite shatters the host rock at grain boundaries, disaggregating the rock into a gravelly textured saprolite called grus (Migon & Thomas, 2002).

Mignon & Thomas (2002) proposed that grus must contain 75 to 100% sand+gravel, <20% silt+clay, <10% clay and that, though not diagnostic, a small amount of vermiculite, chlorite and occasionally illite may be present. Clay rich saprolites (argillaceous weathering profiles) represent more advanced stages of weathering; they contain >20% clay, of which at least 45 to 50% is kaolinite (Migon & Thomas, 2002).

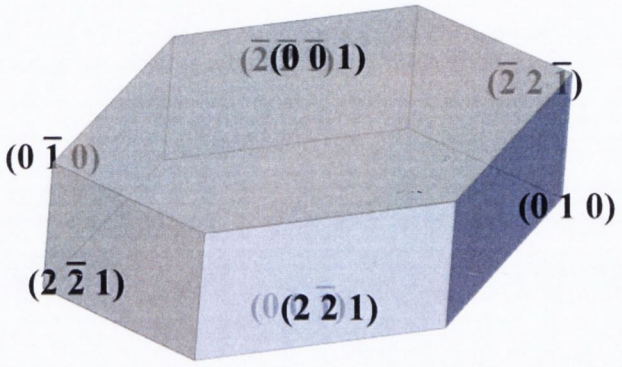

Fig. 6.1: A biotite crystal created by WinXmorph 1.4.5. During weathering, chemical alteration proceeded fastest along biotite's hkl-001 (basal) cleavage plane, causing expansion along the c-axis.

According to Migon & Thomas (2002) grus is "azonal", it can form in any climate regime; it has been found at surface in the sub-Arctic and at the base of deep lateritic and bauxitic weathering profiles in equatorial regions. The degree of grus alteration is controlled by several factors besides climate, including host rock mineralogy, vegetation, drainage conditions, insolation, rainfall and topography. Clay-rich grus varieties (up to 10% clay) are more common in areas of subdued topography, where clay production exceeds its removal by ground water percolation. Clay poor grus on the other hand is generally restricted to hill tops and hill slopes where the drainage is good (Migon & Thomas, 2002).

Clay rich saprolite with >20% clay, especially with kaolinite, gibbsite, hematite and lithiophorite, signify more advanced weathering than grus (Migon & Thomas, 2002). Such clay rich saprolites are typical of humid sub-tropical to equatorial tropical climates and if found in high-latitude regions they can indicate inherited pre-glacial weathering (Migon & Lidmar-Bergstrom, 2002).

Fig. 6.2: An exposure of grus uncovered during building the foundations of house near Ballynastockan Brook, County Wicklow [302422 208779, 240m OD].

The identification of clay-rich saprolites rather than grus, suggests that an associated landscape is pre-glacial and glacial erosion was modest (Migon & Thomas, 2002). For example, a pre-glacial palaeosol with datable pollen near Kilkieran Bay, County Galway indicates that the landscape there dates from late-Pliocene times (Coxon, 2001). Similarly, clay rich grus weathering profiles up to 50 m thick found only on high ground were described by Hall & Sugden (1987) in the Buchan region of north east Scotland. Based on intensity, depth and the restriction of the weathering profiles to hilltops, Hall & Sugden (1986) proposed that the clay rich grus formed during pre-glacial Miocene to Pliocene times in a humid warm temperate climate (Schwarz, 1997) and the associated landscape is pre-glacial.

Grus type weathering profiles were found at several sites in County Wicklow near Ballynastockan Brook [302422 208779, 240m OD] (figure 6.2) and at the Wicklow Gap [306740 200520, 390m OD]. However, an apparently clay rich saprolite was found at a site overlooking Lough Tay [316660 208080, 420 OD] during an undergraduate mapping exercise in 1998 (Jordan, 1999), and it is this more significant site that is described here.

6.3 The Lough Tay "saprolite"

Chemically altered adamellite overlooking Lough Tay was discovered during an undergraduate mapping project in 1998 (figures 6.3 & 6.4) (Jordan, 1999). The chemically altered rock consists of a *c.* 25 meters exposure by the side of the R759 road, at the junction between the adamellite and biotite schist (Jordan, 1999). The site is also the location of a tepid spring (warmer then 12°C).

The spring exits just above the southern end of the exposure amongst a steep gorse and heather covered hill slope. In 1998 water from the spring flowing over the outcrop of chemically weathered rock was found to be warm to the touch. In early October 1998, waters from the spring washed over a clean outcrop, perhaps cleaned due to recent road widening and resurfacing. But by 2005 most of the exposure was buried under loose material washed down slope by the spring. The chemically altered rock is cut by several dark, iron stained quartz veins. Several samples of clay from chemically altered adamellite and schist *c.* 20 metres south of the chemically altered adamellite exposure, were collected.

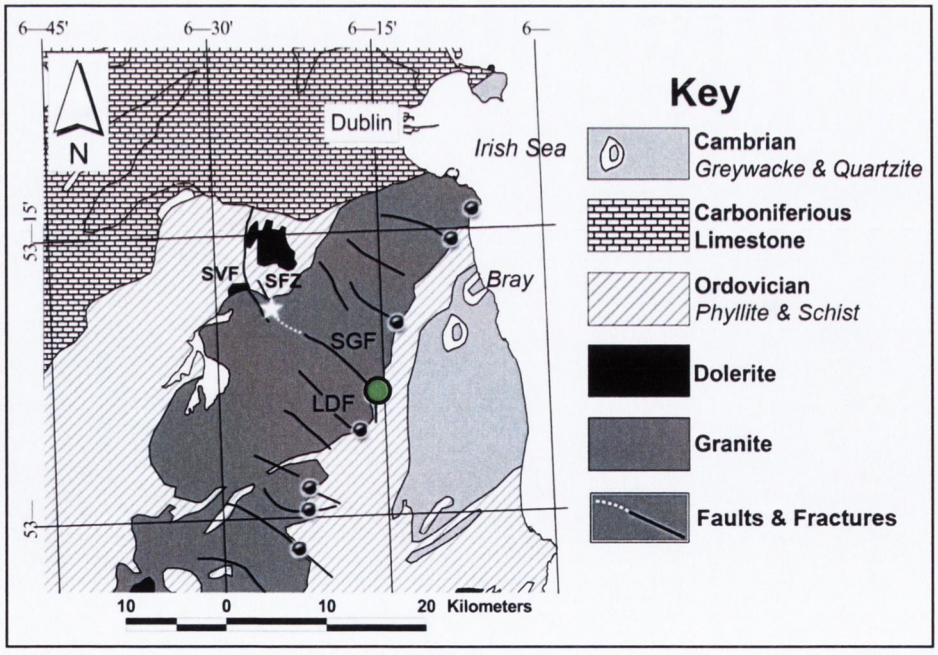

Fig. 6.3: Geological and locality map for the Leinster Mountain chain showing Lough Dan (green) and known historical Pb-Zn sulphide mines. The white star marks the location of the Cloghleagh Iron Mine. SVF – Slade Valley Fault, SFZ – Shankill Fracture Zone, SGF – Sally Gap Fracture, LDF – Lough Dan Fault. Note that Shankill fracture zone appears to connect with the Sally Gap Fracture to its south east.

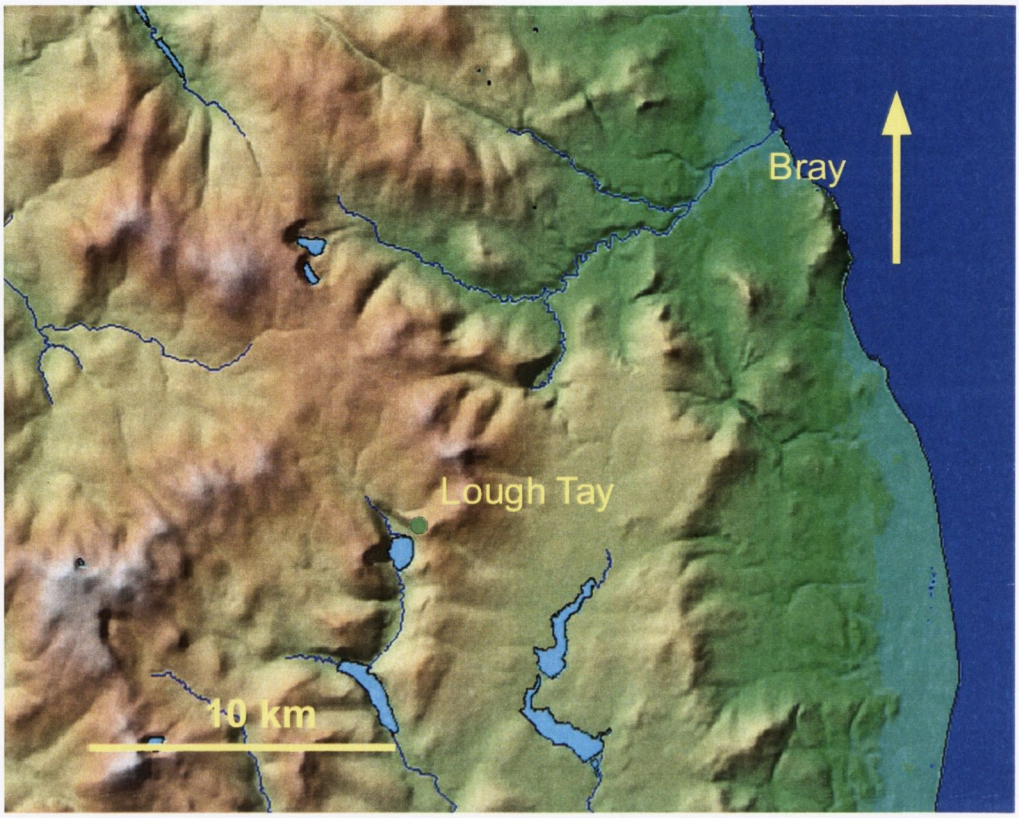

Fig. 6.4: Location of the Lough Tay chemically altered adamellite.

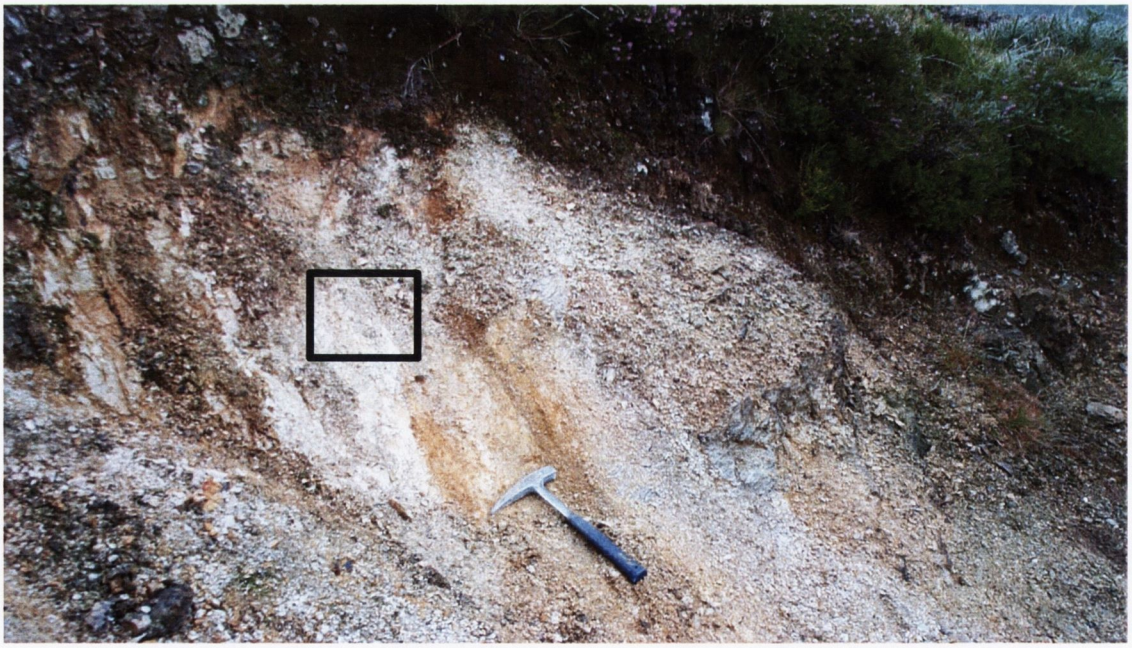

Fig. 6.5: Exposure of chemical altered adamellite at Lough Tay looking south, hammer for scale. The granite is altered to a soft white to light brown clay. The box highlights the sample location detailed in figure 6.6.

Fig. 6.6: Sample collection from the chemically altered adamellite, which was dominated by clay and was greasy smooth to the touch.

6.4 Analysis of Clay Minerals

X-ray diffraction (XRD) analysis was carried out to determine the clay mineral composition of the chemically altered adamellite, and granulometric analysis was carried out in order to determine if the altered adamellite was clay rich i.e. >10% 2μm clay.

6.4.1 XRD

Preparation and XRD analysis of orientated air-dried (2 μm) clay fraction was carried out according to the method described in Moore & Reynolds (1989). Clay minerals identification was aided by the book, *X-ray diffraction and the identification and analysis of clay minerals* by Moore & Reynolds (1989) and the U. S. Geological Survey Open-File Report 01-041, *A Laboratory Manual for X-Ray Powder Diffraction* (Poppe *et al.*, 2001). The open file report includes an on-line interactive flow diagram that aids the identification of clay minerals.

6.4.1.1 XRD analysis procedure

10 g of clay were added to 80 ml of deionised water with 20 ml 10% Calgon dispersing solution ($Na_6P_6O_{18}$) in a 100 ml flask. The flask was sealed and shaken vigorously for 5 minutes, after which the flask was partly submerged in an ultrasonic bath for ~30 seconds (aiding clay dispersal). The flask was shaken for another 5 minutes and then the clays were allowed to settle for 3 hours. An improved equation of Stokes Law that corrects for temperature/viscosity variation of water (equation 6.1) was used to calculate that at 3 hours particles <2 μm would have settled to <3.8 cm depth. Accordingly, the <2 μm clay fraction was drawn by pipette from 3.8 cm depth, placed on a silicon slide and air-dried overnight. The equation is:

$$t = 18\eta\, h / g(d_p - d_l)D^2 \quad \text{(eqn. 6.1)}$$

Where t is settling time, η is the viscosity of the liquid, h is settling distance, g is acceleration due to gravity, (d_p-d_l) is the difference between the density of the mineral particle and liquid and D^2 is the cross-sectional area of the mineral particle.

The gradual settling of platy clay particles, during air-drying on a slide, causes the clay particles to orientate themselves horizontally on the slide. Accordingly, (001) harmonic diffraction peaks are most prominent on orientated air-dried slides. The prepared slides were analysed using a Philips PW-1710 with Cu-Kα radiation (1.5418Å) at 10,000 volts and 6 milliamps. Step size was 0.02 degrees at 1 degree per minute, from 2 to 35 degrees 2-θ.

Three tests were carried out. The first run was air-dried, followed by ethylene glycol solvation (figure 6.7) and then potassium saturation (figure 6.9). Ethylene glycol solvation was achieved by exposing the air-dried slide to ethylene glycol vapours at 60°C for 12 hours. K-saturation was achieved by soaking a test tube of clays in a 3 molar solution of KCl overnight, followed by thorough rinsing with deionised water and preparation of an orientated 2 μm slide as per procedure.

6.4.1.2 XRD results

XRD analysis of the orientated and ethylene glycol solvated slides (figure 6.7), indicated that the clay is dominated by smectite, indicated by the swelling of a 12.74 Å peak to *c.* 17 Å, with subordinate amount of illite and kaolinite. Furthermore, the position of the *hkl*-005 peak *c.* 3.1 Å (figure 6.8) confirms that the smectite contains montmorillonite not saponite. Following K-saturation (figure 6.9) there was only a slight collapse of the *c.* 12.74 Å peak, showing that the smectite does not contain high charge interlayers (Moore & Reynolds, 1989).

Finally, given the identification of smectite, the Greene-Kelly test was carried out to distinguish the smectite interlayer minerals present (Moore & Reynolds, 1989). The clays were exposed to a 3 molar solution of LiCl overnight and then thoroughly rinsed 20 times with deionised water followed by repeated settling by centrifugation, to remove LiCl. An orientated air dried slide was then prepared as standard and then heated to 250°C for 3 hours. This slide was the treated with Glycerol solvation at 60°C overnight and analysed using the Philips PW-1710 XRD machine with Cu-Kα radiation (1.5418Å) at 10,000 volts and 6 milliamps. Step size was 0.02 degrees at 1 degree per minute, from 2 to 35 degrees 2θ. The XRD traces (figure 6.10) reveals that the smectite is an interlayered mixture of montmorillonite-beidellite i.e. Bentonite. Montmorillonite collapsed to 9.38 Å but did not re-expand after Glycerol solvation whereas beidellite re-expanded to *c.* 20 Å.

XRD analysis indicates that the clays are composed predominantly interlayered montmorillonite-beidellite (Bentonite) with a subordinate amount of illite and kaolinite. The clay mineral assemblage of smectite, illite and kaolinite is typical of argillic hydrothermal alteration (Yang *et al.*, 2002).

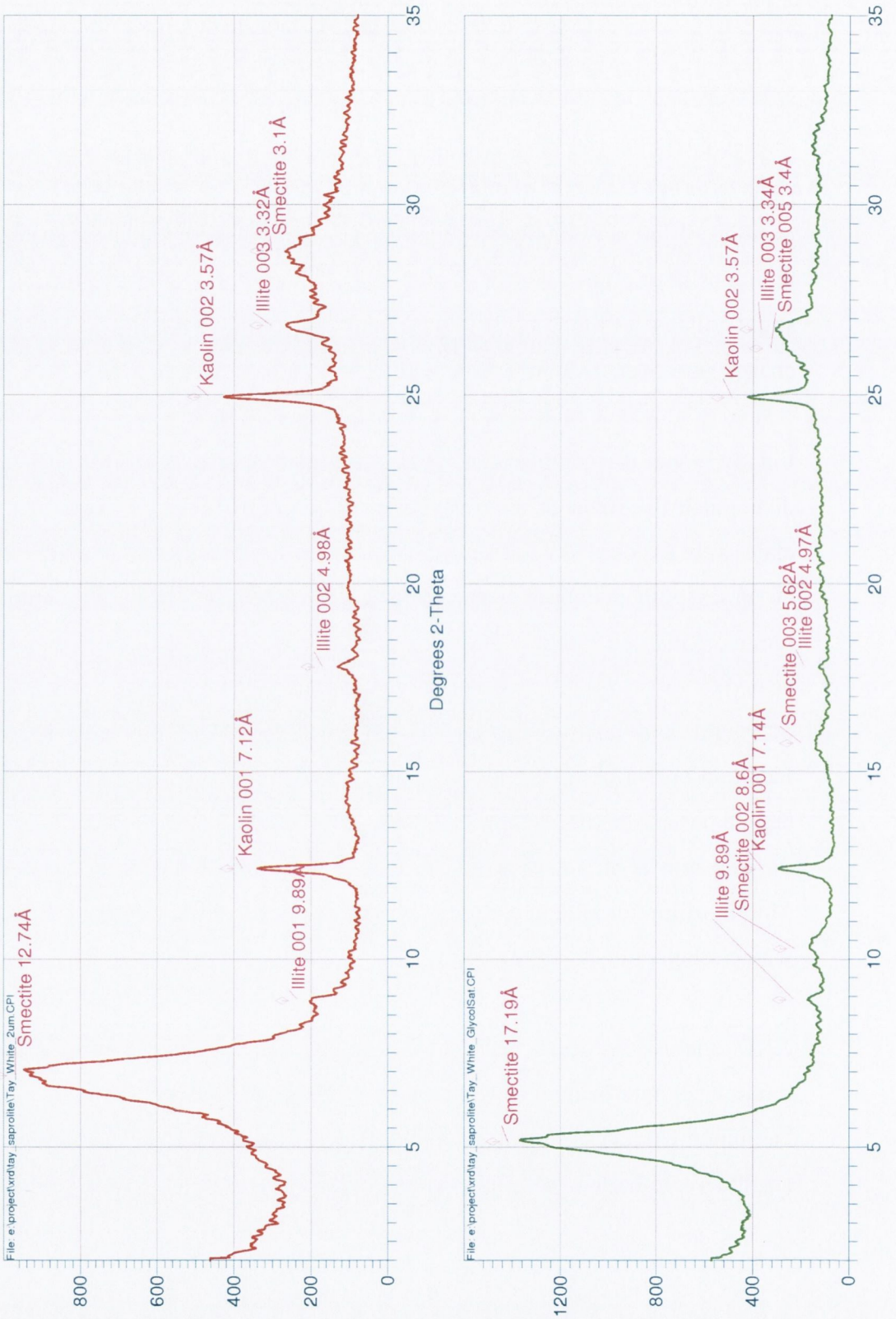

Fig. 6.7: XRD trace of air-dried 2 μm clay fraction (left) and ethylene glycol solvation 2 μm clay fraction (right). Smectite swells to *c.* 17 Å after treatment with ethylene glycol. The clay is dominated by smectite with subordinate kaolinite and illite.

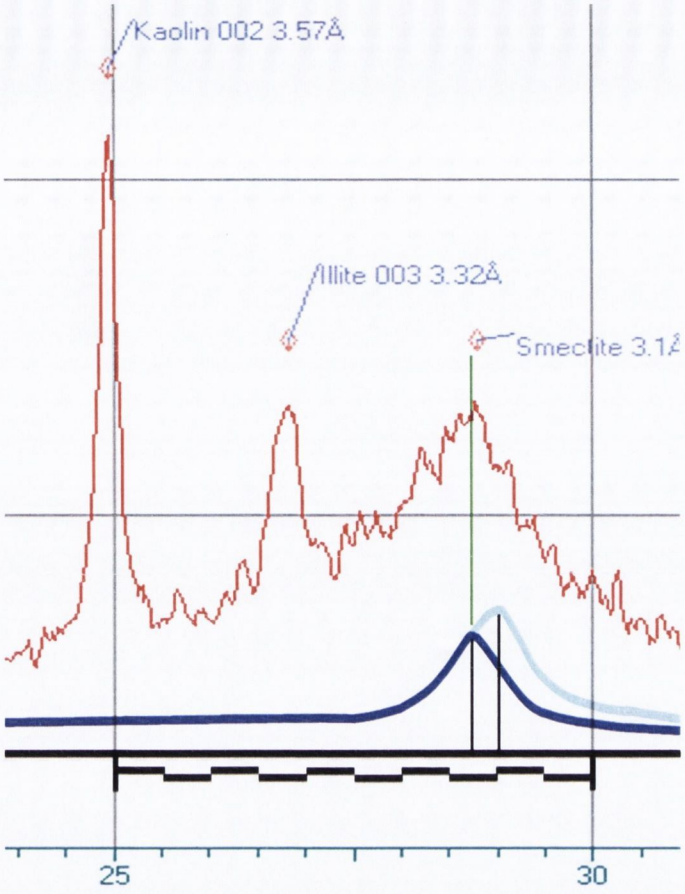

Fig. 6.8: XRD trace of air-dried slide; the *hkl*-005 smectite peak that is near 3.1 Å, indicates that the smectite contains montmorillonite. Comparison peak positions are adapted from U. S. Geological Survey Open-File Report 01-041.

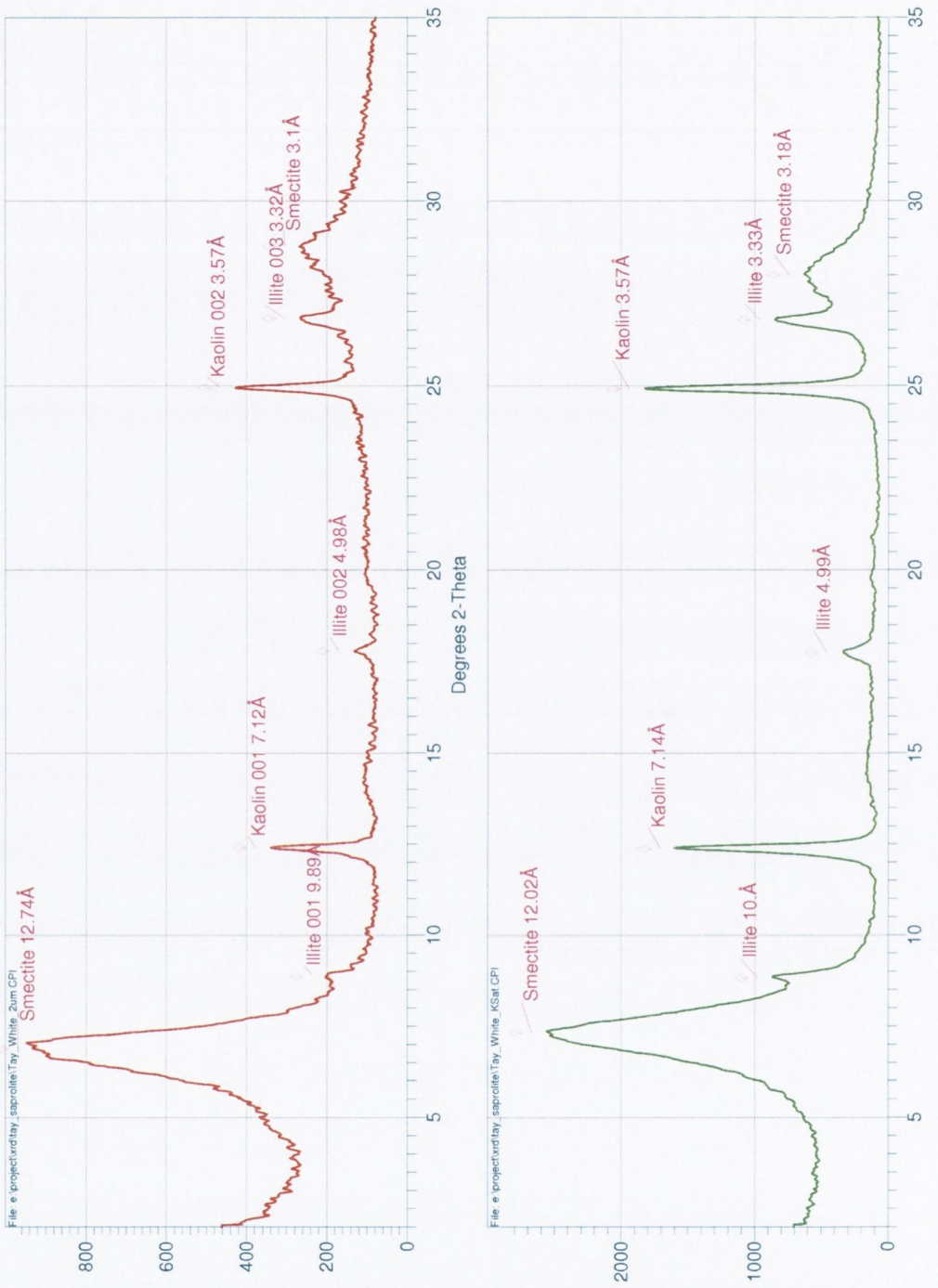

Fig. 6.9: XRD of air-dried 2 μm clay fraction again (left) and K-saturated 2 μm (right). There is only a slight collapse of the *c*. 12.74 Å peak, indicating that the smectite contains few expandable layers.

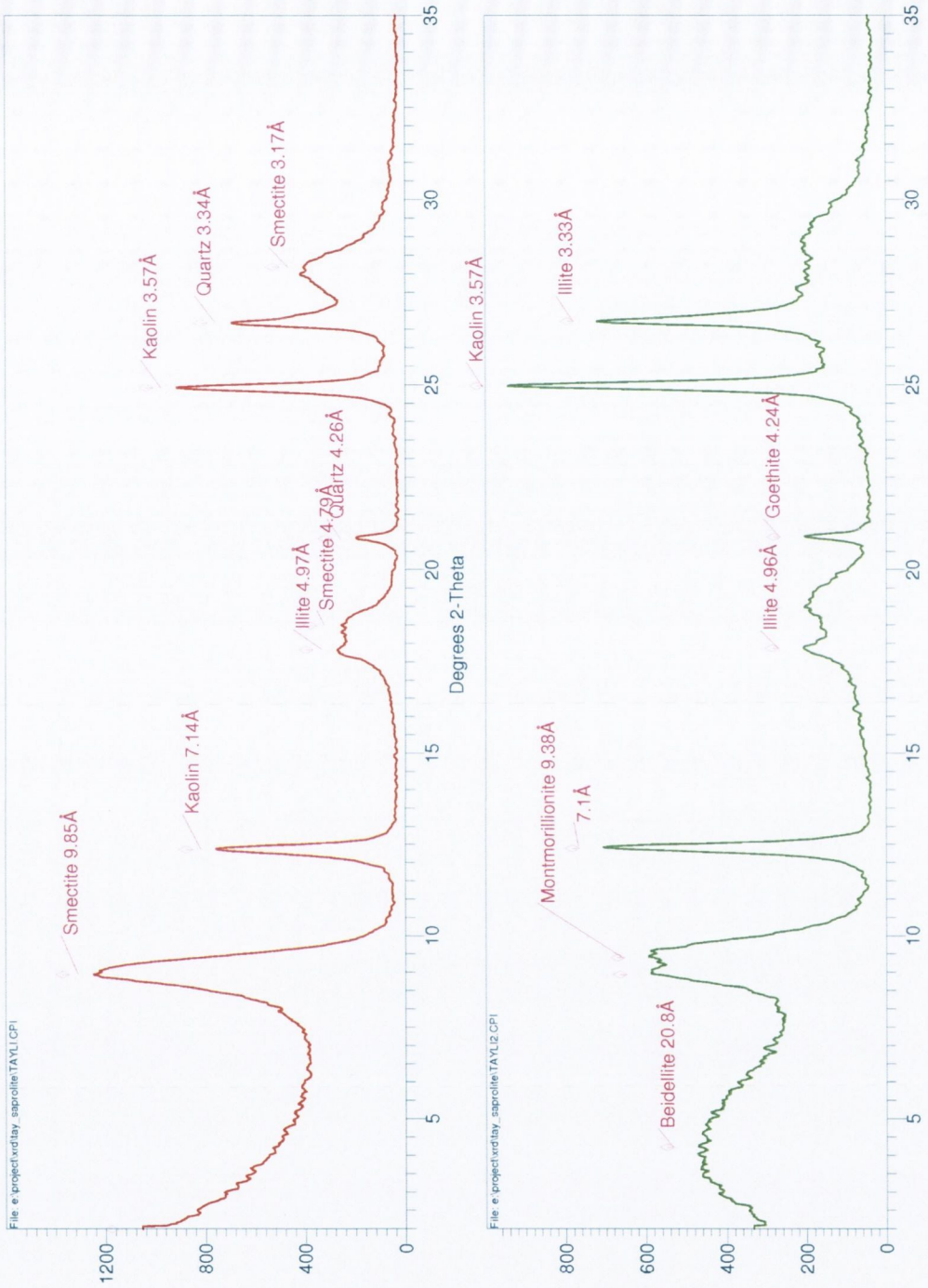

Fig. 6.10: Results of the Greene-Kelly test (right) compared with the XRD trace for the untreated sample (left) indicate the smectite is an interlayered mixture of montmorillonite and beidellite.

6.4.2 Granulometric analysis

Granulometric analysis of the chemically altered adamellite was carried out using wet sieving and the pipette method after Day (1965). Gravel and sand were separated using wet sieving with a 2 mm and 75 μm sieve. The separated gravel and sand fractions were air dried in an oven at 50°C over night and then weighed on an Oertling JB25 laboratory balance.

The remaining silt and clay abundances were determined using the Pipette Method (Day, 1965; Soil Survey Division Staff, 1993). The silt-clay fraction was placed in a 1000 ml cylinder with 20 ml of Calgon and 980 ml of distilled water. The cylinder was agitated for 30 seconds and placed on a bench to settle. A modification of Stokes Law (equation 6.1) was used to calculate the withdrawal time from 3 cm depth, pertaining to <2 μm clays. After 33 minutes of settling, 20 ml of fluid was drawn by pipette from the settling cylinder at 3 cm depth and placed in a 50 ml beaker, dried and then weighed. In addition, because water soluble Calgon was used to disperse the clays, a Calgon Correction Factor (CCF) of 0.04 grams per 20 ml was subtracted from the total weight.

6.4.2.1 Results of granulometric analysis

Gravel	> 2 mm	2.2063 grams – 4.33%
Sand	2 mm to 75 μm	10.9492 grams – 21.5%
Silt	75 μm to 2 μm	35.5962 grams – 69.9%
Clay	<2 μm	2.1700 grams – 4.26%
		(2.17 – 0.1 grams Calgon)
Total Gravel/Sand/Silt/Clay		50.9217 grams
Total Sand/Silt/Clay		48.8587 grams
USDA - Sand/Silt/Clay		22.4% / 73.6% / 4.4%

According to the United States Department of Agriculture (USDA) soil textural classification triangle (Gerakis & Baer, 1999), the altered adamellite is a Silt Loam (figure 6.11)

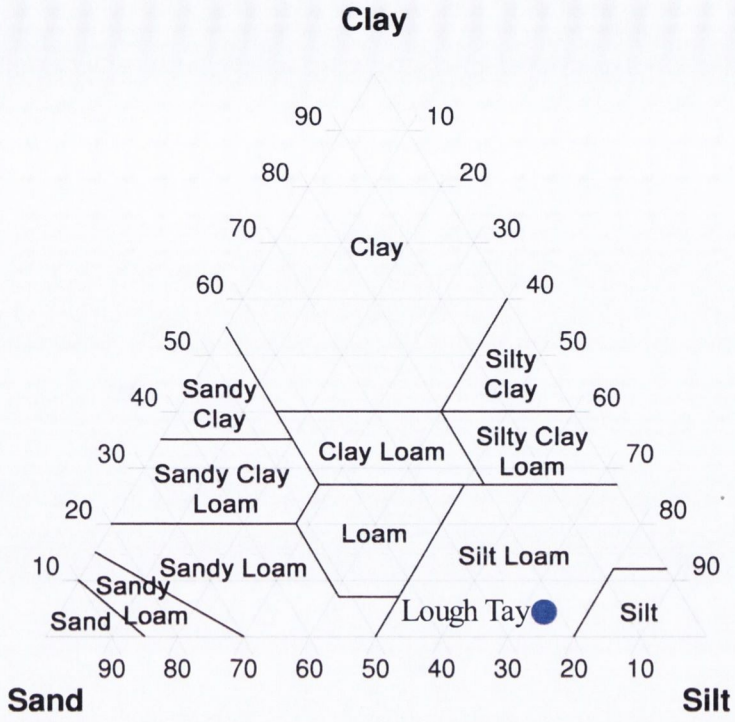

Fig. 6.11: The altered adamellite saprolite plots as a Silt Loam, according to the USDA textural triangle.

6.4.3 Supergene weathering of lead mineralisation

After initial clay mineral analyses were carried out, the site was revisited. On this occasion an exceptionally rich lead sulphide gossan was discovered lying *c*. 2 m left of the sampling site (figure 6.12). Secondary weathering consists of cerussite ($PbCO_3$) and minor anglesite ($PbSO_4$). The cerussite exhibits a pseudomorphous texture after primary (hypogene) cubic galena crystals up to 3 cm on edge. As a result of this discovery, the clay mineral assemblage was reassessed with hydrothermal alteration in mind.

Fig. 6.12; Sample of supergene lead weathering was collected from the outcrop marked with the arrow on the left; the rusty red colour is the gossan weathering. The arrow to the right indicates the approximate location of the exit of the tepid spring in 1998, now covered by debris. The box highlights the sample location

6.5 Discussion

The intimate association of hypogene lead mineralisation, quartz veining and chemical weathering, suggests that the chemical alteration originated though hypogene hydrothermal processes. The interlayered smectite, beidellite-montmorillonite, is diagnostic of argillic alteration and is commonly associated with high-sulphidation epithermal mineralisation and near surface hydrothermal systems.

Intriguingly, Patrier *et al.* (2003) studied clay mineral assemblages associated with hydrothermal activity on Guadeloupe Island, eastern Caribbean Sea, where they found that beidellite-smectite clays are restricted to the very top of geothermal wells and surficial steaming ground. Similarly, Yang *et al.* (2002) found that beidellite-montmorillonite with minor illite is restricted to the low-temperature smectite zone (<180 metres depth) of the Broadlands–Ohaaki geothermal system in New Zealand. These observations indicate that the hydrothermal alteration and associated lead mineralisation at Lough Tay may have been formed less then *c.* 200 metres below ground. The tepid spring could represent waning hydrothermal activity; indeed tepid springs are very rare in Ireland, so the occurrence of this tepid spring beside a zone of hydrothermal alteration is unlikely to be a coincidence. Furthermore, it suggests that the mineralisation and associated alteration is remarkably young.

Given the indications that the mineralisation at Lough Tay is shallow, efforts were undertaken to locate further evidence of shallow mineralisation (e.g. platy calcite and hydrothermal breccia amongst the other nearby lead-zinc veins of east Wicklow).

6.4.4 Platy calcite and hydrothermal breccia

The spoil heaps of the 19th century lead-zinc mines of Glendasan [309840 198320 250m OD] and Glendalough [308640, 212255, 85m OD] *c.* 10 km SSW of Lough Tay, were searched for platy calcite and hydrothermal breccias. Platy calcite is a reliable indicator of near surface fluid boiling (Simmons & Christenson, 1994). Boiling during ore formation causes CO_2 loss,resulting in sudden calcite supersaturation. Calcite, precipitated suddenly from a supersaturated solution forms distinctive thin plates and scales. Observations in the Hishikari low-sulphidation epithermal gold deposit of Japan indicates that platy calcite there was formed just below the zone of fluid boiling (Etoh *et al.*, 2002). Numerous examples of platy calcite were collected from the Glendasan and Glendalough spoil heaps (figure 6.13).

In addition, a sample of hydrothermal breccia was found at Glendasan (figure 6.14) (Drummond & Ohmoto 1985; Dong *et al.*, 1995; Jébrak, 1997). It contains well rounded matrix-supported vein quartz clasts to ~3 mm set in a dark grey flinty quartz matrix. Hydrothermal breccias are more common in the upper 0.5 km of the brittle crust (Sibson, 2000). The platy calcite and hydrothermal breccia indicate that at least some of the mineral veins of Glendasan and Glendalough area were emplaced within *c.* 500 metres of the contemporaneous water-table.

Fig. 6.13: Platy calcite collected from the spoil heaps of Glendasan, County Wicklow. Platy calcite indicates vigorous fluid boiling that caused CO_2 loss resulting in rapid mineralisation (Etoh *et al.*, 2002).

Fig. 6.14: A sample of hydrothermal breccia Glendasan, County Wicklow, with 1 cent coin for scale. The matrix consists of very fine grained flinty quartz. The minute grain size of the ground mass indicates vigorous open-system boiling and rapid cooling of mineralising fluids.

6.6 Conclusions

A weathered lead sulphide deposit at a site overlooking Lough Tay, County Wicklow, is associated with soft clayey argillic hydrothermal wall-rock alteration. It is not palaeoweathering. The clay mineral assemblage of beidellite-montmorillonite, illite and kaolinite is typical of argillic alteration that formed within *c.* 200 metres of the Earth's surface. Its shallow formation indicates that the mineralisation could be remarkably young; indeed the tepid spring may represent ebbing hydrothermal activity. The mineralisation was not formed by waning magmatic heat shortly after the crystallisation of the Leinster Batholith.

With this possibility in mind, other nearby base metal veins were assessed for indicators of shallow mineralisation. Abundant platy calcite was found amongst the spoil heaps of Glendasan and Glendalough lead-zinc mines, and a sample of hydrothermal breccia was located at Glendasan.

Other clay deposits in the study area should be considered with the possibility of hydrothermal phenomena in mind. The identification of hydrothermally altered granite supports the hypothesis that hydrothermal alteration along faults, fractures and minerals veins in the study area influenced topographic development.

Chapter 7 – Surfaces and Rivers

7.1 Chapter summary and introduction

At the outset of this project, attempts were made to test the working hypothesis that the Irish Sea area was uplifted in Paleocene times due to the effects of the buoyant Iceland Plume, forming the Irish Sea Dome (Cope, 1994; Japsen & Chalmers 2000). If the Irish Sea Dome existed, a radial drainage flowing westward across eastern Ireland would have formed. However, no evidence of an early-Cenozoic drainage directed away from the Irish Sea was found in the study area. Instead, an early drainage that flowed south eastward to the Irish Sea, following faults and fractures across a gently tilted landscape, was discovered. In this chapter, that early drainage pattern is described and the nature and origin of landscape tilting is investigated.

This chapter is separated into two main sections, topographic analysis and fluvial analysis. Topographic analysis is separated into two parts; subjective identification of areas of interest that constitute areas of subdued topography, followed by objective statistical analysis of these regions of interest. Objective analysis will show that the northern part of the study area was gently tilted to the south. The cause of this tilting and its implications will be discussed.

Following from surface analysis, the oldest drainage patterns in the southern part of the study area are examined. It will be shown that an early drainage pattern appears to have followed NW-SE faults across a landscape that was gently tilted to the south east. Finally, the bed of a palaeoriver on the summit of Howth Head, County Dublin (*c.* 130 metres OD) provides a valuable clue to the mechanism that caused the observed landscape tilting and uplift.

7.2 Surface Analysis

The following section is divided into two parts. The first part describes the process of subjective identification of areas of interest that include plateau regions. The second part is more objective, and involves applying the objective computer based method Trend Surface Analysis (TSA), to the areas of interest. TSA determines the slope, trend and flatness of a surface.

7.2.1 Subjective surface analysis methods

Areas of interest in the DTMs OSI-50 and SRTM-90, were identified and delineated using three main techniques; hillshading, moving window analysis and slope analysis (see section 3.3.1 for a discussion on the nature and quality of OSI-50 and SRTM-90).

Special care was taken to create high quality shaded relief images of both DTMs in ArcView 3.2. The following procedure was found to produce excellent hillshaded relief maps (figure 7.1):

- The DTM was converted from floating point to integer values using Map Calculator.
- The integer DTM was hillshaded using a vertical exaggeration of 2.
- The integer DTM was then multiplied by 4.7 using map calculator and a relief theme was applied using the Shademax blended colour legend provided by Data Deja View.
- The coloured relief theme was selected and the hillshaded DTM was used as the brightness theme.

The resultant relief theme is a blended combination of the Shademax colour legend and the hillshaded DTM. In addition, 3DEM 18.9 (a GIS program used for the 3D-visualisation of topography) was use to create hillshaded 3-dimensional images and rotating animations of the Calary Plateau area. Three images of the Calary Plateau animation generated by 3DEM 18.9 are presented in figure 7.2.

7.2.2.1 Slope Analysis

Slope analysis is a simple technique that was used to highlight flat and subdued topography; in this case areas with less than 2 degrees slope were highlighted. Slope analysis was carried out using ArcView 3.2 on OSI-50 and SRTM-90, using command derive slope. Slope analysis coloured topography according to its slope, and in this case areas less then 2 degrees were coloured red.

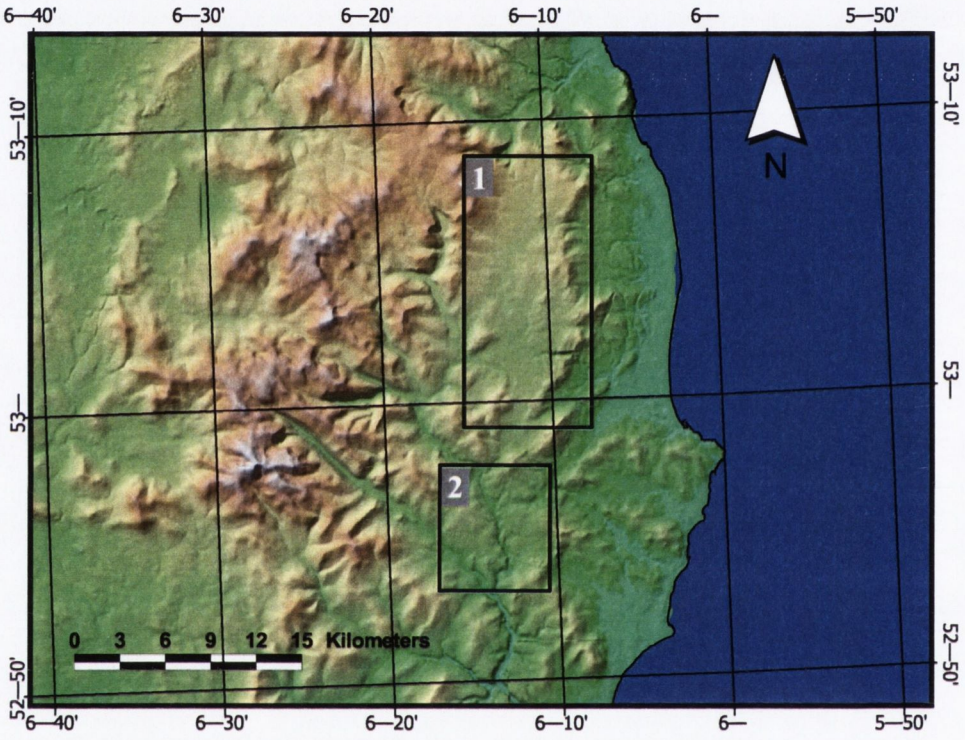

Fig. 7.1: A hillshaded view of the study area produced using the Shademax blended colour legend. Box 1 outlines the Calary Plateau and box 2 outlines the Rathdrum Surface.

7.2.2.2 Moving Window Analysis

Moving window analysis is a technique thathighlights areas within a selected altitude range. Moving window analysis was carried out using ArcView 3.2. Areas within 50 metre altitude range were colour coded red and the image compiled into an animation. In previous studies, the images were viewed in isolation. Animating the moving window analysis greatly improves the visualisation of topography and the identification of areas of low slope. Six images from the slope analysis animation are shown in figures 7.2, 7.3 and 7.4.

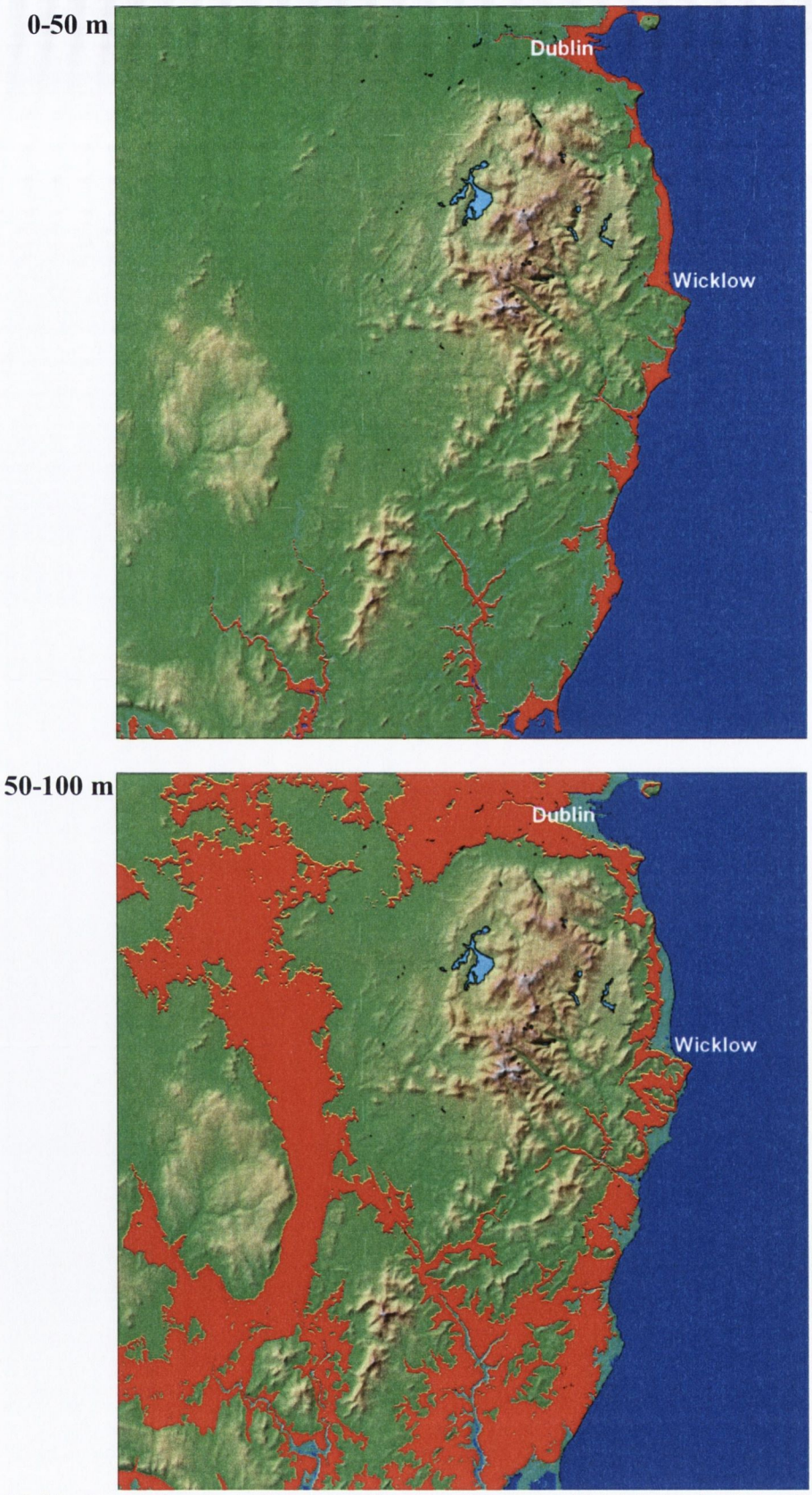

Fig. 7.2: Moving window analysis using a 50 metre window size, highlighting the Coastal Plain.

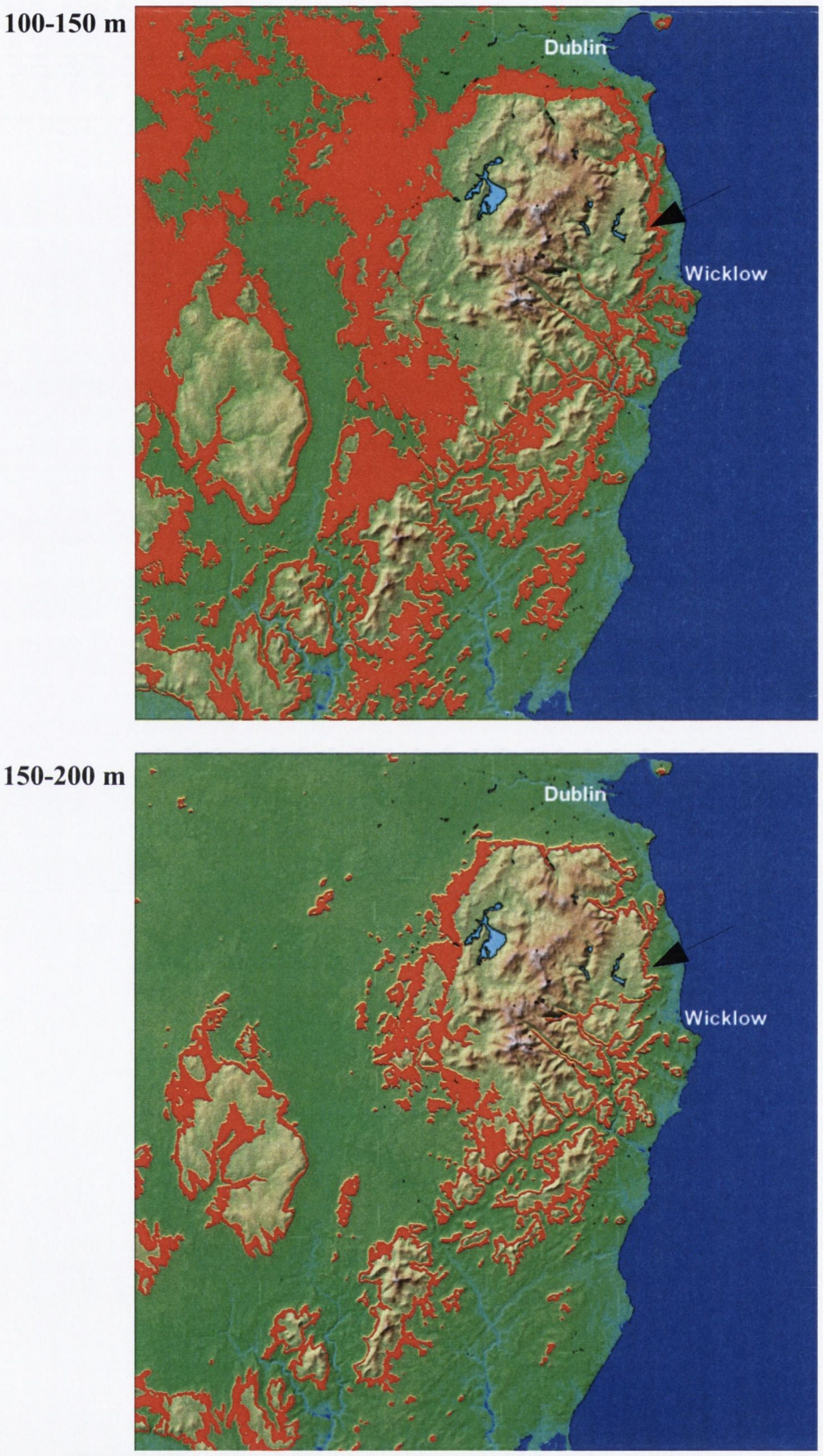

Fig. 7.3: Moving window analysis using a 50 metre window size, highlighting a scarp (arrowed) with increased slope separating the Coastal Plain from the Calary and Rathdrum surfaces.

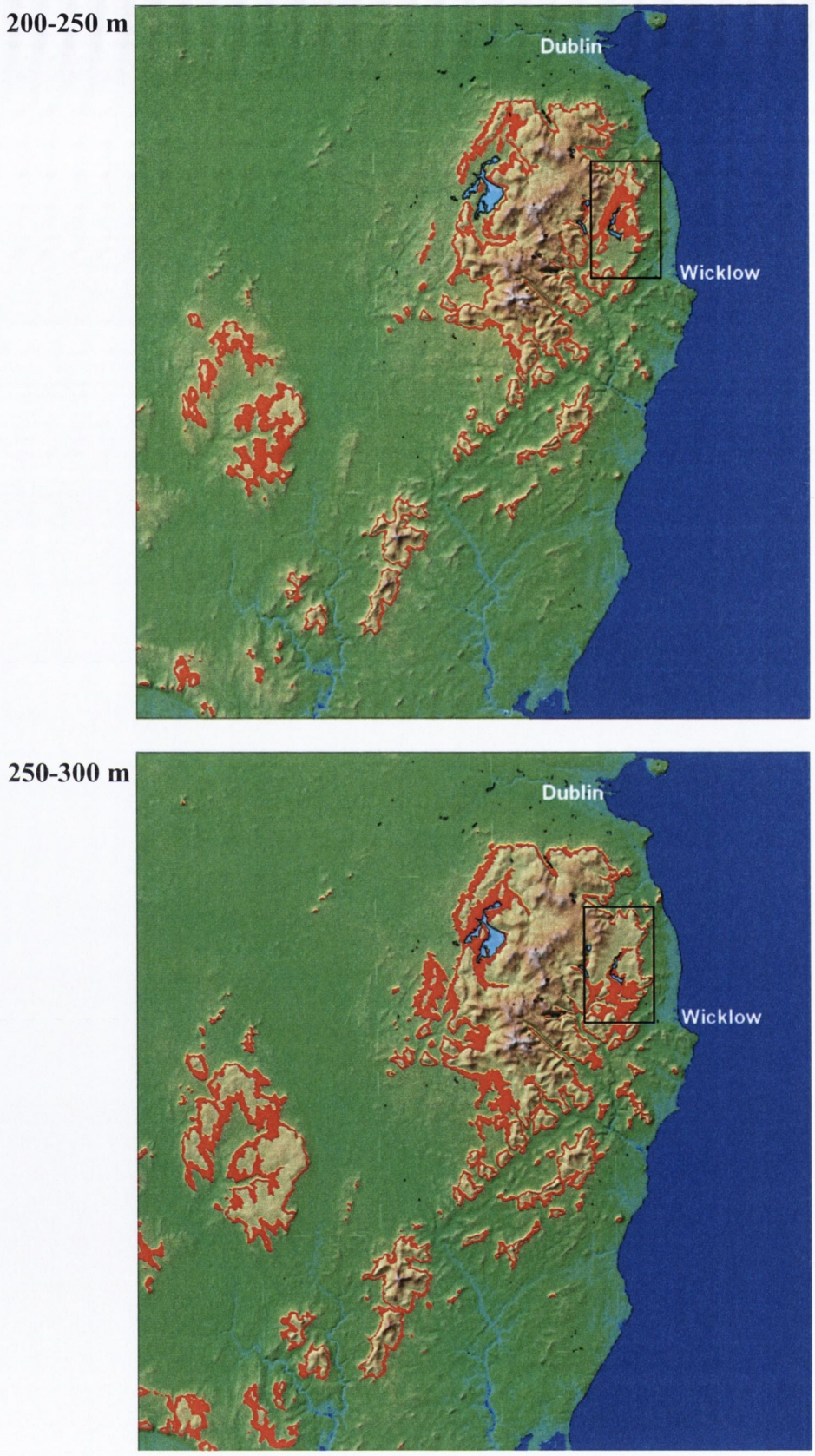

Fig. 7.4: Moving window analysis using a 50 metre window size, the Calary Plateau (highlighted) appears to be gently tilted to the south.

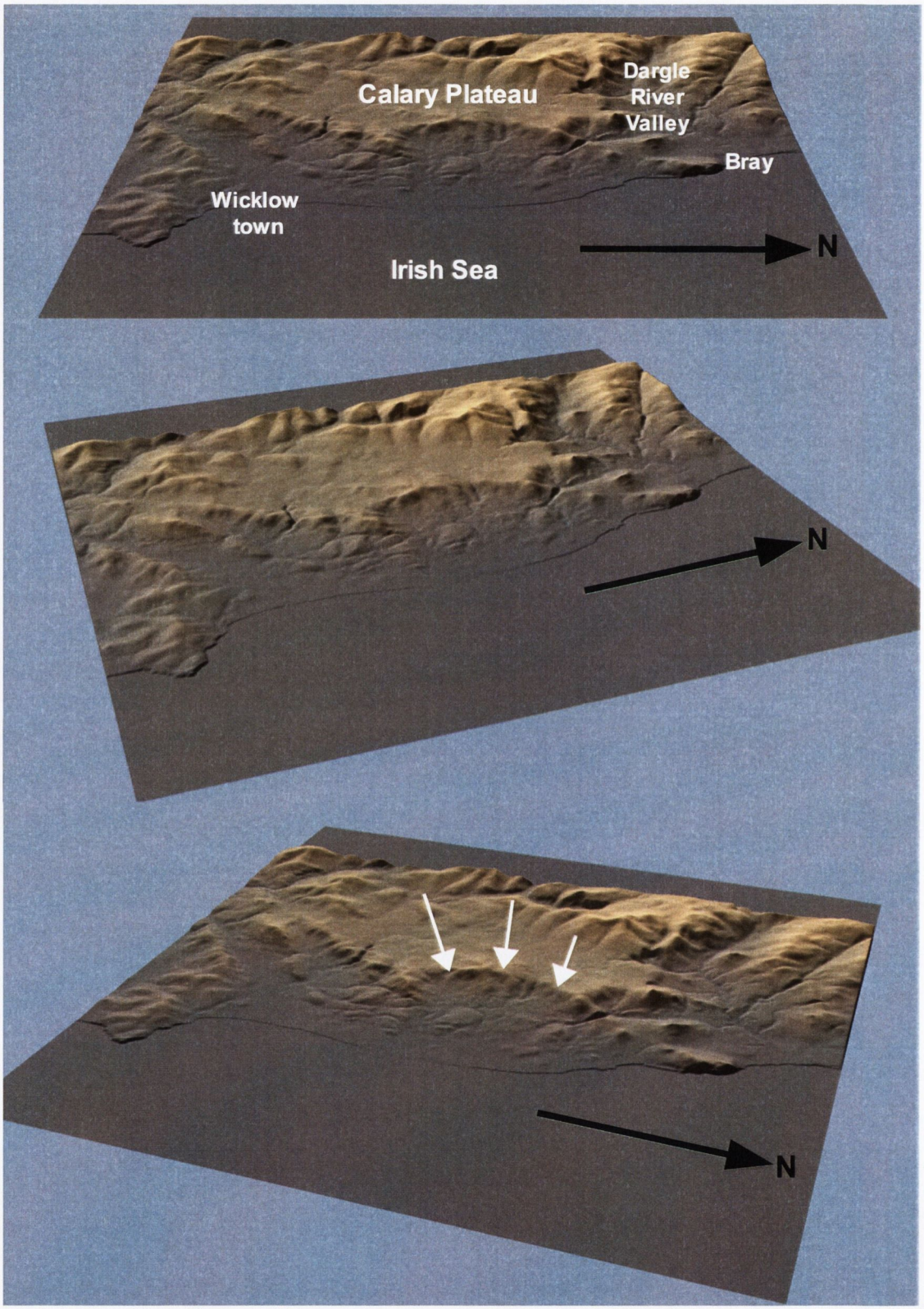

Fig. 7.5: The Calary Plateau looking to the west, visualised using 3DEM 18.9 with OSI-50 DTM. The arcuate scarp (white arrow bottom image) is plainly visible. Note that the broad Dargle River valley truncates the Calary Plateau at its northern extremity (vertical exaggeration is 200%).

7.2.3 Subjective observations

The images clearly show the Calary Plateau and a break in slope consisting of an arcuate scarp front (figure 7.5) separating it from the Coastal Surface to its east, and giving the impression that the scarp formed by erosional retreat directed away from the east. Also, the Dargle River valley truncates the Calary Plateau to its north (figure 7.5) and thus is antecedent to the Calary Plateau.

In addition, compared with the Avoca River which is deeply incised into its bed in a relatively narrow gorge, the Dargle River valley occupies a broad open valley. This suggests that the Dargle River valley is older then the Avoca River valley. It is therefore proposed, that the Dargle Valley is antecedent to the Calary surface.

If the Calary Plateau's arcuate scarp originated through faulting, then the controlling fault must be located near the toe of the scarp. The Bray Fault Zone (BFZ), a normal fault with down to the east motion that bounds the western sector of the Kish Bank Basin (KBB), is the only likely culprit. If the BFZ is the controlling fault, the Calary scarp would have retreated by *c.* 15 km westward (figure 7.6). Indeed, Cunningham (2000) found evidence for a buried Cenozoic river just east of the mouth of the present day Dargle River (figure 7.6).

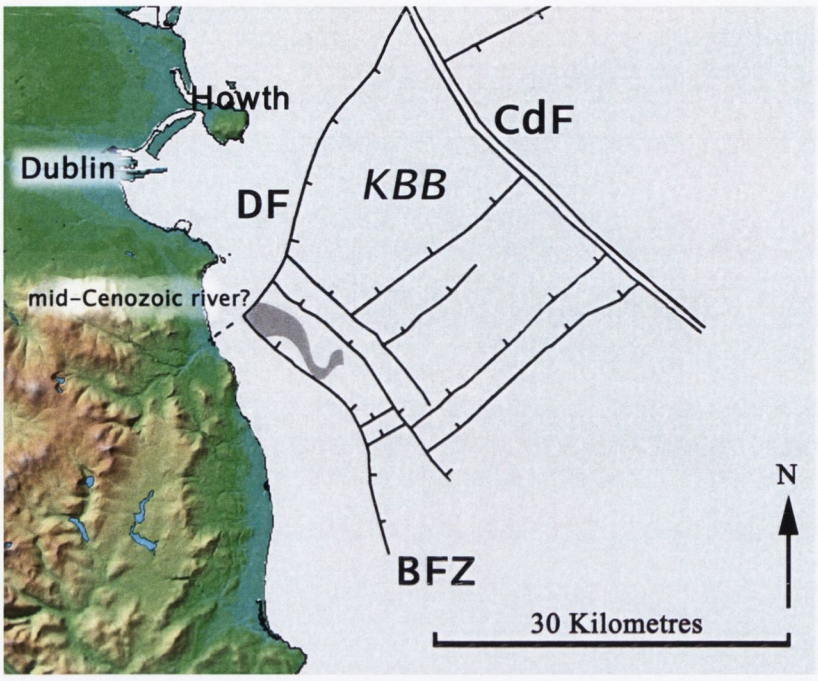

Fig. 7.6: Tectonic map of the KBB with a mid-Cenozoic palaeoriver (grey meandering channel) close to the present day Dargle River (adapted from Cunningham, 2000). Key: KBB – Kish Bank Basin, CdF – Codling Fault, DF – Dalkey Fault, BFZ – Bray Fault Zone.

7.2.4 Selecting areas of interest for objective analysis

In order to analyse the Calary Plateau and Rathdrum Surface using Trend surface Analysis (TSA), it was necessary to extract these surfaces from the DTM covering all of Ireland. In ArcView 3.2, areas with subdued topography of <2 degrees slope were highlighted in red using the command "derive slope". A polygon was then hand drawn around the low slope surfaces, delineating the Calary Plateau and Rathdrum Surface. The polygon was then used to "cookie-cut" just the Calary Plateau and Rathdrum Surface using the ArcView 3.2 script, "grid clip to poly". The result was two smaller DTMs extracted from OSI-50, covering only the Calary Plateau and Rathdrum Surface.

7.3 Trend Surface Analysis

Here TSA is used to objectively measure the slope, trend and flatness of the Calary Plateau, and to test if the Calary Plateau and Rathdrum Surface were originally part of a larger continuous surface.

7.3.1 Methods

TSA was carried out using Microdem 8.0, which employs the least squares method of Davis (1986), a method that can cope with rough terrain. Microdem 8.0 can create trend surfaces up to the 8th order. However, useful results were not gained beyond a 1st order trend surface (figure 7.7).

1st $z = C1 + C2(x) + C3(y)...$

2nd $+C4(x^2) + C5((x)(y)) + C6(y^2)...$

3rd $+C7x^3 + C8((x^2)(y)) + C9((x)(y^2)) + C10(y^3)...$

..... similar progression up to an 8th order trend surface.

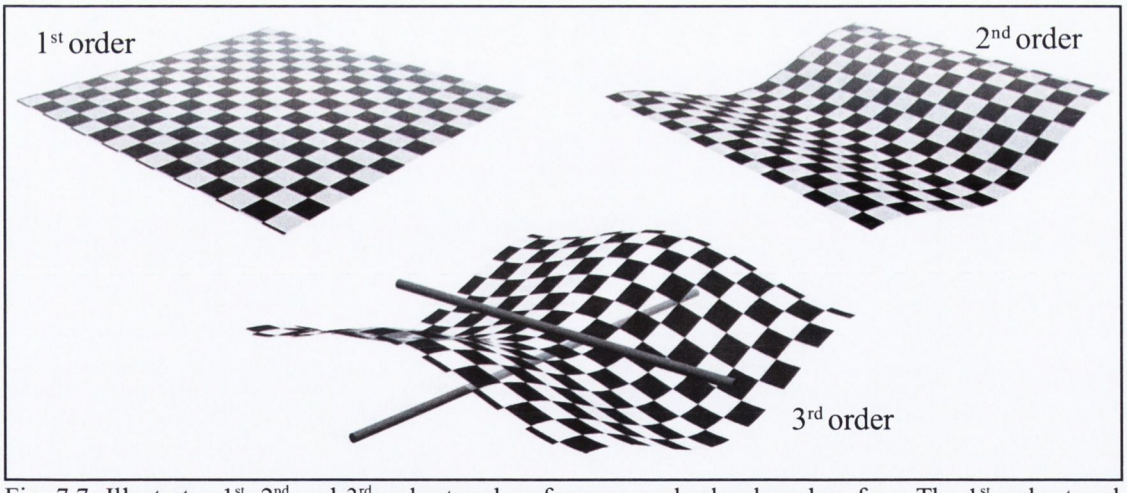

Fig. 7.7: Illustrates 1st, 2nd and 3rd order trend surfaces on a checker board surface. The 1st order trend surface is a simple plane, the 2nd order surface is a curved surface with a single inflexion axis and the 3rd order trend surface is a hyperbolic (saddle shaped) surface with two inflexion axes (highlighted).

The completed TSA analyses includes (figure 7.8) - the Calary Plateau, its residual error surface, the trend surface, a rose diagram depicting the slope and trend of the Calary Plateau and statistical measures of topographic flatness including, Goodness of Fit (R2) and Correlation Coefficient.

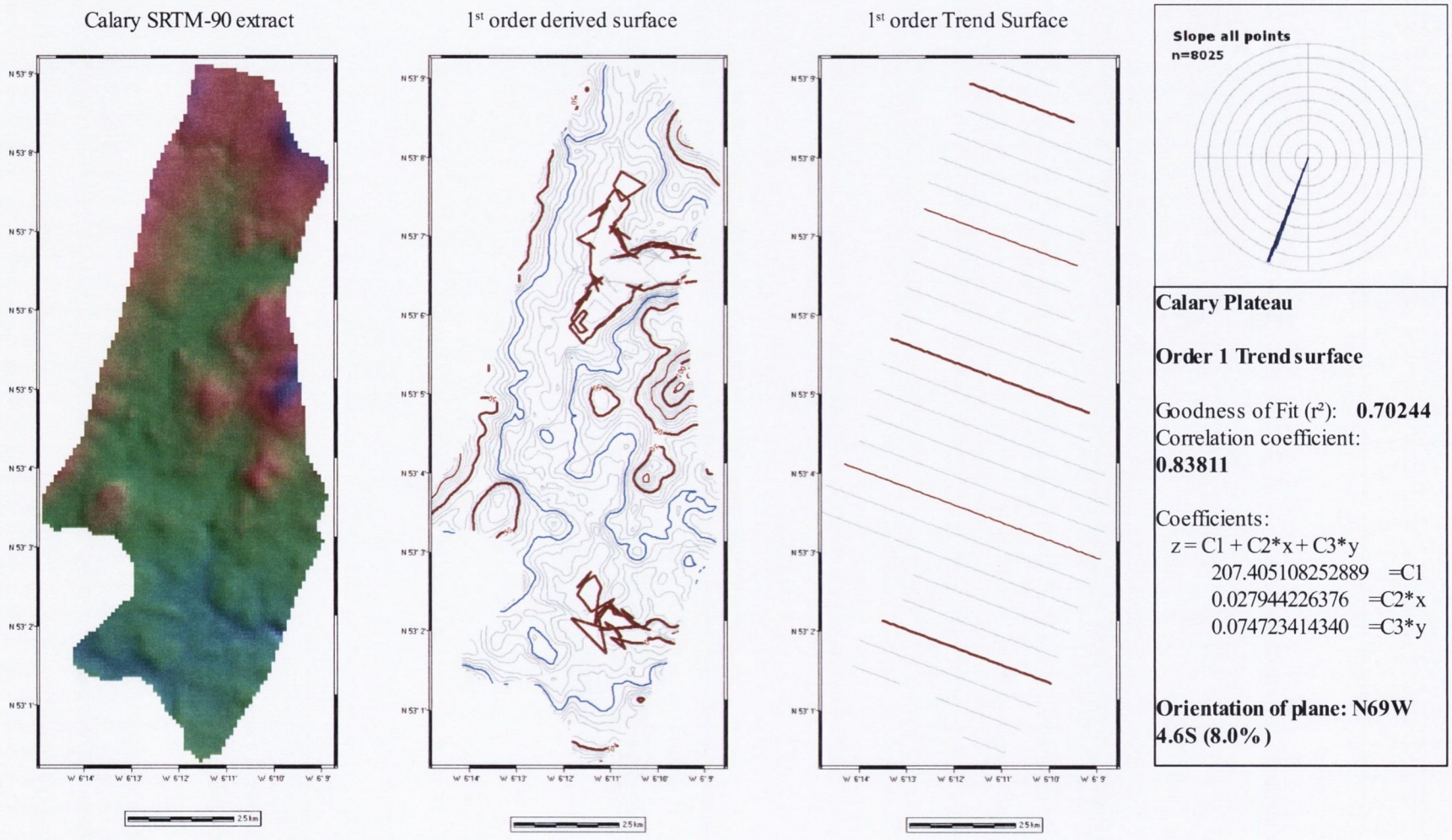

Fig. 7.8: Results of Trend Surface Analysis for the Calary Plateau.

7.3.2 Results of TSA

Cunningham (2000) said that the Calary Plateau is tilted gently to the west. However, results of TSA presented here confirm that the Calary Plateau is gently tilted (8.0% gradient) to the south-south-east; its slope and trend is 69/4.6 S. Additionally, TSA confirms the flatness of the Calary Plateau; it has a Goodness of Fit (r^2) of 0.70244 and a Correlation Coefficient of 0.8381. Furthermore, if the Calary Plateau's 1st order trend surface is extended *c.* 16.25 km south, to the middle of the Rathdrum Surface, the predicted altitude of this extended surface is *c.* 100 metres OD. The Rathdrum Surface is 100 to 130 m OD. This supports the subjective impression that the Calary Plateau and Rathdrum Surface may be fragmented remnants of a larger contiguous palaeosurface tilted to the south.

7.3.3 Discussion

It is likely that the Calary Plateau's scarp originated due to tectonic activity. The Bray Fault Zone, a normal fault in the off-shore Kish Bank Basin, roughly parallels the Calary Plateau's scarp (figure 7.6). Furthermore, Cunningham (2000) studied seismic records for the off-shore Kish Bank Basin and concluded that the Codling Fault, Dalkey Fault, Bray Fault Zone were active during the Cenozoic, evinced by the faults cutting pre-Pleistocene Cenozoic sediments. Accordingly, it is proposed that the Calary Plateau's scarp was formed by Cenozoic activity on the Bray Fault Zone, and that the scarp retreated by *c.* 10 to 15 km. This contradicts Cunningham (2000) who surprisingly placed the Calary Plateau's controlling normal fault at the top of the scarp. Furthermore, the Calary Plateau is tilted *c.* 4.5° to the south-south-west. Mild regional tilting of this type may be caused by isostatic unloading e.g. see Watts *et al.* (2000) regarding the south easterly tilt of England.

7.4 Rivers Pattern Analysis

The working hypothesis at the outset of this study accepted that the Irish Sea area was uplifted during Paleocene times, due to the effects of the buoyant Iceland plume that impinged on the crust, forming a radial drainage flowing away from topography (Cope, 1994; Cunningham, 2000). Accordingly, efforts were made to identify remnants of palaeorivers and transcurrent drainage traversing the Wicklow Mountains and Howth, County Dublin, bordering the western edge of the hypothetical Irish Sea Dome.

7.4.1 Transcurrent drainage

Transcurrent drainage is often found in mountain ranges. It is a type of drainage notable for its disrespect of topography, often flowing perpendicular to the trend of high mountain belts, forming steep sided gorges and valleys in the process (Oberlander, 1985). Often transcurrent drainage is dissected by a later concordant drainage, illustrating that transcurrent drainage is the older drainage pattern.

Drainage pattern evolution studies have examined anomalous transcurrent rivers in several regions of the world, including the Beit-Hakerem and Makhtesh Ramon river valleys, Israel (Matmon *et al.,* 1999), the Rio Almanzora, eastern Spain (Stokes & Mather, 2003) and Umbria-Marche region, Italy (Alvarez, 1999). The origin of transcurrent drainage is not always clear and a number of mechanisms have been developed to explain the formation of transcurrent drainage formation. Four main basic mechanisms are proposed. They are:

- Antecedence: Antecedence implies that transcurrent drainage is older then topography. In this case rivers flow across a flat land surface that gradually evolves towards a landscape with topographic relief over geological time, and if a river posses sufficient erosive power it can maintain its course to form transcurrent drainage that cuts across developed topography.

- Superposition: Drainage flows over a geologically simple surface, gradually erodes down into a complex geology beneath an unconformity, forming transcurrent drainage. First proposed by Jukes (1862) regarding the rivers of southern Ireland.

- Stream capture: Headward erosion of an actively eroding river captures an adjacent river in neighbouring valley, thus connecting the two drainage basins across topography.

- Ponding and overflow: If a river's course suddenly becomes blocked (e.g. landslide) and may form a ponded lake. The ponded lake eventually overflows and finds a new route over topography. The resulting ephemeral flood will cut a gorge and form transcurrent drainage across topography.

Additionally, these three basic mechanisms have been combined by some workers:

- Oberlander's structural superposition: - This is a variation on the superposition model, proposed by Oberlander (1985) who studied the fold belts of the Zagros Mountians, Iran. He proposed that rivers flowing over gradually uplifting anticlines can maintain their course to create transcurrent drainage.

- Hunt's Anteposition: - Hunt's anteposition is a variation on the stream capture model. River capture events are confined to linear lines of weaknesses such as faults and fractures that cut across mountain ranges, resulting in transcurrent drainage.

According to Meek & Douglass (2001), European researchers most often cite antecedence and superposition as the cause of transcurrent drainage, whereas researchers in the United States disproportionately favour stream capture due to the availability of popular texts in the United States describing the mechanism. According to Meek & Douglass (2001), ponding and overflow is an under-appreciated mechanism that can form transcurrent drainage.

7.4.2 Previous work in the study area

The drainage evolution within the study area has received relatively little attention. Workers who commented on the fluvial geomorphology within or near the present study area include: Jukes (1862), Farrington (1929), Davies (1960), Mitchell (1980, 1986) and Cunningham (2000).

The anomalous and transcurrent nature of major rivers in southern Ireland was first noted by Jukes (1862). He described unusual drainages of the Shannon, Blackwater, Barrow, Nore, Suir and Lee, that he termed "transverse ravines". Jukes (1862) believed that the River Barrow at Graiguenamanagh gorge, where it flows between Mount Brandon and Dranagh Mountain, formed by superposition.

Farrington (1929) studied the drainage evolution of the Liffey and King's River basins and attempted to recreate the oldest, pre-glacial, drainage pattern. He gathered outcrop and depth to bedrock data, and constructed a bedrock surface map for the Liffey and Kings River basins. Using the bedrock surface, Farrington (1929) reconstructed the pre-glacial state of the River Liffey and Kings River and described their subsequent drainage development, which involved stream capture of the Kings River by a pirating stream of the River Liffey basin that followed the erodible Pollaphuca Formation.

Mitchell (1980) commented on the anomalous features exhibited by rivers and streams in south east Ireland, basing his findings on Ordnance Survey topographic maps and Landsat®-3 digital imagery. Mitchell (1980) classified drainage into two categories, a transcurrent consequent drainage and a strike parallel subsequent drainage. Mitchell (1980) observed that the transcurrent drainage is heavily dissected by the strike parallel drainage, and from these observations he concluded that the transcurrent drainage is the oldest drainage pattern in the study area. Mitchell (1980) also stated that the transcurrent drainage was initiated during uplift of the Wicklow Mountains and that this early drainage flowed away from the area of greatest uplift in a radial pattern that disregarded the Caledonian structural grain. Later, this early drainage was dissected by a subsequent drainage that followed the Caledonian structural grain.

Mitchell (1986) described the fluvial geomorphology of the Avonmore River, again basing descriptions on topographic maps and Landsat®-3 satellite imagery. The Avonmore River, Mitchell (1986) observed, is deeply entrenched into the Avoca Surface by *c.*120 meters, from Avonmore village to *c.* 4 km west of Arklow in the south. The tributaries of the Avonmore River are also deeply incised and flow radially towards the Avonmore River. Mitchell (1986) proposed that the incision of the Avonmore River is due to tectonic uplift rather then base level fall. If base-level fall was responsible, other rivers in Ireland should be similarly entrenched, but this is not the case. Mitchell (1986) named the uplifted area the Annagh-Avoca Block.

Cunningham (2000) commented briefly on the drainage characteristics within the study area; that a number of rivers in east County Wicklow posses nick points along their courses, suggesting recent tectonic movement, perhaps related to normal faulting to the east.

7.4.3 Materials and Methods

Examination of the fluvial geomorphology of the study area was carried out using ArcView 3.2 with the DTMs OSI-50 and SRTM-90 (see section 3.3.1). River data for south east Ireland provided by the Ordnance Survey of Ireland in DXF format and was converted to shapefile format for use in ArcView 3.2 (see section 3.3.2). This available date was:

- 50 meter resolution DTM from the Ordnance Survey of Ireland (OSI-50).
- 90 meter horizontal resolution Shuttle Radar Topography Mission (SRTM-90)
- River data for study area supplied as ArcView shapefile from the Ordnance Survey of Ireland.

7.4.4 Fluvial geomorphology of the Potters Stream and Three Mile Water

The coastal Potters Stream and Three Mile Water river valleys run roughly parallel to each other, approximately NW-SE. Both river catchments are situated in broad valleys where hill slopes are subdued. Many of the hilltops are near horizontal, giving the landscape the impression of a dissected plateau surface. It appears that long term erosion of the landscape broadened the valleys and reduced hill slope angles.

Near the coast, there is an area of high ground (*c.* 200 meters) separating the Potters Stream and Three Mile Water river valleys. The width of the high ground is greatest towards the coast but progressively narrows inland, consistent with the area of subcropping Ballymoyle Formation, which contains hard wearing rhyolite, rhyolite breccias and volcanic tuffs. The separation between the valleys decreases towards the Deputies Pass (Fig. 7.9).

Immediately to the west of where the two valleys coalesce, the Potters Stream breaches an area of high ground at Deputies Pass as a 60 meters deep, steep sided gorge *c.* 1 km long. Beyond the Deputies Pass, there is a linear area of low ground that trends NE-SW, henceforth referred to as the Glenealy Low. The Glenealy low is between 50 and 80 meters altitude and is surrounded by higher ground between 120 and 200 meters.

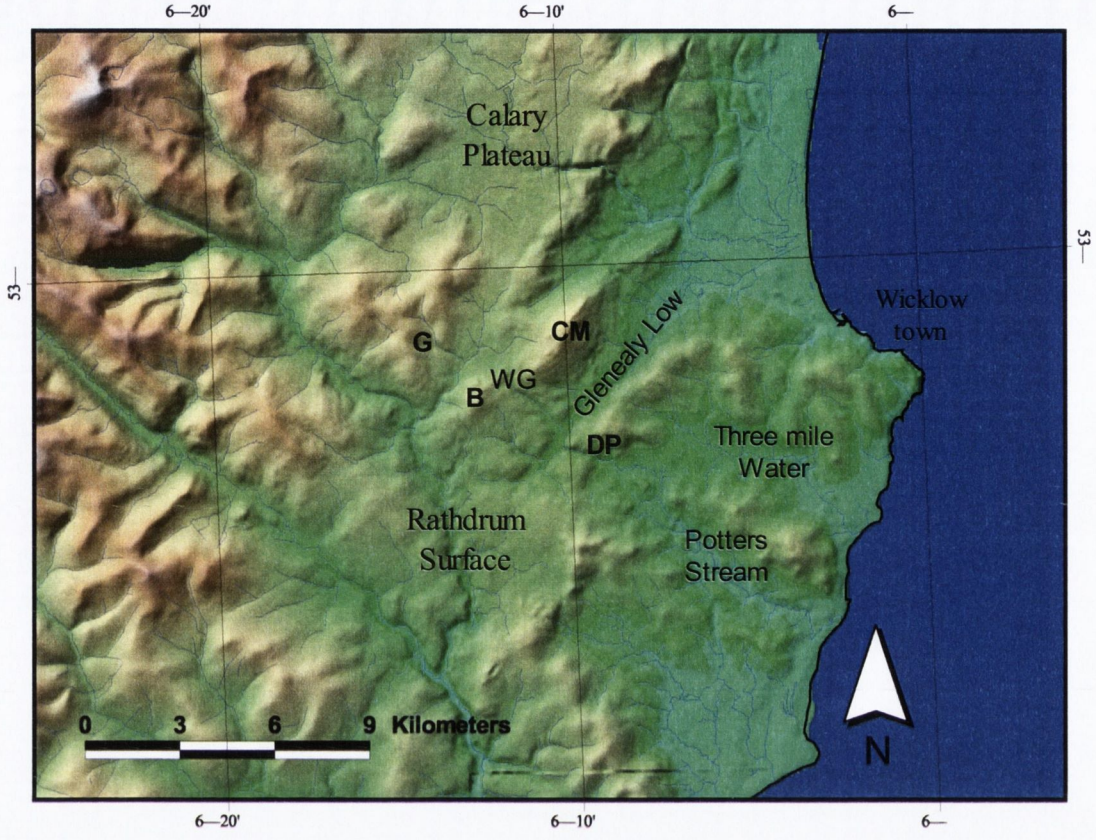

Fig. 7.9: Potters Stream/Three Mile Water area of south east County Wicklow. Key: DP – Deputies Pass, B- Ballinastraw, CM - Carrick Mountain, G- Glenwood, WG – wind gap.

The Potters Stream continues to the north west towards a wind gap between Ballinastraw and Carrick Mountain. The area near the wind gap is underlain by resistant Bray Group quartzite. On the other side of the wind gap, a stream near Glenwood appears to follow the projected continuation of the Potters Stream and this river is also incised deeply into its bed.

7.4.5 Discussion

It is proposed that the Potters Stream and Three Mile Water are antecedent and the rivers follow deeply weathered fractures or faults. Deep chemical weathering may have progressed fastest along NW to SE orientated fractures and faults, due to the focusing of south east directed ground water flow in a landscape that was undergoing gentle tilting to the south east.

The trend of the coastal Potters Stream and Three Mile Water valleys appears to be partly controlled by the subcropping exposure of Ballymoyle Formation that contains resistant rhyolite, rhyolite breccias and other volcanics. This agrees with Cunningham (2000) who observed that rhyolite often forms high ground above other less resistant rock types. The Glenealy Low is predominantly underlain by the Maulin Formation and it is bounded to its north west by resistant Bray Group quartzite and to its south east by relatively resistant Kilmacrea Formation and Oakland's Formation. Thus, it is likely that the Glenealy Low originated through preferential erosion of Maulin Formation. However, the tributaries of the Potters Stream appear offset dextrally, and tectonism is an alternative possibility that seems to have some support.

7.4.6 Tinahely Hills and adjacent areas

This section will discuss the transcurrent drainage of the Tinahely Hills, Croghan Mountain and Annagh Hill.

7.4.6.1 Geology and fluvial geomorphology

The Tinahely Hills follow the boundary between the Tullow Pluton and the country rocks of the Maulin Formation (figure 7.10). North west of the Tinahely Hills there is the extensive subdued topography of the Tullow lowlands, that is underlain by the Tullow Pluton. The Tinahely Hills approximately coincide with the East Carlow Deformation Zone (ECDZ). The ECDZ is a sinistral shear zone that follows the Tullow Pluton and adjacent aureole schists (McArdle *et al.* 1986). Cunningham (2000) proposed that the Tinahely Hills were recently uplifted along the ECDZ, indicated by incision of the River Slaney where is crosses the Tinahely Hills, the presence of 2 wind gaps and 4 water gaps.

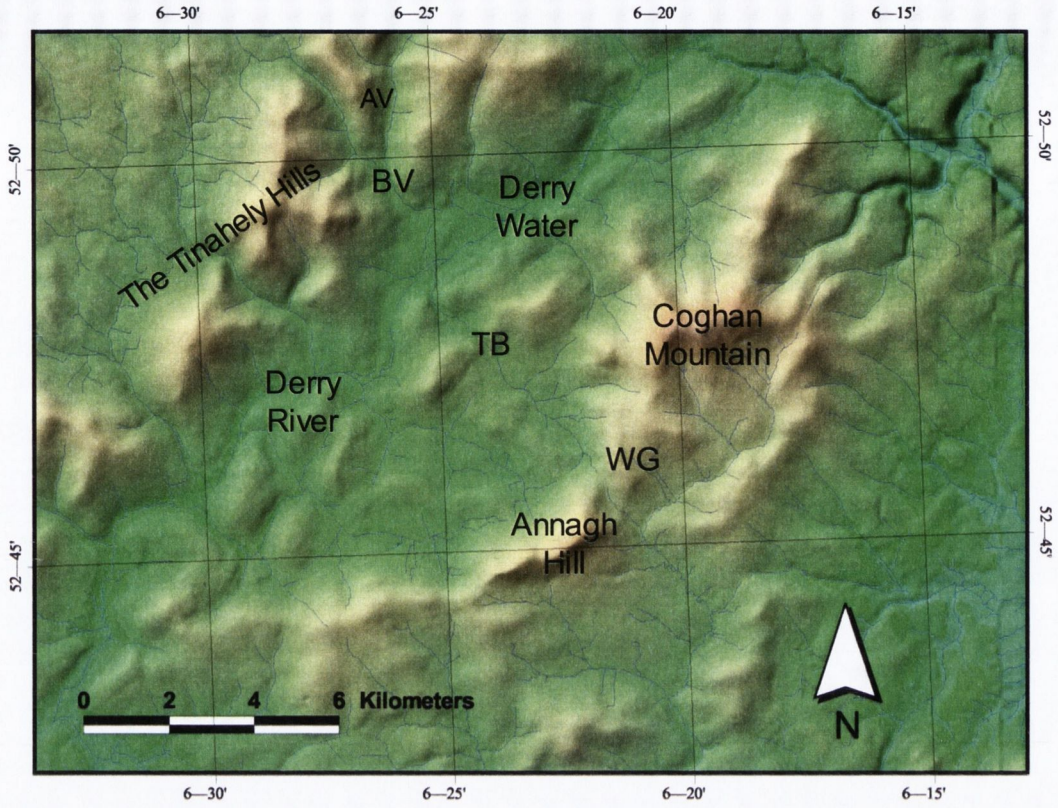

Fig. 7.10: Locality and drainage map for the Tinahely Hills area of south County Wicklow–north County Wexford. Key: WG – Wicklow Gap of Country Wexford, TB - Toberpatrick Bridge, BV - Ballinglen Valley, AV - Askanagh Valley.

Immediately south east of the Tinahely Hills is the Derry Corridor, an area of low ground and former site of a palaeoriver now occupied by the Derry River and Derry Water. The Derry River and Derry Water flow away from each other along the topographic low; the Derry Water flows north east and the Derry River flows south west. Derry Corridor lies along the ECDZ and the south eastern slopes of the Tinahely Hills. Four water gaps and two wind gaps breach the Tinahely Hills. The water gaps include the River Slaney and Derry River. The River Slaney is incised into its bed to 50 meters along a 6 km straight course as it approaches the Tinahely Hills from the Tullow lowlands (Cunningham, 2000). It has a low sinuosity index indicating possible uplift focused along the Tinahely Hills (Cunningham, 2000). Further to the south east are Croghan Mountain and Annagh Hill (figure 7.10).

Between the two hills is the Wicklow Gap of County Wexford. The gap lies on the NW-SE trending Annagh Fault (Mitchell, 1986). Also, the wind gap has a flat bottom to it, *c.* 400 meters wide, much like a dry river bed; other wind gaps in the study area are saddle shaped.

To the north west of the Wicklow Gap, the drainage breaches a line of hills, *c.* 250 meters OD, and the drainage is clearly transcurrent. The river again displays transcurrent drainage to the north east, breaching another line of hills between Coolalug Wood and Killavney Wood. The river then joins the Derry Water and drains to the north east along the Derry Corridor.

On the north west side of the Derry Corridor and slightly offset dextrally in comparison with the apparent continuation of the river flowing north west from the Wicklow Gap, County Wexford, is the steep sided Ballinglen Valley which breaches the Tinahely hills and joins the Tullow lowlands. The Askanagh Valley also joins Ballinglen from the north. The Askanagh Valley is a hanging valley and it is truncated by the Ow river valley to its north east.

7.4.6.2 Discussion

It is proposed that a south easterly directed palaeodrainage developed on a subdued surface that was gradually tilted to the south east. The early drainage pattern was confined along NW-SE faults that may have witnessed hydrothermal alteration and/or deep weathering. Deep weathering may have progressed fastest along NW-SE orientated fault because they focused ground water that flowed to the south east.

The drainage flowing north west from the Wicklow Gap County Wexford is likely the remnant drainage that originally flowed to the south east via the Wicklow Gap of County Wexford. The three gaps, Wicklow Gap in County Wexford, Toberpatrick Bridge and Coolalug Wood/Killavney Wood gaps are all located along the Annagh Fault.

It is likely the Annagh fault captured an early drainage that developed on a subdued landscape that was gently tilted to the south east. In addition, the observation that the Askanagh valley near Ballinglen turns to the south east, agrees with a drainage directed to the south east (figure 7.10).

7.4.7 The Howth Strath Surface

During field work, an enigmatic V-shaped horizontal surface cut into obdurate Cambrian quartzite was found near the summit of Howth Head, County Dublin (near 327990 237875 OD) (figure 7.11). In order to visualise the surface, a photorealistic virtual terrain model was created of Howth Head using the scenery visualisation program Terragen, combined with a 10 metre DTM and *c.* 1 metre resolution aerial photograph. Several images and "flyby" animations were created of the surface, and these greatly aided its visualisation.

Fig. 7.11: An aerial photograph of Howth Head, showing the location of the possible strath surface (yellow box). The surface is located *c.* 130 metres OD near the highest point of the peninsula.

The surface is not obviously related to bedding, jointing or faulting. The quartzite bedrock is massive and it is cut by numerous irregularly orientated quartz veins (van Lunsen & Max, 1975). The flat surface appears to be a strath, the bed or terrace of a bedrock palaeoriver; henceforth referred to as the Howth Strath Surface.

The V-shaped morphology of the Howth Strath Surface is suggestive of a river confluence that flowed towards the north west (figures 7.12 & 7.13). Furthermore, the strath indicates that *c.* 130 metres of differential erosion has taken place since its formation and that it represents the last vestige of the palaeoriver that formed it. Clearly, any contemporaneous palaeorivers that flowed across the nearby limestones terrain, west of Howth Head, have been eroded away.

Fig. 7.12: The Howth Strath Surface looking to the south east from from an altitude of *c.* 200 metres.

Additionally, the loss of 130 metres of limestone likely caused isostatic uplift of Howth Head, proportional to the amount of limestone that was eroded. Accordingly, the limestone surface surrounding Howth Head would have remained close to sea level while Howth gradually gained altitude due to the effects of isostatic unloading (Watts *et al.*, 2000; Simms, 2004). This would explain why a palaeoriver now rests in a horizontal repose near the summit of Howth, marooned *c.* 130 metres above the surrounding limestone plain.

The age of the Howth Strath surface may be estimated by calculating the time needed to erode 130 metres of limestone. Using an erosion rate of 40 to 50 mm ka^{-1}, cited by Drew (2001) for the Burren of Country Clare, the Howth Strath Surface may be 3.25 to 2.6 Ma, mid to late Pliocene.

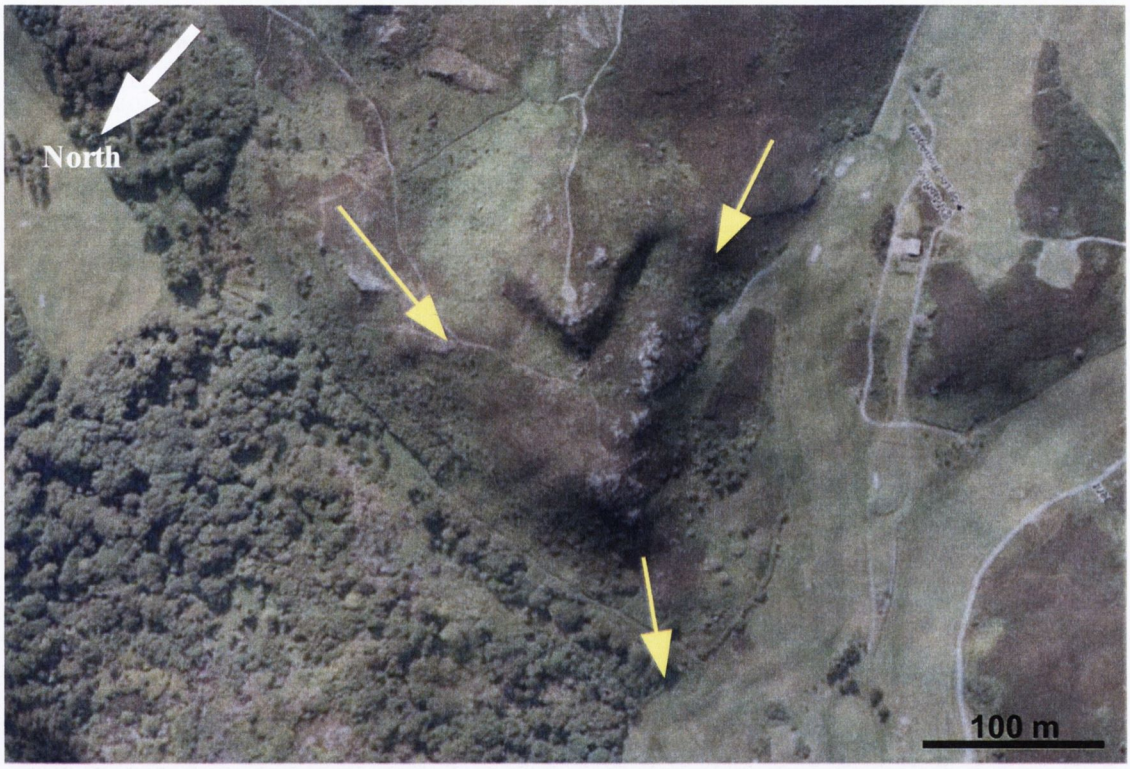

Fig. 7.13: The horizontal surface on Howth viewed from an altitude of *c.* 600 metres, illuminated by sunlight glancing from the south east. The surface forms a V-shaped notch, suggestive of a river confluence that flowed north westwards (river flow directions are indicated by arrows).

It is likely that contemporary pre-glacial (>2.588 Ma) palaeorivers in the limestone terrain near Howth were lost, due to the effects of erosion and concomitant isostatic uplift. Furthermore, regional isostatic uplift could explain the gentle southerly tilt of the Calary Plateau and Rathdrum Surface to the south and the *c.* 200 metre incision of Avonmore River.

7.5 Conclusions

It is proposed that the early parallel north west to south east drainage of the Potters Stream, Three Mile Water and the Tinahely Hills area, formed on subdued landscape that was tilted to the south east in pre-glacial times. It is likely that deep weathering progressed in pace with gradual uplift along fracture systems and faults, and that deeply weathered faults and fractures captured and confined the early drainage. Following tilting to the south east, the northern part of the study area appears to have been gently tilted to the south, evinced by the Calary Plateau – Rathdrum Surface. The strath surface on Howth Head, County Dublin, suggests that landscape tilting and uplift may be related to the erosional isostasy caused by the removal of easily dissolved Carboniferous limestone. It is proposed that obdurate lithologies that form high ground in Ireland, have risen relative the surrounding limestone plain by 100 to 200 metres in the last 3 My, due to isostatic effects.

The Dargle River appears to pre-date the uplift and tilting of Calary Plateau. Indeed, the spatial association between it and a pre-glacial palaeoriver immediately to its east in the offshore KBB, is further evidence of its antiquity.

Finally, apart from a suspected north west directed palaeodrainage on Howth Head, no robust evidence for a radial drainage system directed away from the hypothetical Paleocene Irish Sea Dome was found. Known erosion rates for limestone in Ireland indicate that the suspected palaeoriver on Howth Head posts dates the mid-Pliocene. Accordingly, it is unlikely that pre-Pliocene palaeorivers await discovery in the limestone terrains of Ireland, but they may survive in upland regions where the oldest landscapes of Ireland are preserved.

Chapter 8 – Conclusions and suggestions for further work

The following is a summary of the main findings of this thesis and some suggestions for future avenues of research.

8.1 Conclusions

It is proposed that the weathering profile at Timahoe, County Kildare, is a pocket deposit that formed when the weathering of pyrite liberated sulphuric acid that decalcified limestone. It is proposed that the iron rich dark silica-clays are the residuum of a formally pyrite rich lithology. The work of Chigara & Oyama (1999) suggests that the Timahoe pocket deposit experienced vertical groundwater flow during its formation, in a well drained hilly landscape. The practice of reconstructing the missing section of pocket deposits to the Namurian level is justified if the local Namurain rocks are pyrite rich. The alleged palaeochannels identified by Pasquali (2002), hidden beneath deep overburden in the Irish Midlands, may be pocket deposits.

A simple work flow that incorporates Feature Network Extraction (FNE) was developed in order to detect lineaments in the study area. Significantly, FNE is an automatic computer based technique that minimises user bias and error. Numerous lineaments were detected using FNE and most of them coincide with rivers. Two previously unrecognised major lineaments were discovered, namely the Billy Byrne's Gap Lineament and the Woodenbridge Lineament. It is suggest that lineaments find expression in the landscape by virtue of fault hosted hydrothermal fluids that caused chemical alteration of wall-rocks.

The Shankill Fracture Zone that closely parallels the northern section of the Billy Byrne's Gap Lineament, channelled hydrothermal fluids. A mineralised section of the fault at the Cloghleagh Iron Mine is host to a rare type of epithermal manganese deposit that likely formed <500 metres beneath a landscape that was above sea-level. These observations agree with the hypothesis that lineaments find expression in the landscape due to fault/fracture hosted hydrothermal fluids.

The serendipitous discovery of structures that resemble fossilised microbial life at the Cloghleagh Iron Mine was explored in chapter 5. It is proposed that they are inorganic structures that formed in a fault zone composed of solidifying iron-oxyhydroxide rich silica gel, the natural analogue of the Silica Garden. These proposals support the observations of Di Toro *et al.* (2004) who witnessed silica gel formation and friction reduction in a simulated fault zone. Finally, a convincing inorganic mimic of microbial life calls into question the supposed microbial fossils of the pre-Cambrian, for which evidence of biogenicity often relies only on morphology.

The chemically altered granite over looking Lough Tay is not a saprolite. Detailed XRD analysis revealed a clay mineral assemblage composed of beidellite-montmorillonite, illite and kaolinite. It is a type of argillic alteration that likely formed <200 metres of the surface. The tepid spring at the site may represent ebbing hydrothermal activity and indicate that the mineralisation is remarkably young. Indications of shallow mineralisation in nearby base metal veins were found in the form of platy calcite and hydrothermal breccia. Lastly, the identification of hydrothermally altered granite adds further weight to the hypothesis that hydrothermal alteration along faults, fractures and mineral veins in the study area influences topographic and fluvial development.

Finally, the Calary Plateau and Rathdrum Surface were likely part of the same palaeosurface, that is now gently tilted to the south and obfuscated by erosion and possibly tectonism as well. The Dargle River appears to pre-date the uplift and tilting of the Calary Plateau; indeed its spatial association with a pre-glacial Cenozoic palaeoriver in the offshore Kish Bank Basin supports its antiquity. A possible strath terrace near the summit of Howth Head, County Dublin, suggests that the observed regional landscape tilting may be related to erosional isostasy caused by the removal of relatively more easily denuded Carboniferous Limestone. Finally, there is evidence of an early north-west to south-east palaeodrainage in south County Wicklow and north County Wexford, evinced by the unusual parallel courses of the Potters Stream, Three Mile Water and some of the streams in Tinahely Hills area. It is proposed that these rivers were captured by fractures in a landscape that was gently tilted towards the south east.

8.2 Suggestions for Further Work

A recurring theme in this thesis is the suggestion that some faults and hydrothermal mineralisation in south east Ireland might be young *i.e.* pre-glacial Cenozoic. It is recommended that faults and mineral veins in the study area are dated using applicable radiometric dating tools. Another fruitful research topic might involve coupling Apatite Fission Track analysis (AFT) with the radiometric dating of faults. AFT analysis was used by Cunningham *et al.* (2003) to locate Cenozoic domain boundaries in the study area, separating differentially uplifted fault blocks bounded by suspected Cenozoic faults. The temporal activity of a fault that lies along an identified domain boundary could be dated by radiometric means, thus confirming and refining a suspected Cenozoic age.

Finally, young faults of Cenozoic age might host hot hydrothermal fluids at depth. Thus, they may be a source of geothermal energy, an important energy resource that does not emit greenhouse gases.

References

Adams, D.G. 2000. Heterocyst formation in cyanobacteria. *Current Opinion in Microbiology*, **3**, 618-624.

Alvarez, W. 1999. Drainage on evolving fold-thrust belts: a study of transverse canyons in the Apennines. *Basin Research*, **11**, 267-284.

Aoudjit, H., Elsass, F., Righi, D. & Robert, M. 1996. Mica weathering in acidic soils by analytical electron microscopy. *Clay Minerals*, **31**, 319-332.

Arrhenius, G.O. 2003. Crystals and Life. *Helvetica Chimica Acta*, **86**, 1569-1586.

Azaroual, M., Fouillac, C. & Matray, J.M. 1997. Solubility of silica polymorphs in electrolyte solutions, I. Activity coefficient of aqueous silica from 25° to 250°C, Pitzer's parameterisation. *Chemical Geology*, **140**, 155-165.

Azaroual, M., Fouillac, C. & Matray, J.M. 1997. Solubility of silica polymorphs in electrolyte solutions, II. Activity of aqueous silica and solid silica polymorphs in deep solutions from the sedimentary Paris Basin. *Chemical Geology*, **140**, 167-179.

Bada, J.L. & Lazcano, A. 2002. Some Like It Hot, But Not the First Biomolecules. *Science*, **296**, 1982-1983.

Balköse, D., Özkan, F., Köktürk, U., Ulutan, S., Ülkü, S. & Nisli, G. 2002. Characterization of Hollow Chemical Garden Fibers from Metal Salts and Water Glass. *Journal of Sol-Gel Science and Technology*, **23**, 253-263.

Ball, V. 1888. On the probable mode of transport of the fragments of granite and other rocks which are found imbedded in the Carboniferous limestone of the neighbourhood of Dublin. *Quartly Journal of the Geological Society, London*, **44**, 371-374.

Bartel, D.P. & Unrau, P.J. 1999. Constructing an RNA world. Trends in Cell Biology, **9**, M9-M13.

Beese, A.P., Brück, J., Feehan, J. & Murphy, T. 1983. A silica deposit of possible Tertiary age in the carboniferous limestone near Birr, County Offaly, Ireland. *Geological Magazine*, **120**, 331-340.

Ben Amar, M., Combescot, R. & Couder, Y., 1993. Viscous fingering with adverse anisotropy: A new Saffman-Taylor finger. *Physics Review Letters*, **70**, 3047-3050.

Berner, R.A. 1999. Atmospheric oxygen over Phanerozoic time. *Proceedings of the National Academy of Sciences of the United States of America*, 96, 10955-10957.

Bissig, T., Clark, A.H., Lee, J. & Hodgson, C.J. 2002. Miocene Landscape Evolution and Geomorphologic Controls on Epithermal Processes in the El Indio-Pascua Au-Ag-Cu Belt, Chile and Argentina. *Economic Geology*, **97**, 971-996.

Brasier, M.D., Green, O.R., Jephcoat, O.P., Kleppe, A.K., Van Kranendonk, M.J., Lindsay, J.F., Steele A. & Grassineau, N. 2002. Questioning the evidence for Earth's oldest fossils. *Nature*, **416**, 76-81.

Bray, C., Greenaway, I., Morgan, R. & Stewart, S. 2001. A new coordinate system for Ireland. **The Irish Scientist Year Book.**

Brindley, J.C. 1971. The granite dome of the Upper Liffey valley district, Co. Wicklow - A subsidary unit of the Leinster Batholith. *Biology and Environment: Proceedings of the Royal Irish Academy*, **71B**, 109-112.

Brindley, J.C., Gupta, L.N. & Kennan, P.S. 1976. Explosion breccias and related features in the Leinster Caledonian Massif, South-east Ireland. *Biology and Environment: Proceedings of the Royal Irish Academy*, **76B**, 337-349.

Browne, P.R.L. & Lawless, V.L. 2001. Characteristics of hydrothermal eruptions, with examples from New Zealand and elsewhere. *Earth-Science Reviews*, **52**, 299-331.

Brück, P.M. & O'Connor, P.J. 1982. Relationship of hydrothermal phenomena within the Leinster Granite to crustal fractures delineated from Landsat imagery. *Photogrammetria*, **37**, 151-159.

Buka, A., Kertesz J. & Vicsek, T. 1986. Transitions of viscous fingering patterns in nematic liquid crystals. *Nature*, **323**, 424-425.

Byerlee, J. 1978. Friction of rocks. *Pure and Applied Geophysics*, **116**, 615-626.

Capewell, J. 1956. The stratigraphy, structure and sedimentation of the Old Red sandstone of the Comeragh mountains and adjacent areas. *Proceedings of the Geological Society of London*, **1532**, 24-27.

Cartwright, J.H.E., García-Ruiz, J.M., Novellay, M.L. & Otálora, F. 2002. Formation of Chemical Gardens. *Journal of Colloid Interface Science*, **256**, 351-359.

Catling, C. & Moore, J.M. 2003. The nature of coarse-grained crystalline hematite and its implications for the early environment of Mars. *Icarus*, **165**, 277-300.

Chan, C.S., Welch, S.A., Frazer, B.H., Fakra, S. & Banfield, J.F. 2004. Microbial polysaccharides template assembly of nanocrystal fibers. *Science*, **303**, 1656- 8.

Chen, I.A., Roberts, R.W. & Szostak, J.W. 2004. The Emergence of Competition Between Model Protocells. *Science*, **305**, 1474-1476.

Chigira, M. & Oyama, T. 1999. Mechanism and effect of chemical weathering of sedimentary rocks. *Engineering Geology*, **55**, 3-14.

Cipelletti, L., Manley, S., Ball, R.C. & Weitz, D.A. 2000. Universal Aging Features in the Restructuring of Fractal Colloidal Gels. *Physical Review Letters,* **84**, 2275-2278.

Cipelletti, L. & Ramos, L. 2005. Slow dynamics in glassy soft matter. *Journal of Physics: Condensed Matter*, **17**, R253-R285.

Cody, G.D., Boctor, N.Z., Hazen, R.M., Scott, J.H., Sharma, A. & Yoder Jr., H.S. 2000. Primordial Carbonylated Iron-Sulfur Compounds and the Synthesis of Pyruvate. *Science*, **289**, 1337-1340.

Cohn, C.A., Borda, M.J. & Schoonen, M.A. 2004. RNA decomposition by pyrite-induced radicals and possible role of lipids during the emergence of life. *Earth and Planetary Science Letters*, **225**, 271-278.

Cole, G.A.J. 1922. Memoir and Map of Localities of Minerals of Economic Importance and Metalliferous Mines in Ireland. *Memoirs of the Geological Survey of Ireland*,155pp.

Cope, J.C.W. 1994. A latest Cretaceous hotspot and the southeasterly tilt of Britain. *Journal of the Geological Society*, **151**, 905-908.

Coxon, P. 2001. Understanding Irish landscape evolution: pollen assemblages from Neogene and Pleistocene palaeosurfaces in western Ireland. *Biology and Environment: Proceedings of the Royal Irish Academy*, **101B**, 85-97.

Cravotta III, C.A., Brady, K.B.C., Rose A.W. & Douds J.B. 1999. Frequency distribution of the pH of coal-mine drainage in Pennsylvania U.S. *Geological Survey Toxic Substances Hydrology Program: Proceedings of the Technical Meeting*, **1**, 313-324.

Cunningham, M.J.M. 2000. Mesozoic-Tertiary tectonics of SE Ireland and genetic link to offshore extensional basins. Unpublished Ph.D. Thesis, Trinity College Dublin.

Cunningham, M., Densmore, A., Allen, P., Phillips, W., Bennett, S., Gallagher, K. & Carter, A. 2003. Evidence for post-early Eocene tectonic activity in southeastern Ireland. *Geological Magazine*, **140**, 101-118.

Daccord, G., Nittmann, J. & Stanley, H.E. 1986. Radial viscous fingers and diffusion-limited aggregation: Fractal dimension and growth sites. *Physical Review Letters*, **56**, 336-339.

Darwin, C.R. 1995. *The Origin of Species*. Gramercy Books, New York.

Davies, G.L. 1960. The age and origin of the Leinster mountain chain: a study of the evolution of south-eastern Ireland from the upper Palaeozoic to the later Tertiary. *Biology and Environment: Proceedings of the Royal Irish Academy*, **61B**, 79-107.

Davis, J.C. 1986. *Statistics and data analysis in geology*. John Wiley & Sons; 2nd edition, New York.

Day, P.R. 1965. Particle fractionation and particle-size analysis, *In: Black A.C.* (ed.) *Methods of soil analysis, Part 1*. American Society of Agronomy, Inc., Madison, Wisconsin, 545-567.

Deamer, D.W. 1997. The First Living Systems: a Bioenergetic Perspective. *Microbiology and Molecular Biology Reviews*, **61**, 239-261.

Di Toro, G., Goldsby, D.L. & Tullis, T.E. 2004. Friction falls towards zero in quartz rock as slip velocity approaches seismic rates. *Nature*, **427**, 436-439.

Dickin, A.P. 1997. *Radiogenic Isotope Geology*. Cambridge University Press, Cambridge.

Dong, G., Morrison, G. & Jaireth, S. 1995. Quartz textures in epithermal veins, Queensland; classification, origin and implications. *Economic Geology*, **90**, 1841-1856.

Dörfelt, H., Schmidt, A.R. & Wunderlich, J. 2000. Rosaria succina spec. nov. – a fossil cyanobacterium from Tertiary amber. *Journal of Basic Microbiololgy*, **40**, 327-332

Dreher, A.N, Vlach, S.R.F. & Martini, S.L. 1998. Adularia associated with epithermal gold veins in the Tapajós Mineral Province, Pará State, northern Brazil. *Revista Brasileira de Geociências*, **28**, 397-404.

Drew, D.P. & Jones, Ll. G. 2000. Post-Carboniferous pre-Quaternary karstification in Ireland. *Proceedings of the Geologists' Association*, **111**, 345-353.

Drew, D. 2001. *Classic Landforms of the Burren Karst.* The Geographical Association, Sheffield.

Drummond, S. & Ohmoto, H. 1985. Chemical evolution and mineral deposition in boiling hydrothermal systems. *Economic Geology*, **80**, 126-147.

Durn, G., Ottner, F. & Slovence, D. 1999. Mineralogical and geochemical indicators of the polygenetic nature of terra rossa in Istria, Croatia. *Geoderma*, **91**, 125-150.

Ericson, K., Migon, P. & Olvmo. M. 2004. Fractures and drainage in the granite mountainous area. A study from Sierra Nevada, USA. *Geomorphology*, **64,** 97-116.

Etoh, J., Izawa, E., Watanabe, K., Taguchi, S. & Sekine, R. 2002. Bladed Quartz and Its Relationship to Gold Mineralization in the Hishikari Low-Sulfidation Epithermal Gold Deposit, Japan. *Economic Geology*, **97**, 1841-1851.

Eugster, H.P. 1968. Hydrous sodium silicates from Lake Magadi, Kenya: precursors of bedded chert. *Science*, **157**, 1177-1180.

Farrington, A. 1929. The pre-glacial topography of the Liffey Basin. *Biology and Environment: Proceedings of the Royal Irish Academy*, **38B**, 148-170.

Fenchel, T.M. 2002. *The Origin and Early Evolution of Life*. Oxford University Press, Oxford.

Fisher, P., Wood, J. & Cheng, T. 2004. Where is Helvellyn? Fuzziness of Multiscale Landscape Morphometry. *Transactions of the Institute of British Geographers*, **9**, 106-128.

Garcia-Ruiz, J.M., Hyde, S.T., Carnerup, A.M., Christy, A.G., Van Kranendonk, M. & Welham, N.J. 2003. Self-Assembled Silica-Carbonate Structures and Detection of Ancient Microfossils. *Science*, **302**, 1194-1197.

Garrity, G.M. & Boone, D.R. 2001. *Bergey's Manual of Systematic Bacteriology*. Williams & Wilkins, Baltimore.

Geoffory, L., Bergerat, F. & Angelier, J. 1996. Brittle tectonism in relation to the Palaeogene evolution of the Thulean/NE Atlantic domain: a study in Ulster. *Geological Journal*, **31**, 259-269.

Gerakis, A. & Baer, B. 1999. A Computer Program for Soil Textural Classification. *Soil Soil Science Society of America Journal*, **63**, 807-808.

Glauber, J.R. 1651. *Furni novi philosophici (A description of new philosophical furnaces)*. Richard Coats, London.

Golubic, S. & Seong-Joo, L. 1999. Early cyanobacterial fossil record: preservation, palaeoenvironments and identification. *European Journal of Phycology*, **34**, 339-348.

Gualtieri, A.F. & Venturelli, P. 1999. In situ study of the goethite-hematite phase transformation by real time synchrotron powder diffraction. *American Mineralogist*, **84**, 895-904.

Gugger, M.F. & Hoffmann, L. 2004. Polyphyly of true branching cyanobacteria (Stigonematales). *International Journal of Systematic Evolutionary Microbiology*, **54**, 349-357.

Génin, J.-M.R., Refait, P., Bourrie, G., Abdelmoula, M. & Trolard, F. 2001. Structure and stability of the Fe(II)-Fe(III) green rust "fougerite" mineral and its potential for reducing pollutants in soil solutions. *Applied Geochemistry*, **16**, 559-570.

Génin, J.-M. , Rabha, A., Gehin, A., Abdelmoula, M., Benali, O., Ernstsen, V., Ona-Nguema, Upadhyay, C. & Ruby, C. 2005. Fougerite and Fe^{II-III} hydroxycarbonate green rust; ordering, deprotonation and/or cation substitution; structure of hydrotalcite-like compounds and mythic ferrosic hydroxide $Fe(OH)_{(2+x)}$. *Solid State Sciences*, **7**, 545-572.

Hall, A.M. & Sugden, D.E. 1987. Limited modification of mid-latitude landscapes by ice sheets: The case of northeast Scotland. *Earth Surface Processes and Landforms*, **12**, 531-542.

Hammarstrom, M.J., Sibrell, P.L. & Belkin, H.E. 2003. Characterization of limestone reacted with acid-mine drainage in a pulsed limestone bed treatment system at the Friendship Hill National Monument Site, Pennsylvania, USA. *Applied Geochemistry*, **18**, 1705-1721.

Hass Jr., J. 1971. The effect of salinity on the maximum thermal gradient of a hydrothermal system at hydrostatic pressure. *Economic Geology*, **66**, 940-946.

Hautmann, S. & Lippolt, H.J. 2000. $^{40}Ar/^{39}Ar$ dating of central European K-Mn oxides -- a chronological framework of supergene alteration processes during the Neogene. *Chemical Geology*, **170**, 37-80.

Hills, E.S. 1964. Elements of structural geology, *In:* anonymous (eds) Methuen, London, 439p.

Hoffman, B.A. & Farmer, J.D. 2000. Filamentous fabrics in low-temperature mineral assemblages: are they fossil biomarkers? Implications for the search for a subsurface fossil record on the early Earth and Mars. *Planetary Space and Science*, **48**, 1077-1086.

Holland, H. 1999. When did the Earth's atmosphere become oxic? A Reply. *The Geochemical News*, **100**, 20-22.

Hone, J., Craig, M. & Fewer, M. 2002. *The new neighbourhood of Dublin.* Farmer, Dublin.

Hopkinson, L., Roberts, S., Wilkinson, J.J. & Herrington, R.J. 1998. Self-Organization of submarine hydrothermal siliceous deposits: Evidence from the TAG Hydrothermal Mound 26°N Mid Atlantic Ridge. *Geology*, **26**, 347-350.

Hutchinson, E.F. 1989. A new procedure for gridding elevation and stream line data with automatic removal of spurious pits. *Journal of Hydrology*, **106**, 211-232.

Génin, J.-M.R., Refait, P., Bourrie, G., Abdelmoula, M. & Trolard, F. 2001. Structure and stability of the Fe(II)-Fe(III) green rust "fougerite" mineral and its potential for reducing pollutants in soil solutions. *Applied Geochemistry*, **16**, 559-570.

Japsen, P. & Chalmers, J.A. 2000. Neogene uplift and tectonics around the North Atlantic: overview. *Global and Planetary Change*, **24**, 165-173.

Jones, D.E.H. 2002. Gardening in space: on the space shuttle Columbia, an experiment explores chemical growth without gravity and the challenges of orbital science. *American Scientist*, **90**, 454-461.

Jones, D.E.H. & Walter, U. 1998. The Silicate Garden Reaction in Microgravity: A Fluid Interfacial Instability. *Journal of Colloid and Interface Science*, **203**, 286-293.

Jordan, D. 1999. Geology of the Lough Dan area, County Wicklow. Unpublished Final Year Undergraduate Mapping Thesis, Trinity College Dublin.

Jukes, J.B. 1862. On the river valleys in the south of Ireland. *Quarterly Journal of the Geological Society of London*, **18**, 378-403.

Jébrak, M. 1997. Hydrothermal breccias in vein-type ore deposits: A review of mechanisms, morphology and size distribution. *Ore Geology Reviews*, **12**, 111-134.

Kamei, G. & Ohmoto, H. 2000. The kinetics of reactions between pyrite and O_2-bearing water reviled from in situ monitoring of DO, Eh and pH in a closed system. *Geochimica et Cosmochimica Acta*, **64**, 2585-2601.

Kane, K., Arbogast, B. & Leventhal, B. 1990. Characterization of Devonian Ohio Shale SDO-1 as a USGS Geochemical Reference Sample. *Geostandards Newsletter*, **14**, 169-196.

Kennan, P.S. 1972. Some curious garnet clusters from the Garnetiferous Beds of the Leinster Granite Aureole. *Geological Magazine*, **109**, 165-169.

Kennan, P.S. 1978. The origin of the sulphide deposits in the Leinster Granite. *Journal of Earth Sciences - Royal Dublin Society*, **1**, 41-47.

King, P.R. 1987. The fractal nature of viscous fingering in porous media. *Journal of Physics A: Mathematical and General*, **20**, L529-L534.

Konhauser, K.O., Phoenix, V.R., Bottrell, S.H., Adams, D.G. & Head, I.M. 2001. Microbial-silica interactions in Icelandic hot spring sinter: possible analogues for some Precambrian siliceous stromatolites. *Sedimentology*, **48**, 415-433.

Konhauser, K.O., Jones, B., Phoenix, V.R., Ferris, G. & Renaut, R.W. 2004. The Microbial Role in Hot Spring Silicification. AMBIO: A Journal of the Human Environment. *AMBIO: A Journal of the Human Environment*, **33**, 552-558.

Leal, P.R. 2004. Mineralogy and Geochemistry of an Epithermal Manganese District, Sierras Pampeanas, Argentina. *International Geology Review*, **46**, 75-90.

Leduc, S. 1911. *The Mechanism of Life*. Rebman Limited., London.

Levy, M. & Miller, S.L. 1998. The stability of the RNA bases: Implications for the origin of life. *Proceedings of the National Academy of Sciences*, **95**, 7933-7938.

Little, C.T.S., Glynn., S.E.J. & Mills, S.A. 2004. Four-Hundred-and-Ninety-Million-Year Record of Bacteriogenic Iron Oxide Precipitation at Sea-Floor Hydrothermal Vents. *Geomicrobiology Journal*, **21**, 415-429.

Lynne, B.Y., Campbell, K.A., Moore, J.N. & Browne, P.R.L. 2005. Diagenesis of 1900-year-old siliceous sinter (opal-A to quartz) at Opal Mound, Roosevelt Hot Springs, Utah, U.S.A. *Sedimentary Geology*, **179**, 249-278.

Mann T.A. 1999. *Doctor Faustus : The Life of the German Composer Adrian Leverkuhn As Told by a Friend.* Vintage Books, USA.

Marchant, T.R. & Sevastopulo, G.D. 1980. The Calp of the Dublin District. *Journal of Earth Science of the Royal Dublin Society*, **3**, 195-203.

Marone, C. 2004. Faults greased at high speed. *Nature*, **427**, 405-406.

Martin, W. & Russell, M.J. 2003. On the origins of cells: a hypothesis for the evolutionary transitions from abiotic geochemistry to chemoautotrophic prokaryotes, and from prokaryotes to nucleated cells. *Philosophical Transactions: Biological Sciences*, **358**, 58-85.

Maselko, J. & Strizhak, P. 2004. Spontaneous Formation of Cellular Chemical System that Sustains Itself far from Thermodynamic Equilibrium. *Journal of Physical Chemistry B*, **108**, 4937-4939.

Matmon, A., Enzel, Y., Zilberman, E. & Heimann, A. 1999. Late Pliocene and Pleistocene reversal of drainage systems in northern Israel: tectonic implications. *Geomorphology*, **28**, 43-59.

Maw, G. 1865. On some deposits of chert, white sand, and white clay in the Neighbourhood of Llandudno, North Wales. *Geological Magazine*, **2**, 200-204.

Maw, G. 1867. On the Distribution beyond the Tertiary Districts of white clays and sands subjacent to the boulder-clay drifts. *Geological Magazine*, **4**, 241-251.

Max, M.D., Barber, A.J. & Martinez, J. 1990. Terrane assemblages of the Leinster Massif, SE Ireland, during the Lower Palaeozoic. *Journal of the Geological Society, London*, **147**, 1035-1050.

Maxwell, J.C. 1870. On Hills and Dales. *The London, Edinburgh and Dublin Philosophical*, **40**, 421-425.

McArdle, P. & Kennedy, M.J. 1985. The East Carlow Deformation Zone and its regional implications. *Geological Survey of Ireland Bulletin*, **3**, 237-255.

McCarthy, A.J. 1989. Thermomonospora, *In:* Williams, S.T., Sharpe, M.E. and Holt, J.G. (eds) *Bergey's Manual of Systematic Bacteriology*. Lippincott, Williams & Wilkins, London, 2552-2572.

McConnell, B. & Philcox, M. E. 1994. *Geology of Kildare-Wicklow*. Geological Survey of Ireland, Enniscrone, Sligo.

McKerrow, W.S., MacNiocaill, C. & Dewey, J. 2000. The Caledonian Orogeny Redefined. *Jornal of the Geological Society of London*, **157**, 1149-1154.

Meek, N. & Douglass, J. 2001. Lake overflow: an alternative hypothesis for Grand Canyon incision and development of the Colorado River, *In:* Young, R. & Spamer, E. (eds) *Colorado River, Origin and Evolution, Proceedings of a Symposium Held at Grand Canyon National Park in June 2000*. Grand Canyon Association, 199-204.

Mielke, R.E., Pace, D.L., Porter, T. & Southam, G. 2003. A critical stage in the formation of acid mine drainage: Colonization of pyrite by Acidithiobacillus ferrooxidans under pH-neutral conditions. *Geobiology*, **1**, 81-90.

Migon, P. & Lidmar-Bergstrom, K. 2002. Deep weathering through time in central and northwestern Europe: problems of dating and interpretation of geological record. *CATENA*, **49**, 25-40.

Migon, P. & Thomas, M.F. 2002. Grus weathering mantles-problems of interpretation. *CATENA*, **49**, 5-24.

Mitcham, T.W. 1974. Origin of breccia pipes. *American Journal of Science*, **69**, 412-413.

Mitchell, G.F. 1980. The search for the Tertiary in Ireland. *Journal of Earth Science, Royal Dublin Society*, **3**, 13-33.

Mitchell, G.F. 1986. *The Shell Guide to Reading the Irish Landscape*. Country House, Dublin.

Mitchell, G.F. & Ryan, M. 1997. *Reading the Irish Landscape*. Roberts Rinehart Publishers; 3rd edition, Dublin.

Moorbath, S. 1962. Lead isotope abundance studies on mineral occurrences in the British Isles and their geological significance. *Philosophical Transactions of the Royal Society of London*, **254**, 295-360.

Moore, D.M. & Reynolds R.C. 1989. *X-ray diffraction and the identification and analysis of clay minerals*. Oxford University Press, New York.

Murata, K.L. & Norman, B.M. 1976. An index of crystallinity for quartz. *American Journal of Science*, **276**, 1120-1130.

Murphy, T. 1966. Deep alteration of carboniferous strata in the Middleton, Co. Cork district as detected by gravity surveying. *Biology and Environment: Proceedings of the Royal Irish Academy*, **64B**, 323-334.

Mühlhaus, H.-B., Dufour, F., Moresi, L. & Hobbs, B. 2002. A director theory for visco-elastic folding instabilities in multilayered rock. *International Journal of Solids and Structures*, **39**, 3675-3691.

Nicholson, K. 1986. Geochemistry and mineralogy of iron and manganese veins, Arndilly, Banffshire, Scotland. *Scottish Jornal of Geology*, **22**, 213-224.

Nisbet, E.G. & Sleep, N.H. 2001. The habitat and nature of early life. *Nature*, **409**, 1083-1091.

O'Connel, Y. 2003. Final report on the geophysical survey for the proposed landfill site, Drehed, Co. Kildare for TES Consulting Engineers.

O'Connor, P., Aftalion, M. & Kennan, P. 1989. Isotopic U-Pb ages of zircon and monazite from the Leinster Granite, Southeast Ireland. *Geological Magazine*, **126**, 725-728.

O'Reilly, G. 1992. Petrographic and geochemical evidence for a hypogene origin of granite-hosted, vein-type Mn mineralization at the New Ross Mn deposits, Lunenburg County, Nova Scotia, Canada. *Economic Geology*, **87**, 1275-1300.

Oberlander, T.M. 1985. Origin of drainage transverse to structure in orogens. *Tectonic Geomorphology*, 155-182.

Oehler, J.H. 1976. Hydrothermal crystallization of silica gel. *GSA Bulletin*, **87**, 1143-1152.

Parsons, T. 2002. Nearly frictionless faulting by unclamping in long-term interaction models. *Geology*, **30**, 1063-1066.

Pasquali, R. 2002. Onshore sediment transport routes to the Porcupine Basin during the Tertiary. Unpublished MSc. Thesis, Trinity College Dublin.

Patrier, P., Beaufort, D., Mas, A. & Traineau, H. 2003. Surficial clay assemblage associated with the hydrothermal activity of Bouillante (Guadeloupe, French West Indies). *Journal of Volcanology and Geothermal Research*, **126**, 143-156.

Peacock, C. & Sherman, D. 2004. Vanadium (V) adsorption onto goethite (α-FeOOH) at pH 1.5 to 12: A surface complexation model based on ab initio molecular geometries and EXAFS spectroscopy. *Geochimica et Cosmochimica Acta*, **68**, 1723-1733.

Peretó, J. 2005. Controversies on the origin of life. *International Microbiology*, **8**, 23-31.

Phoenix, V.R., Adams, D.G. & Konhauser, K.O. 2000. Cyanobacterial viability during hydrothermal biomineralisation. *Chemical Geology*, 329-338.

Phoenix, V.R., Konhauser, K.O., Adams, D.G. & Bottrell, S.H. 2001. The role of biomineralization as an ultraviolet shield: Implications for the Archean. *Geology*, **29**, 823-826.

Poppe, L.J., Paskevich, V.F., Hathaway, J.C. & Blackwood, D.S. 2001. A laboratory manual for X-ray powder diffraction. U.S. Geological Survey Open-File Report 01-041.

Post, J.E. 1999. Manganese oxide minerals: Crystal structures and economic and environmental significance. *Proceedings of the National Academy of Science*, **96**, 3447-3454.

Potter, R.M. & Rossman, G.R. 1979. The mineralogy of manganese dendrites and coatings. *American Mineralogist*, **64**, 1219-1226.

Quinby-Hunt, M.S., Wilde, P., Orth, P.C.J. & Berry, W.B.N. 1989. Elemental geochemistry of black shales - statistical comparison of low-calcic shales with other shales, *In:* Grauch, R.I. & Leventhal, J.S. (eds) *Metalliferous Black Shales and related Ore Deposits*. U. S. Geological Survey Circular 1037, 8-15.

Rabus, B., Eineder, M., Roth, A. & Bamler, R. 2003. The shuttle radar topography mission--a new class of digital elevation models acquired by spaceborne radar. *ISPRS: Journal of Photogrammetry and Remote Sensing*, **57**, 241-262.

Readman, P.W., O'Reilly, B.M. & Murphy, T. 1997. Gravity gradients and upper-crustal tectonic fabrics, Ireland. *Journal of the Geological Society*, **154**, 817-828.

Reynolds, G.A. 1974. A geophysical study of an unusual silica deposit at Dunshaughlin Co. Meath, Ireland. Unpublished MSc. Thesis, Trinity College Dublin.

Reysenbach, A.L. & Cady, S. 2001. Microbiology of ancient and modern hydrothermal systems. *Trends in Microbiology*, **9**, 79-86.

Rimstidt, D.L. 1997. Quartz solubility at low temperatures. *Geochimica et Cosmochimica Acta*, **61**, 2553-2558.

Robertson, W.J., Kinnunen, P.H.M., Plumb, J.J., Franzmann, P.D., Puhakka, J.A., Gibson, J.A.E. & Nichols, P.D. 2002. Moderately thermophilic iron oxidising bacteria isolated from a pyritic coal deposit showing spontaneous combustion. *Minerals Engineering*, **15**, 815-822.

Roddy, M.S., Reynolds, S.J., Smith, B. & Ruiz, J. 1988. K-metasomatism and detachment related mineralization, Harcuvar Mountains, Arizona. *Geological Society of America Bulletin*, **100**, 1627-1639.

Rodgers, K.A., Browne, P.R.L., Buddle, T.F., Cook, K.L., Greatrex, R.A., Hampton, W.A., Herdianita, N.R., Holland, G.R., Lynne, B.Y., Martin, R., Newton, Z., Pastars, D., Sannazarro, K.L. & Teece, C. 2004. Silica phases in sinters and residues from geothermal fields of New Zealand. *Earth-Science Reviews*, **66**, 1-61.

Rohwerder, T., Schippers, A. & Sand, A. 1998. Determination of reaction energy values for biological pyrite oxidation by calorimetry. *Termochimica Acta*, **309**, 79-85.

Roig Silva, C., Goldsby, D.L., Di Toro, G. & Tullis, T.E. 2004. The Role of Silica Content in Dynamic Fault Weakening Due to Gel Lubrication. *Eos Transactions, American Geophysical Union, Fall Meeting Abstracts*, **85,** Session T21D-06.

Rose, A.W. & Cravotta III, C.A. 1998. Chapter 1: geochemistry of coal mine drainage, *In:* Sokolow, M.A. (eds) *Coal Mine Drainage Prediction and Pollution Prevention in Pennsylvania*. The Pennsylvania department of environmental protection, Harrisburg, PA, U.S.

Russell, M.J. 2003. GEOCHEMISTRY: The Importance of Being Alkaline. *Science*, **302**, 580-581.

Russell, M.J. & Arndt, N.T. 2005. Geodynamic and metabolic cycles in the Hadean. *Biogeosciences*, **2**, 97-111.

Russell, M.J. & Martin, W. 2004. The rocky roots of the acetyl-CoA pathway. *Trends in Biochemical Sciences*, **29**, 358-363.

Saffer, D.M., Bekins, B.A. & Hickman, S. 2000. Topographically driven groundwater flow and the San Andreas heat flow paradox revisited. *Journal of Geophysical Research*, **108**, 12-1- 12-14.

Sander, L.M. 2000. Diffusion-limited aggregation: a kinetic critical phenomenon?. *Contemporary Physics,*, **41**, 203-218.

Schmidt, A.R. & Schäfe, U. 2005. Leptotrichites resinatus new genus and species: a fossil sheathed bacterium in alpine cretaceous amber. *Journal of Paleontology*, **79**, 175-184.

Scholz, C.H. 2000. Evidence for a strong San Andreas fault. *Geology*, **28**, 163-166.

Schopf, W.J., Kudryavtsev, A.B., Agresti, D.G., Wdowiak, T. & Czaja, A.D. 2002. Laser-Raman imagery of Earth's earliest fossils. *Nature*, **416**, 73-76.

Schwartzman, D.W. & Lineweaver, C.H. 2004. The hyperthermophilic origin of life revisited. *Biochemical Society transactions*, **32**, 168-171.

Schwarz, T. 1997. Lateritic bauxite in central Germany and implications for Miocene palaeoclimate. *Palaeogeography, Palaeoclimatology, Palaeoecology*, **129**, 37-50.

Sebag, D., Verrecchia, E.P., Seong-Joo, L. & Durand A. 2001. The natural hydrous sodium silicates from the northern bank of Lake Chad: occurrence, petrology and genesis. *Sedimentary Geology*, **139**, 15-31.

Segré, D., Ben-Eli, D., Deamer, D.W. & Lancet, D. 2001. The Lipid World. *Origins of Life and Evolution of Biospheres*, **31**, 119-145.

Shuster, D.L., Vasconcelos, P.M., Heim, J.A. & Farley, K.A. 2005. Weathering geochronology by (U-Th)/He dating of goethite. *Geochimica et Cosmochimica Acta*, **69**, 659-673.

Sibson, R.H. 1987. Earthquake rupturing as a mineralizing agent in hydrothermal systems. *Geology*, **15**, 701-704.

Sibson, R.H. 2000. Fluid involvement in normal faulting. *Journal of Geodynamics*, **29**, 469-499.

Simmons, S.F. & Christenson, B.W. 1994. Origins of calcite in a boiling geothermal system. *American Journal of Science*, **294**, 361-400.

Simms, M.J. 2004. Tortoises and hares: dissolution, erosion and isostasy in landscape evolution. *Earth Surface Processes and Landforms*, **29**, 477-494.

Soil Survey Division Staff. 1993. *Soil Survey Manual*. Soil Conservation Service. U.S. Department of Agriculture Handbook 18, New York.

Spencer, J.E. & Welty, J.W. 1986. Possible controls of base- and precious-metal mineralization associated with Tertiary detachment faults in the lower Colorado River trough, Arizona and California. *Geology*, **14**, 195-198.

Stal, J.L. 2000. Cyanobacteria Mats and Stromatolites, *In:* B.A. Whitton, M. Potts (eds) *The Ecology of Cyanobacteria: Their Diversity in Time and Space*. Kluwer Academic Publishers, Dordrecht, The Netherlands, 37-59.

Stokes, M. & Mather, A.E. 2003. Tectonic origin and evolution of a transverse drainage: the Rio Almanzora, Betic Cordillera, Southea. *Geomorphology*, **50**, 59-81.

Stone, D.A. & Goldstein, R.E. 2004. Tubular precipitation and redox gradients on a bubbling template. *Proceedings of the National Academy of Sciences of the United States*, **101**, 11537-11541.

Sun, G., Ranson, K.J., Kharuk, V.I. & Kovacs, K. 2003. Validation of surface height from shuttle radar topography mission using shuttle laser altimeter. *Remote Sensing of Environment*, **88**, 401-411.

Symons, D., Smethurst, M. & Ashton, J. 2002. Paleomagnetism of the Navan Zn-Pb Deposit, Ireland. *Economic Geology*, **97**, 997-1012.

Theiler, J. 1990. Estimating fractal dimension. *Journal Optical Society America B*, **7**, 1055-1073.

Thiry, M. & Simon-Coinçon, R. 1996. Tertiary palaeoweathering and silcretes in the southern Paris Basin. *Catena*, **26**, 1-26.

Thouvenel-Romans S. & Steinbock, O. 2003. Oscillatory Growth of Silica Tubes in Chemical Gardens. Journal of the American Chemical Society, **125**, 4338-4341.

Twidale, C.R. 2002. The two stage concept of landform and landscape development involving etching: origin, development and implications of an idea. *Earth-Science Reviews*, **57**, 37-74.

Twidale, C.R. 2004. River patterns and their meaning. *Earth-Science Reviews*, **67**, 159-218.

van Lunsen, H.A. & Max, M.D. 1975. The geology of Howth and Ireland's Eye, Co. Dublin. *Geological Journal*, 35-38.

van Veen, W.L., Mulder, E.G. & Deinema, M.H. 1978. The Sphaerotilus-Leptothrix group of bacteria. *Microbiol Rev*, **42**, 329-256.

Vikre, P.G. 1994. Gold mineralization and fault evolution at the Dixie Comstock Mine, Churchill. County, Nevada. *Economic Geology*, **89**, 707-719.

Waggoner, B.M. 1996. Bacteria and protists from Middle Cretaceous amber of Ellsworth County, Kansas. *PaleoBios*, **17**, 20-26.

Walsh, P.T., Boulter, M.C., Mohammed, I. & Urbani, D.M. 1972. The preservation of the Neogene Brassington Formation of the southern Pennines and its bearing on the evolution of Upland Britain. *Journal of the Geological Society, London*, **128**, 519-559.

Walsh, P.T., Boulter, M.C. & Morawiecka, I. 1999. Chattian and Miocene elements in the modern landscape of western Britain and Ireland, *In:* Smith B. J., Whalley W.B., & Warke P.A. (eds) *Uplift, erosion and stability: perspectives on long-term landscape development*. Geological Society Special Publication no. 162, 45-63.

Walsh, P.T. & Brown E.H. 1971. Solution subsidence outliers containing probable Tertiary sediment in North-east Wales. *Geological Journal*, **7**, 299-320.

Walsh, P.T., Morawiecka, I. & Skawinska-Wieser, K. 1996. A Miocene palynoflora preserved by karstic subsidence in Anglesey and the origin of the Menaian Surface. *Geological Magazine*, **133**, 713-719.

Ward, D.M & Castenholz, R. 2000. Cyanobacteria in geothermal habitats, *In:* Whitton, B. A. and Potts, M. (eds) *Ecology of Cyanobacteria: Their Diversity in Time and Space*. Kluwer Academic Publishers, Dordrecht, 591-611.

Watts, A., McKerrow, W. & Fielding, E. 2000. Lithospheric flexure, uplift, and landscape evolution in south-central England. *Journal of the Geological Society*, **157**, 1169-1177.

Whitton, B.A. & Potts, M., (eds) 2000. *The Ecology of Cyanobacteria - Their Diversity in Time and Space*. Kluwer Academic Publishers, Dordrecht.

Wibberley, C.A.J. & Shimamoto, T. 2005. Earthquake slip weakening and asperities explained by thermal pressurization. *Nature*, **436**, 689-692.

Witten Jr., T.A. & Sander, L.M. 1981. Diffusion-Limited Aggregation, a Kinetic Critical Phenomenon. *Physics Reviews Letters*, **47**, 1400-1403.

Witten Jr., T.A. & Sander, L.M. 1983. Diffusion-limited aggregation. *Physical Review B*, **27**, 5686-5697.

Wächtershäuser, G. 1990. The case for the chemoautotrophic origin of life in an iron-sulfur world. *Origins of Life and Evolution of Biospheres (Formerly Origins of Life and Evolution of the Biosphere)*, **20**, 173-176.

Wächtershäuser, G. 2003. From pre-cells to Eukarya - a tale of two lipids. *Molecular Microbiology*, **47**, 13-22.

Yang, K., Browneb, P.R.L, Huntingtona, J.F. & Walshe, J L. 2001. Characterising the hydrothermal alteration of the Broadlands–Ohaaki geothermal system, New Zealand, using short-wave infrared spectroscopy. *Journal of Volcanology and Geothermal Research*, **106**, 53-65.

Yee, N., Phoenix, V.R., Konhauser, K.O., Benning, L.G. & Ferris, F.G. 2003. The effect of cyanobacteria on silica precipitation at neutral pH: Implications for bacterial silicification in geothermal hot springs. *Chemical Geology*, **199**, 83-90.

Zhang, J.-h. & Liu, Z.-h., 1998. Study of the relationship between fractal dimension and viscosity ratio for viscous fingering with a modified DLA model. *Journal of Petroleum Science and Engineering*, **21**, 123-128.